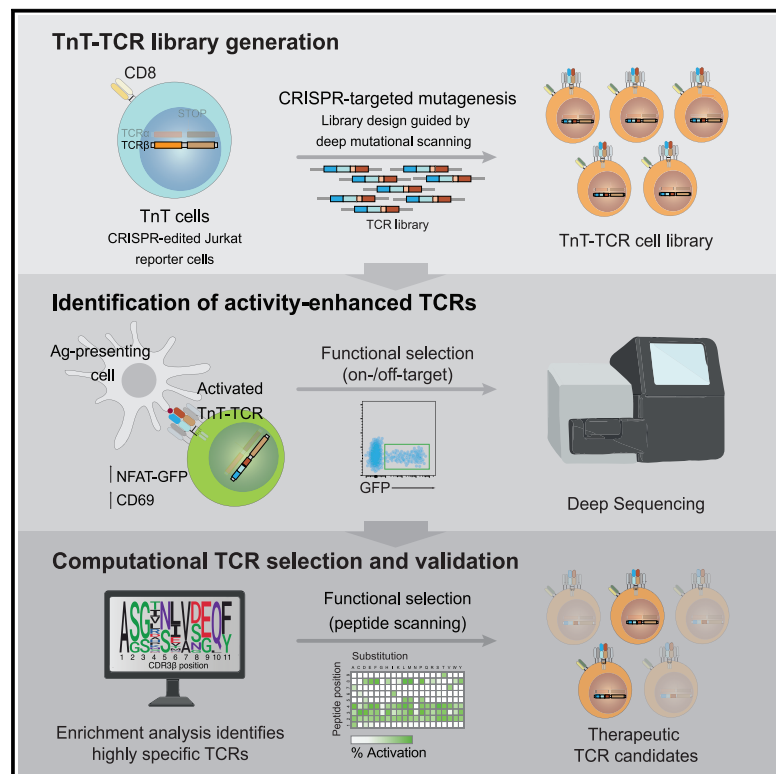


Immunity

High-throughput T cell receptor engineering by functional screening identifies candidates with enhanced potency and specificity

Graphical abstract



Authors

Rodrigo Vazquez-Lombardi,
Johanna S. Jung,
Fabrice S. Schlatter, ...,
Alfred Zippelius, Heinz Läubli,
Sai T. Reddy

Correspondence

rodrigo.vl@engimmune.com (R.V.-L.),
sai.reddy@ethz.ch (S.T.R.)

In brief

Vazquez-Lombardi et al. developed a high-throughput method combining mammalian display, CRISPR-targeted mutagenesis, functional screening, and deep sequencing for the engineering of T cell receptors (TCR-Engine). They applied TCR-Engine to identify potent and specific therapeutic candidates against MAGE-A3, an attractive cancer target for TCR immunotherapy previously complicated by off-target activity.

Highlights

- CRISPR-targeted genome editing enables display of functional T cell receptors
- Deep mutational profiling reveals discordance between TCR binding and function
- Specificity-guided functional screening of TCR mutagenesis libraries
- Functional selections identify TCR variants with enhanced potency and specificity



Resource

High-throughput T cell receptor engineering by functional screening identifies candidates with enhanced potency and specificity

Rodrigo Vazquez-Lombardi,^{1,2,*} Johanna S. Jung,¹ Fabrice S. Schlatter,¹ Anna Mei,¹ Natalia Rodrigues Mantuano,³ Florian Bieberich,¹ Kai-Lin Hong,¹ Jakub Kucharczyk,¹ Edo Kapetanovic,¹ Erik Aznauryan,¹ Cédric R. Weber,¹ Alfred Zippelius,³ Heinz Läubli,³ and Sai T. Reddy^{1,4,*}

¹Department of Biosystems Science and Engineering, ETH Zurich, Mattenstrasse 26, 4058 Basel, Switzerland

²Engimmune Therapeutics AG, Hegenheimermattweg 167A, 4123 Allschwil, Switzerland

³Department of Biomedicine, Universitätsspital Basel, Basel, Switzerland

⁴Lead contact

*Correspondence: rodrigo.vl@engimmune.com (R.V.-L.), sai.reddy@ethz.ch (S.T.R.)

<https://doi.org/10.1016/j.immuni.2022.09.004>

SUMMARY

A major challenge in adoptive T cell immunotherapy is the discovery of natural T cell receptors (TCRs) with high activity and specificity to tumor antigens. Engineering synthetic TCRs for increased tumor antigen recognition is complicated by the risk of introducing cross-reactivity and by the poor correlation that can exist between binding affinity and activity of TCRs in response to antigen (peptide-MHC). Here, we developed TCR-Engine, a method combining genome editing, computational design, and deep sequencing to engineer the functional activity and specificity of TCRs on the surface of a human T cell line at high throughput. We applied TCR-Engine to successfully engineer synthetic TCRs for increased potency and specificity to a clinically relevant tumor-associated antigen (MAGE-A3) and validated their translational potential through multiple *in vitro* and *in vivo* assessments of safety and efficacy. Thus, TCR-Engine represents a valuable technology for engineering of safe and potent synthetic TCRs for immunotherapy applications.

INTRODUCTION

T cells genetically modified to express T cell receptors (TCRs) recognizing tumor-associated antigens (TAAs) offer a promising approach for cancer immunotherapy (Johnson et al., 2009; Morgan et al., 2006; Parkhurst et al., 2011; Rapoport et al., 2015; Robbins et al., 2015; Stadtmauer et al., 2020; Strønen et al., 2016). However, the discovery, engineering, and selection of potent and safe therapeutic TCRs is often complicated by low affinities to peptide-MHC antigen targets and the inherent risk of cross-reactivity to off-target peptides on healthy cells (Uttenthal et al., 2012). Due to central and peripheral negative selection processes, naturally occurring TCRs with high affinity toward self-tumor antigens are extremely rare (Chapuis et al., 2019; Johnson et al., 2006; Spindler et al., 2020). To overcome this, synthetic TCRs have been engineered using protein mutagenesis and selection methods that rely on antigen binding (e.g., phage and yeast display) (Kieke et al., 1999; Li et al., 2005). However, such technologies are limited because the binding affinity of a TCR to antigen does not necessarily correlate with T cell activation in response to antigen presentation on cells, the latter being more physiologically relevant (Duong et al., 2019; Hebeisen et al., 2015; Sibener et al., 2018; Thomas et al., 2011). Moreover, the generation of synthetic TCRs can be complicated

by the introduction of unpredicted cross-reactivity leading to severe toxicity (Linette et al., 2013; Morgan et al., 2013).

An important consideration for both the assessment of cross-reactivity and the engineering of synthetic TCRs is that TCR affinity and activity are not necessarily correlated with each other. For example, although TCRs with high affinities to antigen (1–5 μM) tend to display high activity *in vitro*, TCRs with lower affinities (5–100 μM) often display a poor correlation between affinity and activity (Hebeisen et al., 2015; Sibener et al., 2018). In addition, TCRs engineered for supraphysiological affinity (<1 μM) may in fact display sub-optimal therapeutic activity by promoting T cell dysfunction (Hebeisen et al., 2013; Presotto et al., 2017), inability to undergo serial TCR triggering (Thomas et al., 2011), and potential for reactivity against the presenting HLA molecule (Duong et al., 2019; Holler et al., 2003; Tan et al., 2015).

Traditional TCR engineering methods require re-formatting of TCRs into single-chain fragments, which are then screened on the surface of phage or yeast for binding toward peptide-MHC multimers. In one notable example, phage display was used to generate a high-affinity synthetic TCR targeting the MAGE-A3 TAA. When applied in a cell therapy clinical trial, this synthetic TCR showed an unexpected cross-reactivity toward a self-antigen expressed by beating cardiomyocytes, which ultimately resulted in treatment-induced patient deaths (Cameron et al.,



2013; Linette et al., 2013). Thus, the development of TCR display platforms enabling simultaneous TCR engineering and detection of cross-reactivity on the basis of their activity (i.e., antigen-induced signaling) would be highly desirable. Although a number of TCR engineering methods have been developed in mammalian cell lines (Chervin et al., 2008; Karapetyan et al., 2019; Malecek et al., 2013; Spindler et al., 2020; Wagner et al., 2019; Schmitt et al., 2017) and primary T cells (Kessels et al., 2000; Schmitt et al., 2017), most of these have only reported selections based on antigen binding. Recently, Garcia and colleagues applied peptide-MHC yeast display coupled with soluble TCR binding to discover a biophysical mechanism by which certain high-affinity TCR-peptide-MHC interactions fail to trigger TCR signaling, namely the occurrence of ‘slip’ bonds that rupture under force (Sibener et al., 2018). The opposing mechanism, which is the formation of “catch” bonds that persist under force, has been recently exploited by the same group for structure-based TCR library design and functional screening leading to the identification of TCRs with enhanced activity and specificity against HIV-Pol and MAGE-A3 antigens (Zhao et al., 2022). In all of these previous efforts in mammalian cells, viral transduction or plasmid transfection were used for TCR reconstitution, which are associated with limitations including random integration, constitutive TCR expression, and possible expression of multiple TCRs by a single cell.

Here, we present TCR-Engine, a TCR engineering method leveraging genome editing, deep sequencing, computationally guided design and selection, and functional screening to profile at high-throughput the activity and specificity of TCRs on the surface of a CRISPR-engineered human T cell platform. We use this approach to express >30 individual TCRs and perform functional screening of 437 single amino acid variants and ~260,000 combinatorial variants. We reveal a substantial discordance between TCR binding and activation in response to antigen and identify several TCRs that are strongly activated by antigen despite showing undetectable binding to peptide-MHC multimers. In addition, we use our platform and target peptide scanning to accurately predict TCR off-target antigens. Finally, we apply TCR-Engine to a low-avidity TCR targeting the clinically relevant tumor antigen MAGE-A3, an attractive but challenging TAA (Linette et al., 2013; Morgan et al., 2013). This resulted in engineered TCR variants with enhanced potency and specificity thus representing therapeutic candidates.

RESULTS

Development of TCR-accepting T cells (TnTs) for high-throughput activation and specificity profiling

We developed TCR-Engine, a platform technology combining CRISPR-targeted mutagenesis, deep sequencing, and computationally guided design and selection that enables engineering of TCRs on the basis of their activity. We first established the TCR-accepting T cell (TnT) line (originating from the human leukemia Jurkat T cell line) by five sequential steps of CRISPR-Cas9 genome editing to knockout endogenous TCR expression and introduce additional functional components, culminating in the ability to detect TCR-mediated activation through nuclear factor of activated T cells (NFAT) response elements (Karttunen et al., 1992) linked to a GFP reporter or surface expression of the early

T cell activation marker CD69. Each genome editing step consisted of transfection with a gene-targeting guide RNA (gRNA) and, when required, a homology-directed repair (HDR) template encoding desired transgenes (Figure 1 and STAR Methods for details). This was followed by single-cell fluorescence-activated cell sorting (FACS), cell expansion, and clone validation by flow cytometry and Sanger sequencing. The resulting TnT cell line constitutively expresses Cas9 nuclease, human CD8, and mRuby, harbors an NFAT-GFP reporter of TCR signaling, and lacks expression of CD4, endogenous TCR, and Fas (Figure 2A). Reconstitution of TnT cells with transgenic TCRs was targeted by CRISPR-Cas9 to the endogenous TCR β genomic region, specifically to the recombined complementarity determining region 3 β (CDR3 β) sequence, thus providing a monoallelic target supporting a single integration event per cell and physiological expression of transgenic TCRs (Figures 2B and S1A–S1C). The lack of a constant TCR β domain (TRBC) in the transgenic TCR construct design made splicing with endogenous Jurkat TRBC exons a requirement for transgenic TCR expression. This feature allowed us to detect targeted genomic integration based on restored surface expression of CD3 following transfection of TnT cells with CDR3 β gRNA and designed HDR templates (PCR product) (Figure 2C). Furthermore, our strategy ensured that cells displaying restored CD3 expression underwent knockout of the endogenous Jurkat TCR β chain, as integration of transgenic TCRs relied on the introduction of a double-stranded DNA break at the targeted CDR3 β genomic region. The development of an enhanced transfection protocol led to HDR efficiencies in the range of 5%–20% (Figure 2C). Targeted TCR reconstitution for the generation of TnT-TCR cells was further validated by detecting binding to cognate peptide-MHC dextramer using flow cytometry (Figure 2D), PCR amplification of the Jurkat TCR β genomic locus (Figure 2E), and reverse-transcriptase PCR (RT-PCR) using reverse primers annealing to endogenous Jurkat TRBC sequences (Figures S2D and S2E).

To validate their functionality, we reconstituted TnT cells with three TCRs recognizing HLA-A*0201-restricted TAAs: TCR $_{1G4}$, with specificity to NY-ESO-1, and TCR $_{DMF4}$ and TCR $_{DMF5}$, with specificity to MART-1 (Table S1). TnT-TCR cell activation was assessed by NFAT-GFP expression following co-culture with peptide-pulsed, HLA-A*0201-positive T2 cells (Luft et al., 2001). Co-culture of TnT-TCR $_{1G4}$ cells with non-pulsed (no peptide) T2 cells yielded no detectable expression of NFAT-GFP, whereas co-culture with T2 cells pulsed with NY-ESO-1 $_{157-165}$ cognate peptide induced robust expression of the NFAT-GFP reporter (Figure 2F). To further assess the specificity of TCR-redirected TnT cells, we performed co-cultures of TnT, TnT-TCR $_{1G4}$, TnT-TCR $_{DMF4}$, and TnT-TCR $_{DMF5}$ cells with T2 cells pulsed with NY-ESO-1 $_{157-165}$ peptide, MART-1 $_{26-35(27L)}$ peptide, or no peptide. NFAT-GFP expression was fully restricted to correct TCR-peptide-MHC pairings, with no detectable NFAT-GFP expression across negative controls (Figure 2G). We next compared the binding and signaling avidities of TnT-TCR $_{1G4}$, TnT-TCR $_{DMF4}$, and TnT-TCR $_{DMF5}$ cells (Figures 2H and 2I). TnT-TCR $_{DMF5}$ cells displayed the highest binding avidity to their target peptide-MHC (EC50 = 7 pM), followed by TnT-TCR $_{1G4}$ (EC50 = 57 pM) and TnT-TCR $_{DMF4}$ (EC50 = 267 pM), with picomolar EC50 values reflecting the highly multivalent nature of peptide-MHC dextramers (10–20 peptide-MHC copies per

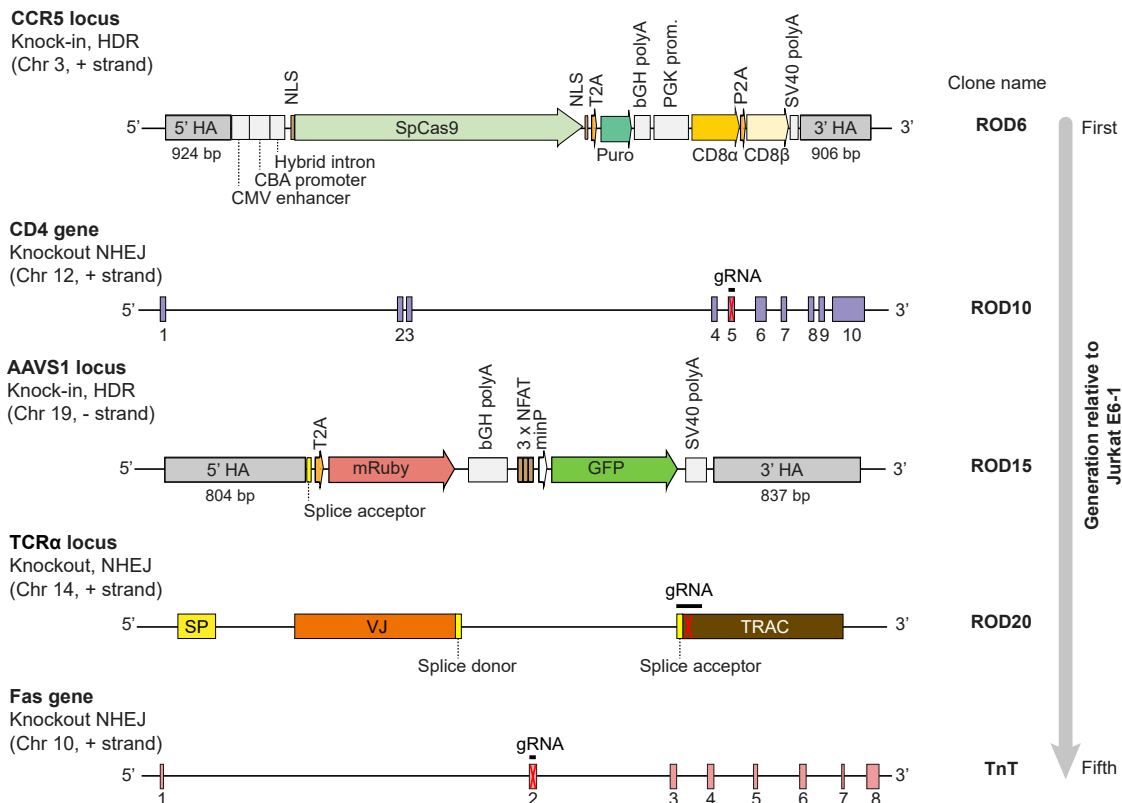


Figure 1. Development of the TCR-accepting T cell (TnT) platform through multistep CRISPR-Cas9 genome editing

Schematic representation of the genome editing steps performed for generating the TnT platform.

AAVS1, adeno-associated virus integration site 1; bGH polyA, bovine growth hormone polyadenylation signal; GFP, green fluorescent protein; gRNA, guide RNA; HA, homology arm; HDR, homology-directed repair; minP, minimal promoter; NHEJ, non-homologous end joining; NLS, nuclear localization signal; P2A, 2A peptide from porcine teschovirus-1 polyprotein; PGK, phosphoglycerate kinase; Puro, puromycin; SP, signal peptide; SpCas9, *Streptococcus pyogenes* Cas9; T2A, 2A peptide from *Thosea asigna* virus capsid protein; TRAC, T cell receptor alpha constant region; SV40 polyA, simian virus 40 polyadenylation signal.

See also Figure S1.

molecule) (Figure 2H). TnT-TCR cells co-cultured with T2 cells pulsed with serial dilutions of cognate peptide revealed a dose-dependent response (Figure 2I). TnT-TCR_{DMF5} displayed the highest signaling avidity (EC50 = 6 nM), followed by TnT-TCR_{DMF4} (EC50 = 11 nM) and TnT-TCR_{1G4} (EC50 = 90 nM). In contrast to their 39-fold difference in binding to peptide-MHC dextramer, the difference between TnT-TCR_{DMF4} and TnT-TCR_{DMF5} in terms of signaling avidity was only 2-fold. Assessment of TCR surface expression levels by means of flow cytometry revealed a substantial deficit for TCR_{DMF4} relative to TCR_{DMF5}, which, in addition to a 5-fold lower reported affinity (Figures S2A and S2B), explains the low capacity for dextramer binding to TCR_{DMF4} both in terms of EC50 and maximal dextramer fluorescence intensity (Figure S2C).

We next investigated the ability of TCR_{DMF4} to potently respond to antigen despite its reduced surface expression and moderate affinity. We used multiple readouts to profile the activation of TnT-TCR_{DMF4}, TnT-TCR_{DMF5}, and TnT-TCR_{1G4} in response to a variety of antigen-independent and antigen-dependent stimuli (Figure S2D). PMA-ionomycin stimulation induced robust expression of NFAT-GFP, CD69, and secretion of IL-2 effector cytokine across all tested TnT-TCR cells, and stimulation with TCR/CD3 engagers strongly correlated with TCR sur-

face expression (TCR_{1G4} > TCR_{DMF5} > TCR_{DMF4}) (Figure S2D). By contrast, antigen-induced stimulation with decreasing concentrations of peptide confirmed robust expression of NFAT-GFP and CD69 in TnT-TCR_{DMF4} cells despite lower affinity relative to TCR_{DMF5} and reduced surface expression relative to both TCR_{1G4} and TCR_{DMF5} (Figure S2E). Notably, maximal IL-2 secretion was elevated in both TnT-TCR_{1G4} and TnT-TCR_{DMF5} relative to TnT-TCR_{DMF4}. Overall, our results show that strong binding avidity is not required for antigen-induced expression of NFAT-GFP and CD69 in TnT-TCR cells, thus enabling high-sensitivity functional selections by means of flow cytometry.

TCRs have divergent sequence landscapes for antigen binding versus antigen-induced activity

In contrast to previous TCR engineering platforms (Kieke et al., 1999; Li et al., 2005), TnT cells allow for the assessment of TCRs across multiple parameters, including surface expression with CD3, binding to peptide-MHC multimers and activation in response to antigen presentation. We selected the MART-1-specific TCR_{DMF4} and the MAGE-A3-specific TCR_{A3} for mutational profiling (Figure 3A; Table S1). TCR_{A3} is a low-avidity TCR isolated from a melanoma patient treated with a viral vaccine encoding the HLA-A*0101-restricted MAGE-A3_{168–176}

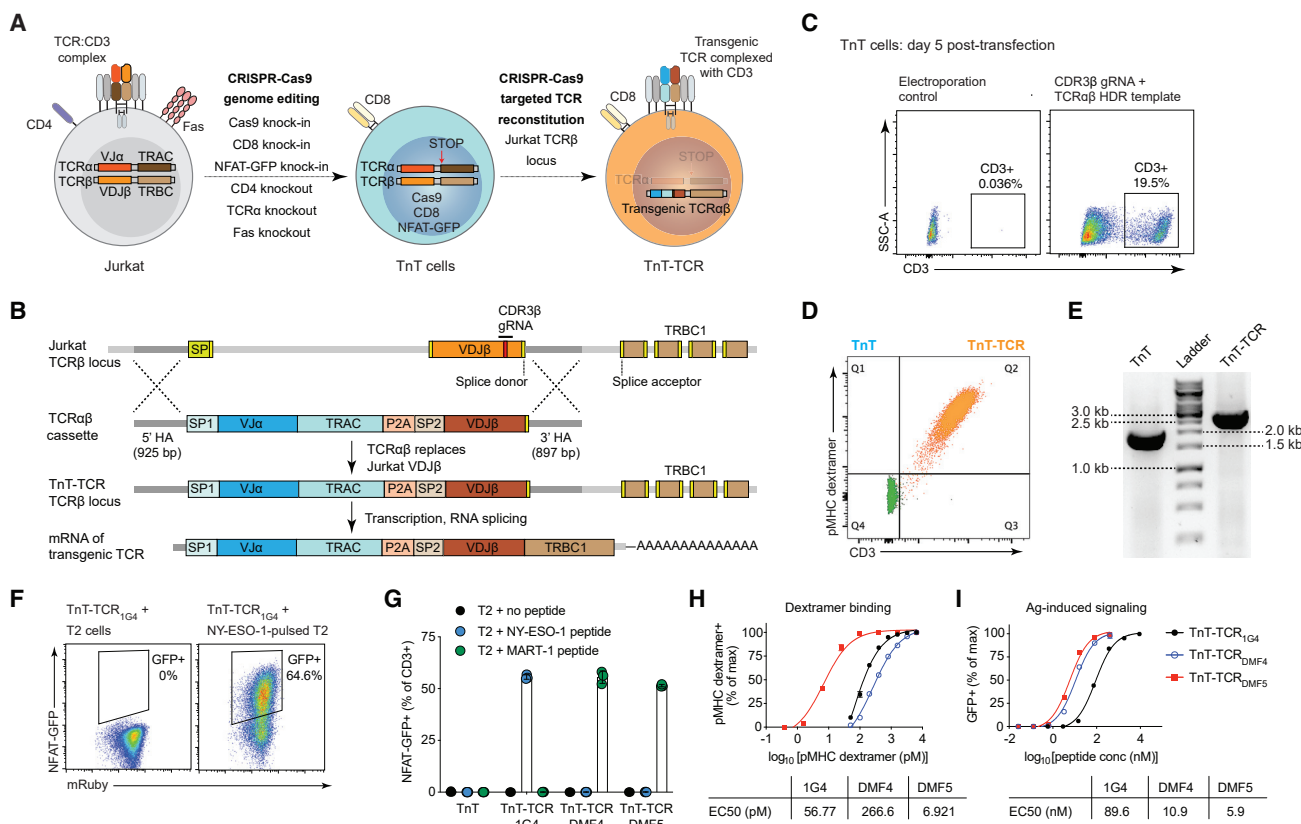


Figure 2. The TnT platform supports targeted reconstitution and functional display of transgenic TCRs

(A) The Jurkat E6-1 cell line was subjected to sequential CRISPR-Cas9 genome editing steps to generate the TnT platform. TnT cells constitutively express Cas9 and human CD8, harbor an NFAT-GFP reporter of TCR signaling, and lack expression of CD4, Fas, and endogenous TCR. Reconstitution of TnT cells with transgenic TCRs via CRISPR-Cas9 HDR results in TnT-TCR cells with restored surface expression of the TCR:CD3 complex.

(B) TCR reconstitution of TnT cells targeted to the Jurkat TCRβ locus. An HDR template encoding transgenic TCRαβ chains is integrated into TnT cells via Cas9 and a gRNA targeting the endogenous Jurkat CDR3β sequence. Transgenic TCR expression is dependent on correct RNA splicing with endogenous Jurkat TRBC1.

(C) Flow cytometric assessment of CD3 restoration in TnT cells after their targeted reconstitution with TCR_{1G4} (specific for NY-ESO-1₁₅₇₋₁₆₅ peptide).

(D) Representative flow cytometry plot showing peptide-MHC dextramer binding to TnT cells (no TCR expression) and MART-1-specific TnT-TCR_{DMF5} cells.

(E) Validation of targeted TCR reconstitution in TnT-TCR_{DMF5} cells by genomic PCR of the Jurkat VDJβ region.

(F) Representative flow cytometry dot plots displaying NFAT-driven GFP expression in TnT-TCR_{1G4} cells, but not TnT cells, after overnight co-culture with T2 cells pulsed with NY-ESO-1₁₅₇₋₁₆₄ peptide.

(G) NFAT-GFP expression in TnT and TnT-TCR cells after overnight co-culture with T2 cells pulsed with NY-ESO-1₁₅₇₋₁₆₄, MART-1_{26-35(27L)}, or no peptide.

(H) Serially diluted target peptide-MHC dextramers were used to assess the binding avidities of TnT-TCR_{1G4}, TnT-TCR_{DMF4}, and TnT-TCR_{DMF5} ($n = 3$). Peptide-MHC dextramer concentrations resulting in half-maximal proportions of dextramer positive cells (EC50) were derived from non-linear least squares fits.

(I) Normalized NFAT-GFP expression in TnT-TCR cells after overnight co-culture with T2 cells pulsed with serially diluted cognate peptide ($n = 2$). Peptide pulse concentrations resulting in half-maximal proportions of NFAT-GFP+ cells (EC50) were derived from non-linear least squares fits. Data are displayed as mean \pm SD. Experiments were performed at least twice.

See also Figures S1 and S2.

peptide (EVDPIGHLY) (Connerette et al., 2008; Karanikas et al., 2003). In a previous effort, TCR_{A3} ($K_D \sim 500 \mu\text{M}$) was engineered by phage display to generate TCR_{a3a}, a variant containing four mutations at the CDR2 α region and conferring >200-fold higher affinity to MAGE-A3₁₆₈₋₁₇₆ peptide-MHC (Figure S3A). However, use of TCR_{a3a} in a TCR-T cell clinical trial resulted in fatal cardiac toxicity due to cross-reactivity to a peptide derived from the protein titin expressed in heart and muscle tissue. Consistent with previous findings, we found that TnT-TCR_{A3} cells showed low but detectable binding to MAGE-A3 peptide-MHC dextramer, TnT-TCR_{a3a} cells showed high binding to MAGE-A3 peptide-MHC dextramer, and only

TnT-TCR_{a3a} cells displayed binding to titin peptide-MHC dextramer (Figure S3B). Co-culture experiments with the MAGE-A3-positive EJM myeloma cell line (HLA-A*0101-positive) revealed that the low avidity of TCR_{A3} was not sufficient to induce NFAT-GFP expression in TnT-TCR_{A3} cells, and only a marginal elevation of CD69 was observed (Figure S3C).

We conducted deep mutational scanning (DMS) of the TCR_{A3} CDR3 β region as it is typically enriched for direct contacts to peptide antigen rather than to MHC (Borbulevych et al., 2011). TnT cells reconstituted with DMS libraries and displaying restored TCR-CD3 surface expression were isolated by FACS (SEL 1), expanded, and re-sorted based on binding to cognate

peptide-MHC dextramer (SEL 2A) or activation following co-culture with cells displaying target antigen (SEL 2B) (Figure 3B). Following FACS, deep sequencing was performed to identify TCR variants that were enriched across selection steps. As expected, the mutational landscapes for antigen binding (SEL 2A) and activation (SEL 2B) were more restricted than those seen for TCR-CD3 surface expression (Figures 3C and 3D). In the case of TCR_{A3}, although a similar number of enriched variants in deep sequencing data was observed in binding (SEL 2A) and activation (SEL 2B) selections, there was little correlation between individual variants in the two fractions (Figure 3C). For TCR_{DMF4}, there was a modest correlation between enrichment of individual variants in binding (SEL 2A) and activation (SEL 2B) fractions (Figure 3D). In order to validate our results experimentally, we reconstituted TnT cells with variants showing enrichment above wild-type TCR. Consistent with sequence enrichment data, TCR_{A3} variants S3G, P4L, M6L, and A7V displayed the largest increases in terms of both binding and activation (Figures 3E and 3F), which could not be explained by differences in TCR surface expression (Figure S3D). For TCR_{DMF4} variants, only modest improvements were observed relative to wild type (Figures 3G–3I), namely enhanced binding of variants I2L, E4V, and E4F to MART-1 peptide-MHC dextramer. Notably, TCR_{DMF4} variants I2H and I2L showed similar antigen-induced activation (and TCR surface expression, Figure S3E) despite I2H showing no detectable binding to MART-1 peptide-MHC dextramer, further highlighting the discordance between binding and activation in certain TCRs. Although there was a strong correlation between antigen binding and antigen-induced signaling for TCR_{A3} single mutants ($R^2 = 0.8742$, Figure 3F), this was not the case for TCR_{DMF4} ($R^2 = 0.000098$, Figure 3I), consistent with reports describing better correlations between TCR binding and signaling at lower levels of affinity (TCR_{A3} $\sim 500 \mu\text{M}$, TCR_{DMF4} = $29 \mu\text{M}$) (Tan et al., 2015). Finally, we compared deep sequencing enrichment data with flow cytometry validation data in terms of antigen binding and antigen-induced signaling (Figures S3F–S3I).

TCR-Engine enables engineering of synthetic TCRs with enhanced activity and specificity to tumor antigen

Next, we applied TCR-Engine to the low-avidity TCR_{A3} to enhance its activity and specificity to MAGE-A3. First, we computationally designed a combinatorial library using deep sequencing enrichment data obtained from CDR3 β DMS (Figure 3C), as this allowed us to maximize both library functionality and size for screening in TnT cells (Figure S4) (Mason et al., 2018). The designed TCR_{A3} library (diversity $\sim 2.6 \times 10^5$) was generated by restriction cloning, amplified by PCR and integrated into TnT cells by CRISPR targeting of the TCR β genomic locus (Figure 4A). Resulting TnT-TCR cells were subjected to positive and negative selection steps based on TCR surface expression, binding to peptide-MHC dextramers and activation in response to cell-displayed MAGE-A3 and titin antigens, with deep sequencing performed at every step (Figures 4B–4E).

Different to wild-type TnT-TCR_{A3} cells, a fraction of cells in the TCR_{A3} library displayed robust NFAT-GFP expression after co-culture with MAGE-A3 expressing EJM myeloma cells, thus indicating the presence of TCR_{A3} variants with enhanced activity (Figure 4D). A subset of TnT-TCR cells still expressed NFAT-GFP

in response to titin-pulsed Colo 205 cells despite the exclusion of titin peptide-MHC binders in SEL 2, highlighting once again the presence of TCRs with discordant levels of binding and activation (Figures 4D and 4E). Bioinformatic analysis of the protein sequence space landscape across selections revealed a number of notable trends, including the preference of alanine codons at position CDR3 β -1 for TCR:CD3 expression (SEL 1) and a substantial increase in the frequency of glutamate residues at CDR3 β -6 in SEL 3B (titin activation), suggesting this substitution as a potential determinant of titin cross-reactivity (Figure 4F). A total of 195 unique variants displayed greater than 2-fold enrichment in SEL 3A (MAGE-A3 activation) and were either absent or not enriched in SEL 3B (titin activation) (Table S2). We scored these TCR_{A3} variants based on read frequency and enrichment, which revealed 29 potential candidates, of which we selected 14 for further experimental characterization (Figure 4G; Table S3). All 14 selected TCR_{A3} synthetic (TCR-Engine) variants showed enhanced MAGE-A3 peptide-MHC dextramer binding and, importantly, had low or undetectable binding to titin peptide-MHC dextramer (Figures 4H and 4I). Our results demonstrate the ability to display and functionally screen TCR combinatorial mutagenesis libraries on the surface of TnT cells for the identification of TCR variants with enhanced target recognition.

TCR-Engine variants display high specificity and mediate potent target cell killing

TnT cells provide an attractive platform for functional profiling of TCR specificity and cross-reactivity. We first profiled the previously phage display-engineered TCR_{a3a} with the aim of identifying potential off-targets shared by TCR-Engine TCR_{A3} variants. We used a single-substitution peptide scanning library of MAGE-A3_{168–176} (EVDPIGHLY) antigen, where each individual peptide ($n = 171$ peptide variants) was pulsed on Colo 205 cells (HLA-A*0101-positive, MAGE-A3-negative), and overnight co-cultures were performed with TnT-TCR_{a3a} cells. We next generated peptide sequence space motifs of allowed substitutions at discrete thresholds of activation for TnT-TCR_{a3a} and used them to interrogate the UniProtKB database (Figure 5A; STAR Methods) (Border et al., 2019; Sanderson et al., 2020). The only human peptide with the highest activation threshold (100%) was the target MAGE-A3 peptide, with the second highest activation threshold (88%) being the titin_{24,337–24,345} peptide (ESDPIVAQY) (Figure 5B). We next screened a panel of 11 predicted off-target peptides for validation of TnT-TCR_{a3a} reactivity (Figure 5C). MAGE-A3, MAGE-A6, MAGE-B18, and titin peptides significantly activated TnT-TCR_{a3a} cells, in agreement with a previous report (Cameron et al., 2013). Human peptides derived from the proteins ANR16, CD166, and MRCKA and a HHV8P viral peptide induced significant activation and thus represent previously unreported potential off-targets of TCR_{a3a} (Figures 5D and 5E).

We next used MAGE-A3, titin, and subset of validated TCR_{a3a} off-target peptides to screen the activity of engineered TCR_{A3} variants (Figure S5A). All TnT-TCR_{A3} variants displayed stronger activation to MAGE-A3 target peptide than wild-type TnT-TCR_{A3}, which showed negligible activation. Furthermore, TnT-TCR_{A3–27} and TnT-TCR_{A3–28} were activated by titin-pulsed Colo 205 cells. Although the low response observed in TnT-TCR_{A3–28} cells might be explained by its residual binding to titin peptide-MHC dextramer, the robust activation in TnT-TCR_{A3–27} cells was highly

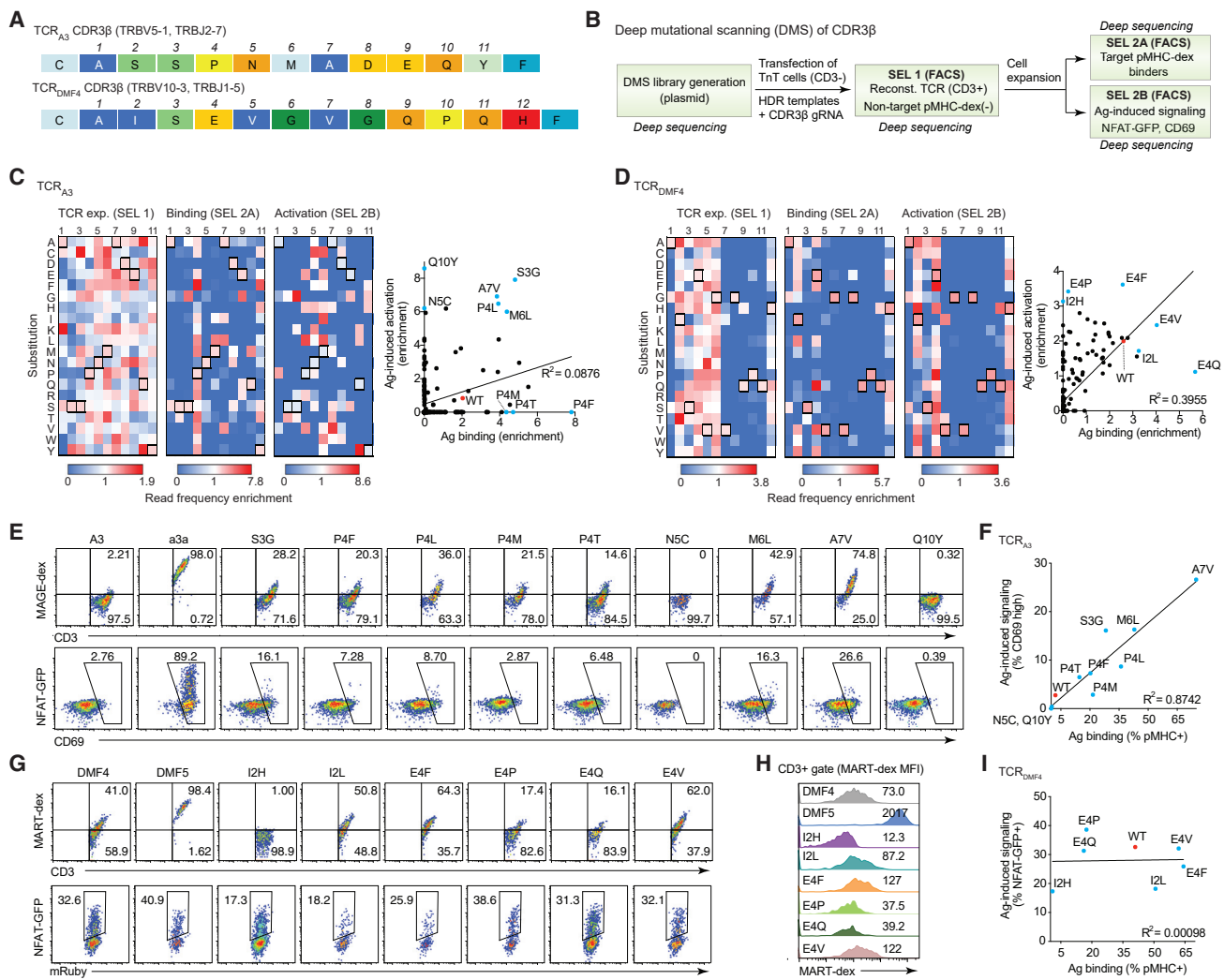


Figure 3. TCRs have divergent sequence landscapes for antigen binding versus antigen-induced activity

- (A) The CDR3 β sequences of TCR_{A3} and TCR_{DMF4} were subjected to deep mutational scanning (DMS).
- (B) DMS libraries were generated by means of plasmid nicking saturation mutagenesis and integrated into TnT cells by Cas9 HDR. Reconstituted cells were selected by FACS based on CD3 surface expression, target peptide-MHC binding, and antigen-induced signaling (co-culture with antigen-presenting cells). Deep sequencing of CDR3 β sequences was performed at every selection step.
- (C and D) Heatmaps display the enrichment of sequencing reads from TCR variants in TCR expression (SEL 1), antigen binding (SEL 2A), and antigen-induced activation (SEL 2B) selections relative to their occurrence in the starting plasmid DMS libraries. (C) shows TCR_{A3} and (D) shows the TCR_{DMF4} variant. Outlined boxes represent wild-type CDR3 β residues. Dot plots display the sequencing read enrichment of individual TCR variants in antigen binding and antigen-induced activation selections. Variants selected for further validation are highlighted in blue, wild-type TCR_{A3}, and wild-type TCR_{DMF4} are highlighted in red. Linear regression analysis is displayed.
- (E) Flow cytometric assessment of antigen binding and antigen-induced activation in TnT cells reconstituted with TCR_{A3}, TCR_{a3a}, and selected TCR_{A3} variants (CD3+ gate). Binding to MAGE-A3 peptide-MHC dextramer (top row) and activation after overnight co-culture with MAGE-A3+ EJM cells (bottom row, proportion CD69^{high} TnT-TCR) are displayed.
- (F) Graph displays antigen binding and antigen-induced activation in TCR_{A3} single mutants relative to wild-type TCR_{A3} (data from E).
- (G-I) Flow cytometric assessment of antigen binding and antigen-induced signaling in TnT cells reconstituted with TCR_{DMF4}, TCR_{DMF5}, and selected TCR_{DMF4} variants (CD3+ gate).
- (G) Binding to MART-1 peptide-MHC dextramer (top row) and activation after overnight co-culture with MART-1-pulsed T2 cells (bottom row, proportion NFAT-GFP+ TnT-TCR) are displayed.
- (H) Histograms displaying the levels of MART-1 peptide-MHC dextramer bound by TnT-TCR cells.
- (I) Graph displays antigen binding and antigen-induced activation in TCR_{DMF4} single mutants relative to wild-type TCR_{DMF4} (data from G). Experiments were performed once.

See also Figure S3.

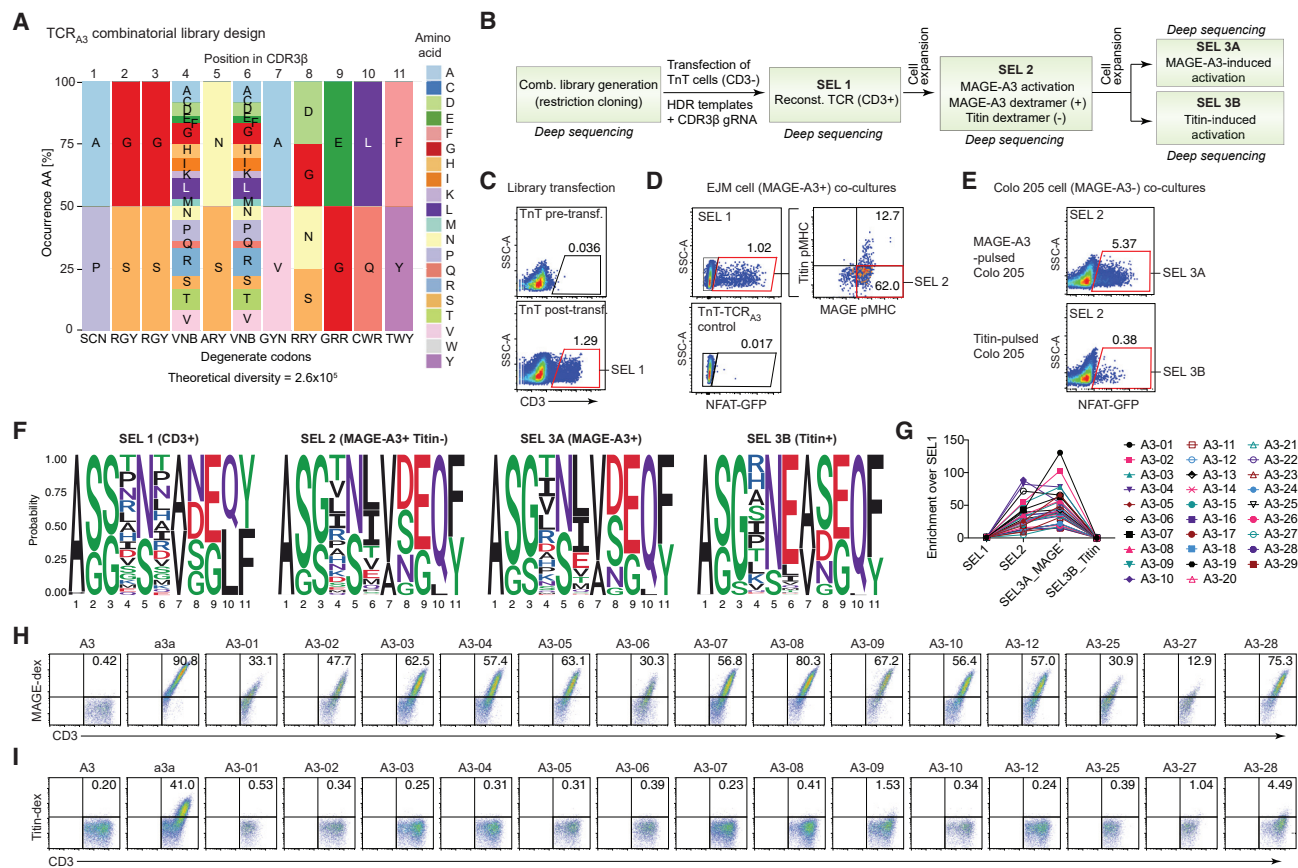


Figure 4. Application of TCR-Engine for engineering synthetic TCRs with enhanced activity and specificity to tumor antigen

(A) Data obtained from TCR_{A3} CDR3 β DMS was utilized as input to design a combinatorial mutagenesis library that has a theoretical diversity of 2.6×10^5 variants. Degenerate codons were designed to recapitulate the amino acid frequencies observed in DMS selections based on MAGE-A3 peptide-MHC dextramer binding and MAGE-A3-induced signaling.

(B) Strategy for the selection of TCR_{A3} combinatorial mutagenesis variants with enhanced recognition of the MAGE-A3₁₆₈₋₁₇₆ peptide (EVDPIGHLY), although avoiding cross-reactivity to the known titin_{24,337-24,345} off-target peptide (ESDPIVAQY). Deep sequencing of CDR3 β sequences was performed at every selection step.

(C) Flow cytometry plots show selection of TCR_{A3} variants from the combinatorial library that are capable of surface expression in TnT cells. TnT cells with restored CD3 surface expression were bulk sorted (SEL 1).

(D) Flow cytometry plots showing TnT-TCR cells (from SEL 1) with positive MAGE-A3-induced signaling (NFAT-GFP+), positive MAGE-A3 peptide-MHC binding, and negative titin peptide-MHC binding; cells were bulk sorted (SEL 2) and expanded in culture ($n = 1$).

(E) Expanded SEL 2 cells were co-cultured overnight with either MAGE-A3 peptide-pulsed or titin peptide-pulsed Colo 205 cells and bulk sorted for activation by NFAT-GFP+ expression (SEL 3A and SEL 3B).

(F) Amino acid sequence logos showing the frequency of specific residues at each CDR3 β position across selections (logos weighted on unique clone frequencies).

(G) TCR_{A3} variants with predicted high specificity for MAGE-A3 and their enrichment across selections based on deep sequencing data. High confidence TCRs ($n = 29$) fulfilled the following criteria: (1) ≥ 2 -fold enrichment SEL3A/SEL1, (2) ≤ 1 -fold enrichment SEL3B/SEL1, and (3) combined frequency rank plus enrichment rank ≤ 202 (arbitrary threshold).

(H and I) Flow cytometry plots of TnT cells reconstituted with TCR_{A3}, TCR_{a3a}, and 14 selected TCR_{A3} combinatorial variants ($n = 1$). Selection criteria (from 29 high confidence pool): top 10 TCRs with highest SEL3A/SEL1 enrichment; 4 test TCRs in which SEL4 reads were detected. Cells were assessed for CD3 expression, MAGE-A3 peptide-MHC binding (H), and titin peptide-MHC binding (I). Cells in the CD3+ gate are shown. Degenerate nucleotide symbols: R = A, G; Y = C, T; S = G, C; W = A, T; K = G, T; M = A, C; B = C, G, T; D = A, G, T; H = A, C, T; V = A, C, G; N = any base. Experiments were performed once.

See also Figures S4 and S5 and Table S3.

unexpected considering its minimal binding to titin peptide-MHC (Figure 4I). These results emphasize that it is insufficient to only measure binding as activation provides a more accurate assessment of TCR specificity and cross-reactivity. Negative selection against titin peptide recognition did not appear to impede the emergence of cross-reactivity against other peptides for some synthetic TCR_{A3} variants. This was clearly the case for

TCR_{A3-09} (cross-reactive to ANR16 and MRCKA) and TCR_{A3-12} (cross-reactive to CD166 and MRCKA), which provide examples of increased cross-reactivity following TCR engineering (Figure S5A). In contrast, we found that TCR_{A3-03}, TCR_{A3-04}, TCR_{A3-05}, TCR_{A3-08}, and TCR_{A3-10} showed low or negligible activation in response to all tested peptides and were thus selected for further analysis (Figure S5A).

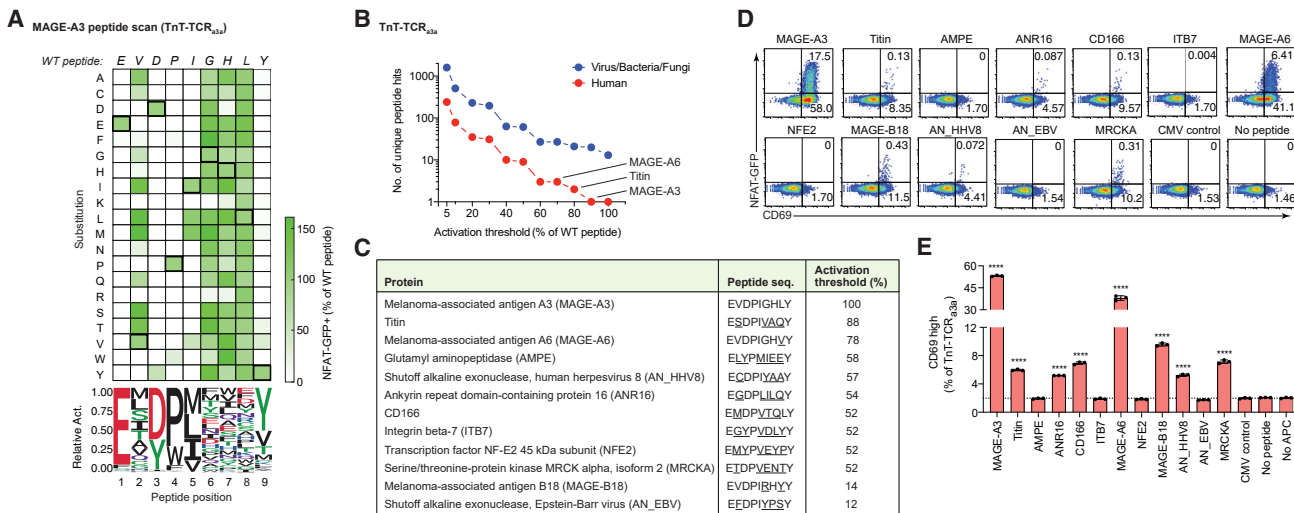


Figure 5. TCR cross-reactivity and off-targets are accurately predicted by activation profiling

(A) The cross-reactivity profile of TnT-TCR_{a3a} cells was assessed using single mutant variants of the wild-type MAGE-A3 peptide (peptide scanning library), which were pulsed on Colo 205 cells for individual co-culture assays (171 peptides). Heatmap shows the proportion of NFAT-GFP-positive TnT-TCR_{a3a} cells after co-culture, as determined by flow cytometry ($n = 1$). Data are normalized to the response induced by the MAGE-A3 wild-type peptide (boxed residues). Sequence logo shows the relative activity of peptide DMS library members carrying mutations at the same peptide position.

(B) The sequences of peptides mediating 5%, 10%, 20%, 30%, 40%, 50%, 60%, 70%, 80%, 90%, and 100% activation relative to the MAGE-A3 wild-type peptide were utilized to generate motifs to query the UniProtKB database. Dot plot displays the number of human (red) and non-human (blue) unique peptide hits resulting from these searches. The first (MAGE-A3), second (titin), and third (MAGE-A6) highest predicted activating peptides are highlighted.

(C) Peptide sequences and maximum activation thresholds of predicted off-targets selected for experimental validation. Differences to the wild-type MAGE-A3 peptide sequence are underlined.

(D) Flow cytometry assessment of CD69 and NFAT-GFP expression following co-culture with peptide-pulsed Colo 205 cells shows cross-reactivity of TnT-TCR_{a3a} cells against a subset of predicted off-target peptides. The CMV peptide (HLA-A⁰¹⁰¹-restricted, VTEHDTLLY) is included as a negative control ($n = 1$).

(E) Bar graph shows repeat of the experiment in (C) performed in triplicate. The percentages of CD69^{high} TnT-TCR_{a3a} cells after co-culture with peptide-pulsed Colo 205 cells were utilized to assess reactivity to each peptide. Dotted line reflects the mean of CMV-pulsed controls ($Y = 1.98$). Asterisks indicate significant differences to CMV controls as determined by two-way ANOVA with Bonferroni post hoc test for multiple comparisons. Data are displayed as mean \pm SD. * $p < 0.05$, ** $p < 0.01$, *** $p < 0.001$, **** $p < 0.0001$, ns, not significant. Experiments were performed once.

We further characterized the activities of selected synthetic TCR_{A3} variants in primary human CD8+ T cells by applying a CRISPR-Cas9 genome editing approach enabling dual knockout of endogenous TCR chains and transgenic TCR integration targeted to the TRAC locus (Figures S5B–S5E) (Roth et al., 2018; Schober et al., 2019). We first co-cultured genome-edited T cells with EJM (MAGE-A3-positive) or Colo 205 cells (MAGE-A3-negative) and assessed their activation by means of IFN- γ enzyme-linked immunosorbent spot (ELISpot) assay (Figure S5F). No significant MAGE-A3-induced activation was observed in T cells transfected with wild-type TCR_{A3}, TCR_{A3-04}, or no TCR. In contrast, T cells expressing TCR_{a3a}, TCR_{A3-03}, TCR_{A3-05}, TCR_{A3-08}, and TCR_{A3-10} were strongly and significantly activated after co-culture with EJM cells. Consistent with our results using TnT-TCR cells, we observed significant TCR_{a3a} cross-reactivity against titin-pulsed Colo 205 cells, whereas titin-induced activation in our synthetic TCR_{A3} variants was either absent or of lower magnitude (Figure S5G). Importantly, primary T cells expressing variants TCR_{A3-03}, TCR_{A3-05}, or TCR_{A3-10} displayed a significant MAGE-A3-induced IFN- γ response but undetectable activation following co-culture with titin-pulsed Colo 205 cells. Furthermore, primary T cells expressing wild-type TCR_{A3} showed a similarly negligible titin-induced activation in this assay. Assessment of TCR cross-reactivity against multiple candidate off-target peptides revealed that pri-

mary T cells expressing TCR_{A3-05} or TCR_{A3-10} displayed high specificity to the MAGE-A3 target peptide, with no other peptide inducing detectable activation (Figure S5H). Next, we expressed soluble versions of TCR variants and performed biolayer interferometry affinity measurements to MAGE-A3 peptide-MHC, which confirmed substantial improvements in the binding affinity of TCR_{A3-05} ($K_D = 6 \mu\text{M}$) and TCR_{A3-10} ($K_D = 10 \mu\text{M}$) relative to parental TCR_{A3} (K_D not determined) and represent affinities in the range of TCRs previously utilized in cell therapy clinical trials (Figure S6) (Borbulevych et al., 2011).

Based on our results, we selected TCR_{A3-05} and TCR_{A3-10} to further characterize using an enhanced peptide scanning assay (see STAR Methods). Specificity profiling of TCR_{a3a}, TCR_{A3-05}, and TCR_{A3-10} revealed that most MAGE-A3 peptide mutations at positions 1, 3, 4, 5, and 9 were detrimental for TnT-TCR_{A3-05} and TnT-TCR_{A3-10} activation (Figure 6A). By contrast, several peptides with mutations at positions 6 and 7, which were mostly activating in TnT-TCR_{a3a} cells, led to substantially reduced activation in TnT-TCR_{A3-05} and TnT-TCR_{A3-10} cells. Of note, the presence of valine at peptide position 6, a substitution present in the titin off-target peptide (ESDPIVAQY), drastically reduced responses in both TnT-TCR_{A3-05} and TCR_{A3-10} (2%–7% of the wild-type MAGE-A3 peptide response), which rationalizes the lack of cross-reactivity of these synthetic TCRs to titin. As a way of comparison, the same peptide induced a response of

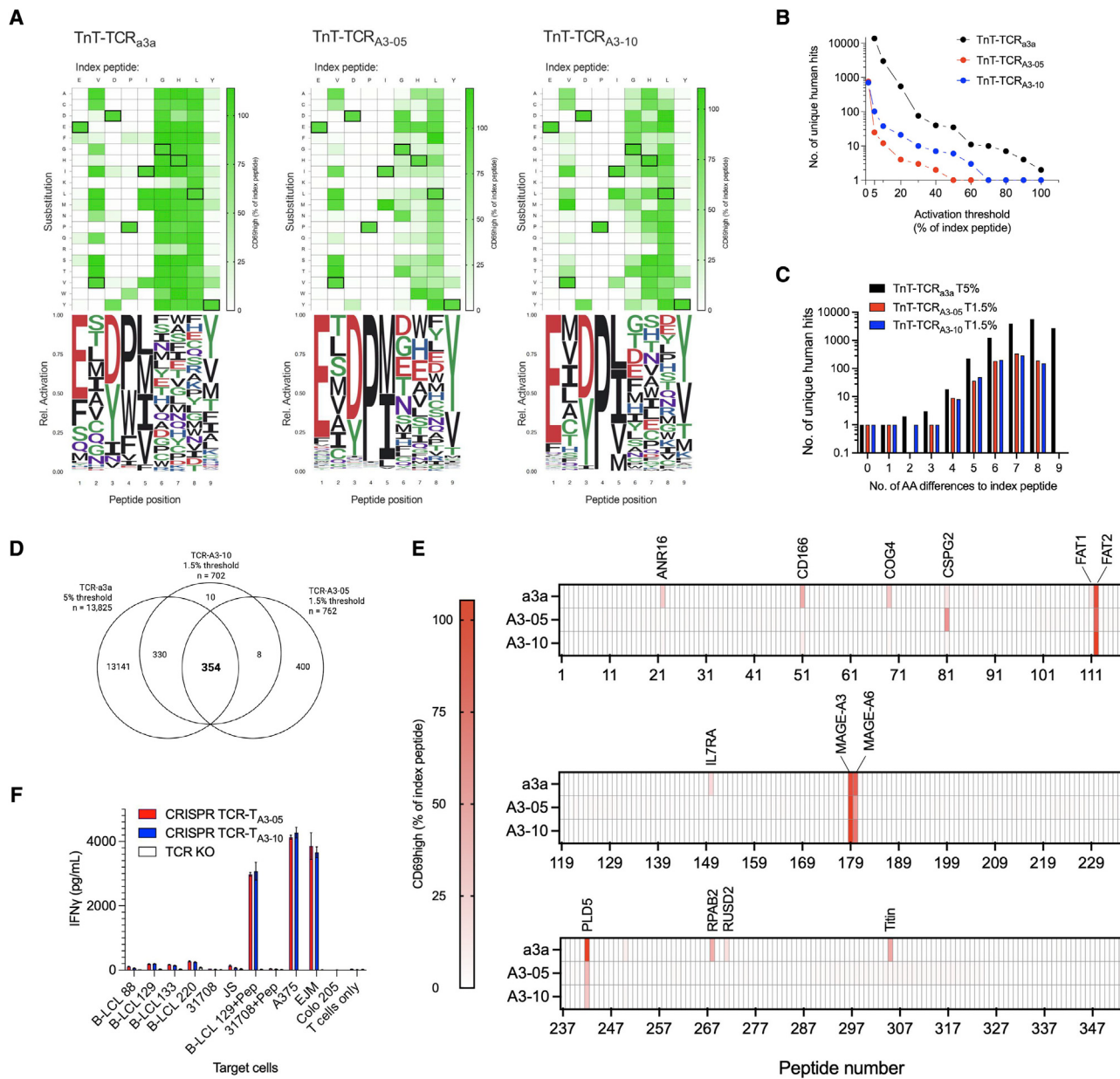


Figure 6. TCR-Engine variants recognizing the MAGE-A3_{168–176} tumor antigen display highly favorable cross-reactivity and alloreactivity profiles

(A) The cross-reactivity profiles of TnT-TCR_{a3a}, TnT-TCR_{A3-05}, and TnT-TCR_{A3-10} cells were assessed by individual co-cultures with IFN- γ pre-treated Colo 205 cells pulsed with single mutant variants (peptide scanning library) of the wild-type MAGE-A3_{168–176} peptide (171 peptides). Heatmaps represent the proportions of CD69^{high} TnT-TCR cells after overnight co-culture, as determined by flow cytometry ($n = 1$). Data are normalized to the response induced by wild-type peptide (boxed residues, $n = 4$). Sequence logos show the relative activity of peptide scanning library members carrying mutations at the same peptide position.

(B) The sequences of peptides mediating 1.5% (TCR_{A3-05} and TCR_{A3-10} only), 5%, 10%, 20%, 30%, 40%, 50%, 60%, 70%, 80%, 90%, and 100% activation relative to wild-type peptide were utilized to generate motifs to query the UniProtKB database. Dot plots display the number of unique human activating peptides resulting from these searches.

(C) The distribution of amino acid differences from the target peptide MAGE-A3_{168–176} in candidate off-target peptides highlights a predominant prediction of highly divergent hits.

(D) Venn diagram illustrating the overlap between predicted candidate off-targets for TCR_{a3a} (5% threshold), TCR_{A3-05} (1.5% threshold), and TCR_{A3-10} (1.5% threshold), highlighting 354 peptides shared by all three TCRs.

(E) The cross-reactivity profiles of TnT-TCR_{a3a}, TnT-TCR_{A3-05}, and TnT-TCR_{A3-10} against a peptide library of 354 shared candidate off-targets were assessed by individual co-cultures with IFN- γ pre-treated, peptide-pulsed Colo 205 cells. Heatmaps represent the proportions of CD69^{high} TnT-TCR cells after overnight co-culture, as determined by flow cytometry. Data are normalized to the response induced by the MAGE-A3_{168–176} peptide for each TnT-TCR line. Highlighted are peptides mediating higher than 10% activation in relative to MAGE-A3_{168–176} target peptide in TnT-TCR_{a3a} cells.

(legend continued on next page)

106% relative to wild-type MAGE-A3 in TnT-TCR_{a3a} cells (see **Figure 6A**), which also led to titin being predicted at the 100% activation threshold (together with MAGE-A3) when using the high sensitivity peptide scanning protocol (**Figure 5B**). The highly sensitive nature of the assay enabled the generation of motifs at extremely low thresholds of TnT-TCR activation (i.e., equivalent to 1.5% activation), thus maximizing the prediction of potential off-targets. Querying of the UniProtKB database with motifs derived from peptide scanning data of TnT-TCR_{a3a} was only possible with a threshold as low as 5% due to a prohibitively large number of predicted hits when using the ScanProsite search tool ($n = 13,825$ unique human hits) (de Castro et al., 2006). By contrast, motifs derived from TnT-TCR_{A3-05} and TnT-TCR_{A3-10} peptide scanning returned only 25 and 102 human hits at the same 5% threshold, respectively (**Figure 6B**). Using the lowest possible threshold of activation of 1.5%, we obtained 762 and 702 human hits for TCR_{A3-05} and TCR_{A3-10}, respectively, still a ~20-fold reduction compared with the number predictions (13,825) for TCR_{a3a}. The majority of candidate off-targets predicted in this analysis had five or more amino acid differences compared with the target peptide MAGE-A3_{168–176}, thus highlighting the ability to predict candidate off-targets that are highly divergent from the intended target (**Figure 6C**). To experimentally validate our predictions, we selected 354 candidate off-targets shared by all three TCRs for screening on Colo205 cells (**Figure 6D; Table S4**). In addition to epitopes derived from MAGE-A6 and titin, TnT-TCR_{a3a} cells responded to additional peptides (i.e., with higher than 10% activity relative to the MAGE-A3_{168–176} target), which included the recently reported off-target FAT2, as well nine additional peptides (ANR16, CD166, COG4, CSPG2, FAT1, IL7RA, PLD5, RPAB2, and RUSD2). Combined with MRCKA and the viral peptide AN_HHV8 (see **Figure 5**), we report eleven potential TCR_{a3a} off-targets in total. In contrast, only three and two off-target peptides in addition to the highly homologous MAGE-A6_{168–176} peptide activated TnT-TCR_{A3-05} and TnT-TCR_{A3-10} cells, respectively (**Figure 6E**).

In addition to cross-reactivity, alloreactivity of TCRs to other HLA alleles also poses a concern for safety. Therefore, we screened for alloreactivity using a panel of human B-LCL lines harboring the seven most common HLA-A alleles across major ethnicities (**Table S5**). CRISPR-edited primary human T cells expressing TCR_{A3-05} and TCR_{A3-10} demonstrated robust T cell activation in response to EJM myeloma cells (HLA-A*0101-positive, MAGE-A3-positive), A375 melanoma cells (HLA-A*0101-positive, MAGE-A3-positive), and MAGE-A3_{168–176}-pulsed 31708 B-LCL cells (HLA-A*0101-positive), but negligible activation in response to any of the tested B-LCL lines or MAGE-A3_{168–176}-pulsed B-LCL-129 cells (HLA-A*0101-negative), indicating that TCR-Engine variants are not alloreactive to the tested HLA class I alleles (**Figure 6F**).

We next determined the potency of TCR-Engine variants in primary human T cells. Experiments using CRISPR-edited TCR-T

cells revealed large and significant improvements in the IFN- γ responses of TCR_{A3-05} and TCR_{A3-10} against both MAGE-A3-pulsed Colo 205 cells (**Figure 7A**) and EJM cells (**Figure 7B**) relative to the parental TCR_{A3-WT}. Despite the low frequencies of transgenic T cells obtained from genome editing (typically 1%–2%, see **Figure S5E**), potent killing of EJM myeloma cells was induced by TCR-T_{A3-05} and TCR-T_{A3-10} cells (E:T ratio approx. 1:6), with cytotoxicity comparable with TCR_{a3a} (**Figure 7C**). Finally, we investigated the translational potential of TCR-Engine variants for TCR-T cell therapy. We generated larger numbers of primary human T cells expressing TCR_{A3-WT}, TCR_{a3a}, TCR_{A3-05}, or TCR_{A3-10} by lentiviral transduction (LV TCR-T cells). We first used LV TCR-T cells to assess cross-reactivity to iPSC-derived beating cardiomyocytes, which express high levels of titin (Cameron et al., 2013). Here, only LV TCR-T_{a3a} cells secreted substantial and significantly higher amounts of IFN- γ than the parental TCR_{A3-WT} in the presence of HLA-A1-transfected cardiomyocytes (**Figure 7D**). Next, we assessed the ability of LV TCR-T cells to target EJM myeloma and A375 melanoma cells for T-cell-mediated killing at multiple effector-to-target ratios. In these experiments, we observed potent killing of target cells by LV TCR-T cells expressing TCR_{A3-05} or TCR_{A3-10}, with TCR_{A3-10} showing marginally higher activity than TCR_{a3a} (**Figure 7E**). Based on this observation, we evaluated the antitumor activity in an A375 melanoma xenogeneic tumor model using immunocompromised NSG mice. In these experiments, a single i.v. infusion of LV TCR-T_{A3-10} cells led to significant reductions in the growth of established A375 tumors and significantly prolonged survival relative to mice treated with untransduced T cells or PBS (**Figure S7**). Finally, LV TCR-T_{A3-10} cells showed a substantial and significant improvement in antitumor activity relative to LV TCR-T cells expressing the parental TCR_{A3-WT}, with similar efficacy to that of LV TCR-T cells expressing the affinity-enhanced TCR_{a3a} previously utilized in the clinic (**Figure 7F**) (Linette et al., 2013). Overall, our results demonstrate the application of TCR-Engine for the identification of synthetic TCR variants with favorable therapeutic properties.

DISCUSSION

Here, we describe the development and application of TCR-Engine, a method enabling functional engineering and cross-reactivity profiling of TCRs. A key component of TCR-Engine is the use of TnT cells, which harbor fully defined genomic changes that facilitate the display and functional screening of transgenic TCRs at high-throughput. As such, TnT cells provide important advantages over alternative TCR engineering platforms that rely exclusively on affinity-based readouts, especially in light of the poor correlation that can exist between TCR affinity and function (Hebeisen et al., 2015; Sibener et al., 2018). Furthermore, TCR reconstitution by CRISPR-Cas9 targeting of the endogenous TCR β locus offers several advantages over plasmid

(F) The alloreactivity profiles of CRISPR-edited T cells expressing TCR_{A3-05}, TCR_{A3-10}, or TCR knockout (KO) was assessed by co-culture with HLA-typed B-LCL lines expressing the most frequently occurring HLA-A alleles across major ethnicities. Co-cultures with EJM myeloma, A375 melanoma and MAGE-A3_{168–176}-pulsed 31708 B-LCL cells are included as positive controls. Co-cultures with MAGE-A3_{168–176}-pulsed B-LCL-129 cells and Colo 205 cells are included as negative controls. 3×10^4 target cells plus 3×10^4 FACS-enriched CRISPR TCR-T cells (TRBV5-1-positive) or TCR KO T cells (CD3-negative) were added into each co-culture well ($n = 3$). Data are displayed as mean \pm SD. Experiments were performed once.

See also **Figure S6**.

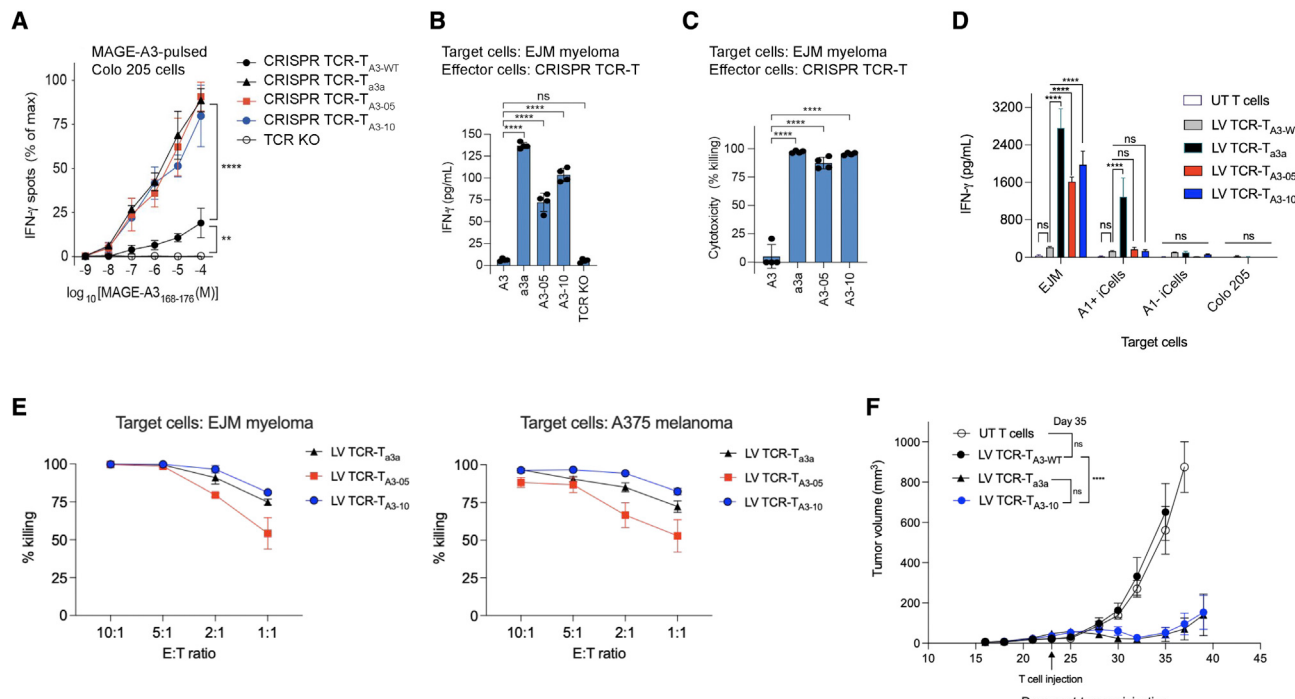


Figure 7. TCR-Engine generates candidates for TCR-T cell therapy of MAGE-A3-positive tumors

(A) Activation of CRISPR-edited CD8+ T cells following overnight co-culture with Colo 205 cells pulsed with serially diluted MAGE-A3_{168–176} target peptide ($n = 3$). 1.25×10^5 T cell transfectants plus 2.5×10^3 Colo 205 cells per well.

(B and C) Activation of CRISPR-edited CD8+ T cells expressing selected TCR_{A3} variants following overnight co-culture with MAGE-A3-positive EJM myeloma cells. 2.5×10^5 T cell transfectants plus 1.5×10^4 EJM cells per well. (B) IFN- γ secretion, as measured by ELISA of harvested supernatants. (C) T cell-mediated killing, as assessed by survival of EJM cells after overnight co-culture with edited CD8+ T cells (normalized to TCR KO response).

(D) Activation of untransduced (UT) or lentivirally transduced (LV) TCR-T cells following overnight co-culture with EJM myeloma cells, iCell beating cardiomyocytes transfected to transiently express HLA-A*0101, untransfected iCell beating cardiomyocytes, or Colo 205 cells, as measured by IFN- γ ELISA. 1×10^5 T cells plus 2×10^4 target cells per well ($n = 3$).

(E) LV TCR-T cell-mediated killing, as assessed by survival of EJM myeloma cells (left panel) and A375 melanoma cells (right panel) after overnight co-culture with LV TCR-T cells ($n = 3$). Target cell survival was assessed by means of flow cytometry and normalized to survival in UT T cell co-cultures at each tested E:T ratio (5×10^4 target cells plus 5×10^4 , 1×10^5 , 2.5×10^5 , or 5×10^5 T cells per well).

(F) The antitumor activity of LV TCR-T_{A3-10} cells was assessed in a xenogeneic A375 melanoma mouse tumor model. NSG mice were injected s.c. in their left flanks with 5×10^6 A375luc2 cells on day 0 ($n = 6–8$), followed by treatment with a single i.v. dose of 1×10^7 UT T cells or 1×10^7 LV TCR-T T cells on day 23. All mice were injected periodically with s.c. injections of recombinant human IL-2 (2.75 μ g per dose) to promote T cell engraftment (dosing schedule described in STAR Methods section). Following treatment, mice were monitored for tumor growth (data displayed as mean \pm SEM). Asterisks indicate significant differences as determined by one-way (A–C) or two-way (D and F) ANOVA with Bonferroni post hoc test for multiple comparisons. Data in (A)–(E) are displayed as mean \pm SD; * $p < 0.05$, ** $p < 0.01$, *** $p < 0.001$, **** $p < 0.0001$, ns, not significant. Experiments were performed once. See also Figure S7.

transfection (Wagner et al., 2019) or viral transduction (Chervin et al., 2008; Karapetyan et al., 2019; Kessels et al., 2000; Malecek et al., 2013; Schmitt et al., 2017; Spindler et al., 2020) such as homogeneous and physiological expression of TCRs and occurrence of a single integration event per cell.

Deep sequencing of original libraries and selections is another important component of the TCR-Engine method as it allows us to accurately determine the enrichment of specific TCR variants across selections. In TCR DMS experiments, we identified several variants that were enriched for antigen binding but not for antigen-induced signaling, and vice versa, which emphasized the discordance between TCR binding affinity and activity. For example, two TCR_{DMF4} variants had nearly identical signaling capacity despite one of them displaying undetectable binding to the MART-1 peptide-MHC dextramer. These results are in agreement with previous reports of peptide-MHC multimers

failing to detect fully functional TCRs (Rius et al., 2018). Crucially, DMS of CDR3 β regions facilitated the computational design of combinatorial libraries encompassing a sequence space enriched for productive TCR variants. This resulted in a 9-log reduction in theoretical library size for TCR_{A3} CDR3 β mutagenesis (from 2×10^{14} to 2.6×10^5 library members), which enabled facile screening in TnT cells.

TnT cells enabled both the engineering and cross-reactivity profiling of TCRs without the need to reformat transgenes for cellular display (Border et al., 2019; Karapetyan et al., 2019; Sanderson et al., 2020) or soluble expression (Gee et al., 2018). By performing mutagenesis of the target MAGE-A3_{168–176} peptide, coupled with a high sensitivity peptide scanning protocol, we predicted and validated known and potential off-targets for the previous clinical candidate TCR_{a3a}. Despite its four amino acid difference to MAGE-A3, the titin peptide

(ESDPIVAQY) alongside the MAGE-A3_{168–176} target were predicted from the activation threshold for TnT-TCR_{a3a}. Furthermore, computationally guided selection of 354 candidate off-target combinatorial peptides and subsequent screening led to the identification of three previously reported (i.e., MAGE-A6, FAT2, and MAGE-B18) and eleven unreported possible off-targets for TCR_{a3a}, thus demonstrating the sensitivity and applicability of our approach for cross-reactivity screening.

TCR-Engine was able to identify variants that displayed high specificity for MAGE-A3, namely TCR_{A3-05} and TCR_{A3-10}, in assays using both TnT-TCR and primary T cells. Functional activation assays in TnT cells with peptide scanning libraries revealed a large reduction in the number of predicted off-targets compared with TCR_{a3a}. Furthermore, screening against a large panel of 354 candidate off-target peptides revealed only three and two potential off-targets for TCR_{A3-05} (FAT2, PLD5, and CSPG2) and TCR_{A3-10} (FAT2 and PLD5), which are shared with TCR_{a3a} and have not been previously highlighted as a source of toxicity. Notably, TCR-Engine offers the possibility to initiate additional engineering campaigns focused on the TCR α chain to remove cross-reactivity against such peptides if found to be problematic.

Finally, we were able to generate compelling proof-of-concept data on the therapeutic potential of TCR-Engine variants. This was achieved through a series of preclinical development assays showing engineered TCRs expressed in primary human T cells: (1) did not display alloreactivity to B-LCL lines expressing highly frequent HLA class I alleles, (2) lacked cross-reactivity to beating cardiomyocytes expressing high levels of titin, (3) demonstrated potent *in vitro* tumor cell killing, and (4) showed significant antitumor activity in a human cell line derived xenograft mouse model.

In summary, here, we develop TCR-Engine for high-throughput engineering and profiling of TCRs on the basis of T cell activation, a method that should greatly accelerate the characterization and development of therapeutic TCRs with improved efficacy and safety profiles.

Limitations of the study

Although we demonstrate that engineering of CDR3 β region was sufficient to generate a promising therapeutic candidate for TCR-T cell therapy, other parental TCRs may require engineering of their TCR α chains to further optimize potency and specificity. This could be particularly important for TCRs recognizing tumor antigens in which there is no prior knowledge of problematic off-targets. In this context, stepwise engineering of TCR β followed by TCR α (or vice versa) provides an attractive strategy to fine-tune TCR potency and specificity having gained insights from the first engineering campaign (e.g., emergence of a previously unknown off-target).

Our approach closely models not only TCR function but also validates surface expression on T cells, which is not possible using other affinity-based platforms such as phage or yeast display. It nevertheless remains a model platform and differences exist between CD69/NFAT-GFP expression in TnT cells and IFN- γ secretion in primary human T cells, which we found overall to be less sensitive for the former. In our study, we were able to largely eliminate this difference by pre-incubating target cells with IFN- γ to increase HLA class I surface expression.

However, the use of primary human T cells will remain a requirement not only for validation purposes but also for formal preclinical development. Since we can also use our method to accurately predict TCR cross-reactivity, TCR-Engine provides a useful tool for the generation of highly de-risked candidates in preparation for resource intensive preclinical development (e.g., screening against large panels of primary human cells and cell lines). In this context, the general applicability of TCR-Engine will be demonstrated in years to come with the generation of additional therapeutic candidates from low-avidity parental TCRs or from TCRs that suffer from safety liabilities.

STAR METHODS

Detailed methods are provided in the online version of this paper and include the following:

- [KEY RESOURCES TABLE](#)
- [RESOURCE AVAILABILITY](#)
 - Lead contact
 - Materials availability
 - Data and code availability
- [EXPERIMENTAL MODEL AND SUBJECT DETAILS](#)
 - Animal studies
 - Cells lines
 - Primary cell cultures
- [METHOD DETAILS](#)
 - Polymerase chain reaction (PCR)
 - Development of TCR-accepting T cells (TnT)
 - Cloning and generation of HDR templates
 - CRISPR-Cas9 genome editing
 - Flow cytometry and FACS
 - Genotyping of cell lines and transfectants
 - Peptides and peptide pulse
 - TnT stimulation and co-culture assays
 - Deep mutational scanning (DMS) library generation
 - DMS library screening and selections
 - Generation of combinatorial TCR_{A3} libraries
 - Combinatorial TCR_{A3} library screening
 - Deep sequencing and analysis of TCR libraries
 - Peptide scanning and off-target validation
 - Primary T cell reconstitution with transgenic TCRs
 - Co-culture of primary T cells and IFN- γ ELISpot
 - Primary T cell cytotoxicity assay
 - B-LCL alloreactivity assay
 - TCR affinity measurements
 - TCR-T cell co-culture with beating cardiomyocytes
 - Xenogeneic A375 melanoma mouse tumor model
- [QUANTIFICATION AND STATISTICAL ANALYSIS](#)

SUPPLEMENTAL INFORMATION

Supplemental information can be found online at <https://doi.org/10.1016/j.immu.2022.09.004>.

ACKNOWLEDGMENTS

We thank Dr. Joseph Taft for his advice on the plasmid nicking mutagenesis method, Darya Palianina for her assistance with ELISpot assays, and Mélanie

Buchi for her assistance with mouse experiments. We thank the ETH Zurich D-BSSE Single-Cell Unit for their assistance with FACS. This study is supported by funding from the Personalized Health and Related Technologies Postdoctoral Fellowship (to R.V.-L.), NCCR Molecular Systems Engineering (to S.T.R.), and Helmut Horten Stiftung (to S.T.R.).

AUTHOR CONTRIBUTIONS

R.V.-L. and S.T.R. designed the study; R.V.-L., J.S.J., F.S.S., A.M., N.R.M., A.Z., H.L., and S.T.R. contributed to experimental design; R.V.-L., J.S.J., F.S.S., A.M., F.B., K.-L.H., E.A., J.K., and E.K. performed experiments; R.V.-L., J.S.J., F.S.S., A.M., N.R.M., F.B., and C.R.W. analyzed data; R.V.-L. and S.T.R. wrote the manuscript with input from all authors.

DECLARATION OF INTERESTS

ETH Zurich has filed for patent protection on the technology and sequences described herein, and R.V.-L., J.S.J., and S.T.R. are named as co-inventors on this patent (WO2021074249A1). R.V.-L and S.T.R. are co-founders and hold shares of Engimmune Therapeutics AG. S.T.R. may hold shares of Alloy Therapeutics. S.T.R. is on the scientific advisory board of Engimmune Therapeutics and Alloy Therapeutics.

Received: May 15, 2022

Revised: August 19, 2022

Accepted: September 2, 2022

Published: September 28, 2022

REFERENCES

- Borbulevych, O.Y., Santhanagopalan, S.M., Hossain, M., and Baker, B.M. (2011). TCRs used in cancer gene therapy cross-react with Mart-1/Melan-A tumor antigens via distinct mechanisms. *J. Immunol.* **187**, 2453–2463.
- Border, E.C., Sanderson, J.P., Weissensteiner, T., Gerry, A.B., and Pumphrey, N.J. (2019). Affinity-enhanced T-cell receptors for adoptive T-cell therapy targeting MAGE-A10: strategy for selection of an optimal candidate. *Oncoimmunology* **8**, e1532759.
- Boulter, J.M., Glick, M., Todorov, P.T., Baston, E., Sami, M., Rizkallah, P., and Jakobsen, B.K. (2003). Stable, soluble T-cell receptor molecules for crystallization and therapeutics. *Protein Eng.* **16**, 707–711.
- Cameron, B.J., Gerry, A.B., Dukes, J., Harper, J.V., Kannan, V., Bianchi, F.C., Grand, F., Brewer, J.E., Gupta, M., Plesa, G., et al. (2013). Identification of a titin-derived HLA-A1-presented peptide as a cross-reactive target for engineered MAGE A3-directed T cells. *Sci. Transl. Med.* **5**, 197ra103.
- Chapuis, A.G., Egan, D.N., Bar, M., Schmitt, T.M., McAfee, M.S., Paulson, K.G., Voillet, V., Gottardo, R., Ragnarsson, G.B., Bleakley, M., et al. (2019). T cell receptor gene therapy targeting WT1 prevents acute myeloid leukemia relapse post-transplant. *Nat. Med.* **25**, 1064–1072.
- Chervin, A.S., Aggen, D.H., Raseman, J.M., and Kranz, D.M. (2008). Engineering higher affinity T cell receptors using a T cell display system. *J. Immunol. Methods* **339**, 175–184. <https://doi.org/10.1016/j.jim.2008.09.016>.
- Connerotte, T., Van Pei, A., Godelaine, D., Tartour, E., Schuler-Thurner, B., Lucas, S., Thielemans, K., Schuler, G., and Coulie, P.G. (2008). Functions of Anti-MAGE T-cells induced in melanoma patients under different vaccination modalities. *Cancer Res.* **68**, 3931–3940.
- de Castro, E., Sigrist, C.J.A., Gattiker, A., Bulliard, V., Langendijk-Genevaux, P.S., Gasteiger, E., Bairoch, A., and Hulo, N. (2006). ScanProsite: detection of PROSITE signature matches and ProRule-associated functional and structural residues in proteins. *Nucleic Acids Res.* **34**, W362–W365.
- Duong, M.N., Erdes, E., Hebeisen, M., and Rufer, N. (2019). Chronic TCR-MHC (self)-interactions limit the functional potential of TCR affinity-increased CD8 T lymphocytes. *J. Immunother. Cancer* **7**, 284.
- Froning, K., Maguire, J., Sereno, A., Huang, F., Chang, S., Weichert, K., Frommelt, A.J., Dong, J., Wu, X., Austin, H., et al. (2020). Computational stabilization of T cell receptors allows pairing with antibodies to form bispecifics. *Nat. Commun.* **11**, 2330.
- Gee, M.H., Han, A., Lofgren, S.M., Beausang, J.F., Mendoza, J.L., Birnbaum, M.E., Bethune, M.T., Fischer, S., Yang, X., Gomez-Eerland, R., et al. (2018). Antigen identification for orphan T cell receptors expressed on tumor-infiltrating lymphocytes. *Cell* **172**, 549–563.e16.
- Hebeisen, M., Allard, M., Gannon, P.O., Schmidt, J., Speiser, D.E., and Rufer, N. (2015). Identifying individual T cell receptors of optimal avidity for tumor antigens. *Front. Immunol.* **6**, 582.
- Hebeisen, M., Baitsch, L., Presotto, D., Baumgaertner, P., Romero, P., Michelin, O., Speiser, D.E., and Rufer, N. (2013). SHP-1 phosphatase activity counteracts increased T cell receptor affinity. *J. Clin. Invest.* **123**, 1044–1056.
- Hockemeyer, D., Soldner, F., Beard, C., Gao, Q., Mitalipova, M., DeKelver, R.C., Katibah, G.E., Amora, R., Boydston, E.A., Zeitler, B., et al. (2009). Efficient targeting of expressed and silent genes in human ESCs and iPSCs using zinc-finger nucleases. *Nature biotechnology* **27**, 851–857.
- Holler, P.D., Chlewicki, L.K., and Kranz, D.M. (2003). TCRs with high affinity for foreign pMHC show self-reactivity. *Nat. Immunol.* **4**, 55–62.
- Jespersen, H., Lindberg, M.F., Donia, M., Söderberg, E.M.V., Andersen, R., Keller, U., Ny, L., Svane, I.M., Nilsson, L.M., and Nilsson, J.A. (2017). Clinical responses to adoptive T-cell transfer can be modeled in an autologous immune-humanized mouse model. *Nat. Commun.* **8**, 707.
- Johnson, L.A., Heemskerk, B., Powell, D.J., Jr., Cohen, C.J., Morgan, R.A., Dudley, M.E., Robbins, P.F., and Rosenberg, S.A. (2006). Gene transfer of tumor-reactive TCR confers both high avidity and tumor reactivity to nonreactive peripheral blood mononuclear cells and tumor-infiltrating lymphocytes. *J. Immunol.* **177**, 6548–6559.
- Johnson, L.A., Morgan, R.A., Dudley, M.E., Cassard, L., Yang, J.C., Hughes, M.S., Kammler, U.S., Royal, R.E., Sherry, R.M., Wunderlich, J.R., et al. (2009). Gene therapy with human and mouse T-cell receptors mediates cancer regression and targets normal tissues expressing cognate antigen. *Blood* **114**, 535–546.
- Karanikas, V., Lurquin, C., Colau, D., van Baren, N., De Smet, C., Lethé, B., Connerotte, T., Corbière, V., Demoitié, M.A., Liénard, D., et al. (2003). Monoclonal anti-MAGE-3 CTL responses in melanoma patients displaying tumor regression after vaccination with a recombinant canarypox virus. *J. Immunol.* **171**, 4898–4904.
- Karapetyan, A.R., Chaipan, C., Winkelbach, K., Wimberger, S., Jeong, J.S., Joshi, B., Stein, R.B., Underwood, D., Castle, J.C., van Dijk, M., and Seibert, V. (2019). TCR fingerprinting and off-target peptide identification. *Front. Immunol.* **10**, 2501.
- Karttunen, J., Sanderson, S., and Shastri, N. (1992). Detection of rare antigen-presenting cells by the lacZ T-cell activation assay suggests an expression cloning strategy for T-cell antigens. *Proc. Natl. Acad. Sci. USA* **89**, 6020–6024.
- Kessels, H.W., van Den Boom, M.D., Spits, H., Hooijberg, E., and Schumacher, T.N. (2000). Changing T cell specificity by retroviral T cell receptor display. *Proc. Natl. Acad. Sci. USA* **97**, 14578–14583.
- Kieke, M.C., Shusta, E.V., Boder, E.T., Teyton, L., Wittrup, K.D., and Kranz, D.M. (1999). Selection of functional T cell receptor mutants from a yeast surface-display library. *Proc. Natl. Acad. Sci. USA* **96**, 5651–5656.
- Li, Y., Moysey, R., Molloy, P.E., Vuidepot, A.-L., Mahon, T., Baston, E., Dunn, S., Liddy, N., Jacob, J., Jakobsen, B.K., and Boulter, J.M. (2005). Directed evolution of human T-cell receptors with picomolar affinities by phage display. *Nat. Biotechnol.* **23**, 349–354.
- Linette, G.P., Stadtmauer, E.A., Maus, M.V., Rapoport, A.P., Levine, B.L., Emery, L., Litzky, L., Bagg, A., Carreno, B.M., Cimino, P.J., et al. (2013). Cardiovascular toxicity and titin cross-reactivity of affinity-enhanced T cells in myeloma and melanoma. *Blood* **122**, 863–871.
- Luft, T., Rizkalla, M., Tai, T.Y., Chen, Q., Macfarlan, R.I., Davis, I.D., Maraskovsky, E., and Cebon, J. (2001). Exogenous peptides presented by transporter associated with antigen processing (TAP)-deficient and TAP-competent cells: intracellular loading and kinetics of presentation. *J. Immunol.* **167**, 2529–2537.
- Malecek, K., Zhong, S., McGary, K., Yu, C., Huang, K., Johnson, L.A., Rosenberg, S.A., and Krosgaard, M. (2013). Engineering improved T cell

- receptors using an alanine-scan guided T cell display selection system. *J. Immunol. Methods* 392, 1–11.
- Mason, D.M., Weber, C.R., Parola, C., Meng, S.M., Greiff, V., Kelton, W.J., and Reddy, S.T. (2018). High-throughput antibody engineering in mammalian cells by CRISPR/Cas9-mediated homology-directed mutagenesis. *Nucleic Acids Res.* 46, 7436–7449.
- Morgan, R.A., Chinnasamy, N., Abate-Daga, D., Gros, A., Robbins, P.F., Zheng, Z., Dudley, M.E., Feldman, S.A., Yang, J.C., Sherry, R.M., et al. (2013). Cancer regression and neurological toxicity following anti-MAGE-A3 TCR gene therapy. *J. Immunother.* 36, 133–151.
- Morgan, R.A., Dudley, M.E., Wunderlich, J.R., Hughes, M.S., Yang, J.C., Sherry, R.M., Royal, R.E., Topalian, S.L., Kammula, U.S., Restifo, N.P., et al. (2006). Cancer regression in patients after transfer of genetically engineered lymphocytes. *Science* 314, 126–129.
- Parkhurst, M.R., Yang, J.C., Langan, R.C., Dudley, M.E., Nathan, D.A., Feldman, S.A., Davis, J.L., Morgan, R.A., Merino, M.J., Sherry, R.M., et al. (2011). T cells targeting carcinoembryonic antigen can mediate regression of metastatic colorectal cancer but induce severe transient colitis. *Mol. Ther.* 19, 620–626.
- Picelli, S., Faridani, O.R., Björklund, A.K., Winberg, G., Sagasser, S., and Sandberg, R. (2014). Full-length RNA-seq from single cells using Smart-seq2. *Nat. Protoc.* 9, 171–181.
- Presotto, D., Erdes, E., Duong, M.N., Allard, M., Regamey, P.-O., Quadrini, M., Doucet, M.-A., Rufer, N., and Hebeisen, M. (2017). Fine-tuning of optimal TCR signaling in tumor redirected CD8 T cells by distinct TCR affinity-mediated mechanisms. *Front. Immunol.* 8, 1564.
- Prommersberger, S., Hudecek, M., and Nerreter, T. (2020). Antibody-based CAR T cells produced by lentiviral transduction. *Curr. Protoc. Immunol.* 128, e93.
- Rapoport, A.P., Stadtmauer, E.A., Binder-Scholl, G.K., Goloubeva, O., Vogl, D.T., Lacey, S.F., Badros, A.Z., Garfall, A., Weiss, B., Finklestein, J., et al. (2015). NY-ESO-1-specific TCR-engineered T cells mediate sustained antigen-specific antitumor effects in myeloma. *Nat. Med.* 21, 914–921.
- Rius, C., Attaf, M., Tungatt, K., Bianchi, V., Legut, M., Bovay, A., Donia, M., Thor Straten, P.T., Peakman, M., Svane, I.M., et al. (2018). Peptide–MHC class I tetramers can fail to detect relevant functional T cell clonotypes and underestimate antigen-reactive T cell populations. *J. Immunol.* 200, 2263–2279. <https://doi.org/10.4049/jimmunol.1700242>.
- Robbins, P.F., Kassim, S.H., Tran, T.L.N., Crystal, J.S., Morgan, R.A., Feldman, S.A., Yang, J.C., Dudley, M.E., Wunderlich, J.R., Sherry, R.M., et al. (2015). A pilot trial using lymphocytes genetically engineered with an NY-ESO-1-reactive T-cell receptor: long-term follow-up and correlates with response. *Clin. Cancer Res.* 21, 1019–1027.
- Roth, T.L., Puig-Saus, C., Yu, R., Shifrut, E., Carnevale, J., Li, P.J., Hiatt, J., Saco, J., Krystofinski, P., Li, H., et al. (2018). Reprogramming human T cell function and specificity with non-viral genome targeting. *Nature* 559, 405–409.
- Sanderson, J.P., Crowley, D.J., Wiedermann, G.E., Quinn, L.L., Crossland, K.L., Tunbridge, H.M., Cornforth, T.V., Barnes, C.S., Ahmed, T., Howe, K., et al. (2020). Preclinical evaluation of an affinity-enhanced MAGE-A4-specific T-cell receptor for adoptive T-cell therapy. *Oncioimmunology* 9, 1682381.
- Sather, B.D., Romano Ibarra, G.S., Sommer, K., Curinga, G., Hale, M., Khan, I.F., Singh, S., Song, Y., Gwiazda, K., Sahni, J., et al. (2015). Efficient modification of CCR5 in primary human hematopoietic cells using a megaTAL nuclease and AAV donor template. *Science translational medicine* 7, 307ra156.
- Schmitt, T.M., Aggen, D.H., Ishida-Tsubota, K., Ochsnerreither, S., Kranz, D.M., and Greenberg, P.D. (2017). Generation of higher affinity T cell receptors by antigen-driven differentiation of progenitor T cells in vitro. *Nat. Biotechnol.* 35, 1188–1195.
- Schober, K., Müller, T.R., Gökmén, F., Grassmann, S., Effenberger, M., Poltorak, M., Stemberger, C., Schumann, K., Roth, T.L., Marson, A., and Busch, D.H. (2019). Orthotopic replacement of T-cell receptor α - and β -chains with preservation of near-physiological T-cell function. *Nat. Biomed. Eng.* 3, 974–984.
- Sibener, L.V., Fernandes, R.A., Kolawole, E.M., Carbone, C.B., Liu, F., McAffee, D., Birnbaum, M.E., Yang, X., Su, L.F., Yu, W., et al. (2018). Isolation of a structural mechanism for uncoupling T cell receptor signaling from peptide-MHC binding. *Cell* 174, 672–687.e27.
- Spindler, M.J., Nelson, A.L., Wagner, E.K., Oppermans, N., Bridgeman, J.S., Heather, J.M., Adler, A.S., Asensio, M.A., Edgar, R.C., Lim, Y.W., et al. (2020). Massively parallel interrogation and mining of natively paired human TCR $\alpha\beta$ repertoires. *Nat. Biotechnol.* 38, 609–619.
- Stadtmauer, E.A., Fraietta, J.A., Davis, M.M., Cohen, A.D., Weber, K.L., Lancaster, E., Mangan, P.A., Kulikovskaya, I., Gupta, M., Chen, F., et al. (2020). CRISPR-engineered T cells in patients with refractory cancer. *Science* 367. <https://doi.org/10.1126/science.aba7365>.
- Strønen, E., Toebe, M., Kelderman, S., van Buuren, M.M., Yang, W., van Rooij, N., Donia, M., Bösch, M.-L., Lund-Johansen, F., Olweus, J., and Schumacher, T.N. (2016). Targeting of cancer neoantigens with donor-derived T cell receptor repertoires. *Science* 352, 1337–1341.
- Tan, M.P., Gerry, A.B., Brewer, J.E., Melchiori, L., Bridgeman, J.S., Bennett, A.D., Pumphrey, N.J., Jakobsen, B.K., Price, D.A., Ladell, K., and Sewell, A.K. (2015). T cell receptor binding affinity governs the functional profile of cancer-specific CD8+ T cells. *Clin. Exp. Immunol.* 180, 255–270.
- Thomas, S., Xue, S.-A., Bangham, C.R.M., Jakobsen, B.K., Morris, E.C., and Stauss, H.J. (2011). Human T cells expressing affinity-matured TCR display accelerated responses but fail to recognize low density of MHC-peptide antigen. *Blood* 118, 319–329. <https://doi.org/10.1182/blood-2010-12-326736>.
- Uttenthal, B.J., Chua, I., Morris, E.C., and Stauss, H.J. (2012). Challenges in T cell receptor gene therapy. *J. Gene Med.* 14, 386–399. <https://doi.org/10.1002/jgm.2637>.
- Vazquez-Lombardi, R., Nevoltris, D., Luthra, A., Schofield, P., Zimmermann, C., and Christ, D. (2018). Transient expression of human antibodies in mammalian cells. *Nat. Protoc.* 13, 99–117.
- Wagih, O. (2017). ggseqlogo: a versatile R package for drawing sequence logos. *Bioinformatics* 33, 3645–3647. <https://doi.org/10.1093/bioinformatics/btx469>.
- Wagner, E.K., Qerqez, A.N., Stevens, C.A., Nguyen, A.W., Delidakis, G., and Maynard, J.A. (2019). Human cytomegalovirus-specific T-cell receptor engineered for high affinity and soluble expression using mammalian cell display. *J. Biol. Chem.* 294, 5790–5804.
- Wrenbeck, E.E., Klesmith, J.R., Stapleton, J.A., Adeniran, A., Tyo, K.E.J., and Whitehead, T.A. (2016). Plasmid-based one-pot saturation mutagenesis. *Nat. Methods* 13, 928–930.
- Zhao, X., Kolawole, E.M., Chan, W., Feng, Y., Yang, X., Gee, M.H., Jude, K.M., Sibener, L.V., Fordyce, P.M., Germain, R.N., et al. (2022). Tuning T cell receptor sensitivity through catch bond engineering. *Science* 376, eabl5282.

STAR★METHODS

KEY RESOURCES TABLE

REAGENT or RESOURCE	SOURCE	IDENTIFIER
Antibodies		
PE-Cy7-conjugated anti-human CD3e (clone UCHT1)	BioLegend	RRID:AB_439781
APC-conjugated anti-human CD3e (clone UCHT1)	BioLegend	RRID:AB_2564151
APC-conjugated anti-human CD4 (clone RPA-T4)	BioLegend	RRID:AB_2564153
PE-conjugated anti-human CD8a (clone HIT8a)	BioLegend	RRID:AB_314112
PE-Cy7-conjugated anti-human CD19 (clone HIB19)	BioLegend	RRID:AB_314246
APC-conjugated anti-human CD69 (clone FN50)	BioLegend	RRID:AB_314845
APC-conjugated anti-human Fas (clone DX2)	BioLegend	RRID:AB_314549
PE-conjugated anti-human TCR α/β (clone IP26)	BioLegend	RRID:AB_314645
TruStain FcX	BioLegend	Cat#422301
NY-ESO-1 peptide-MHC dextramer (SLLMWITQC, HLA-A*0201)	Immudex	Cat#WB2696-APC
MART-1 peptide-MHC dextramer (ELAGIGILTV, HLA-A*0201)	Immudex	Cat#WB2162-APC
MAGE-A3 peptide-MHC dextramer (EVDPIGHLY, HLA-A*0101)	Immudex	Cat#WA3249-PE
Titin peptide-MHC dextramer (ESDPIVAQY, HLA-A*0101)	Immudex	Custom-made
Anti-human CD3e antibody (clone OKT3)	BioLegend	RRID:AB_11150592
Anti-human CD28 antibody (clone CD28.2)	BioLegend	RRID:AB_11150591
Biotinylated MAGE-A3 peptide-MHC class I monomers	BioLegend	Cat#280013
Bacterial and virus strains		
E. coli DH5 α cells	NEB	Cat#C2987H
E. coli DH5 α cells	NEB	Cat#C2987I
Large Scale Lentivirus Production 2nd Generation Strain	Vigene Biosciences	Custom-made
Biological samples		
Human peripheral blood mononuclear cells	Stemcell Technologies	Cat#70025
Chemicals, peptides, and recombinant proteins		
High-glucose DMEM	Thermo Fisher	Cat#10566016
RPMI-1640	Thermo Fisher	Cat#A1049101
ATCC-modified RPMI-1640	Thermo Fisher	Cat#11875093
IMDM	Thermo Fisher	Cat#12440053
Ultra-low IgG Fetal bovine serum	Gibco	Cat#16250-078
Penicillin/Streptomycin	Gibco	Cat#15140-122
Blasticidin	Sigma Aldrich	Cat#15205
TrypLE	Thermo Fisher	Cat#12605010
SpCas9	IDT	Cat#1081059
Alt-R HDR enhancer	IDT	Cat#1081073
DAPI viability dye	Thermo Fisher	Cat#62248
QuickExtract	Lucigen	Cat#0905T
TRIZol	Invitrogen	Cat#15596018
RiboLock RNase inhibitor	Thermo Fisher	Cat#EO0381
Maxima H-minus reverse transcriptase	Thermo Fisher	Cat#EP0751
Custom peptide synthesis	Genscript	N/A
eBioscience Cell Stimulation Cocktail (81 nM PMA, 1.34 μ M ionomycin)	Thermo Fisher	Cat#00497093
soluble PHA	Invivogen	Cat#inh-phap

(Continued on next page)

Continued

REAGENT or RESOURCE	SOURCE	IDENTIFIER
MHC I-Strep HLA-A*0101; CMV pp50 (VTEHDLLY)	IBA	Cat#6-7024-001
recombinant human IFN- γ	Peprotech	Cat#300-02
recombinant human IL-2	Peprotech	Cat#200-02
anti-CD3/anti-CD28 tetrameric antibody complexes	Stemcell Technologies	Cat#10971
Human T Activator Dynabeads	Thermo Fisher	Cat#11131D
TMB substrate	Mabtech	Cat#3651-10
Calibrite beads	BD	Cat#349502
eFluor780 fixable viability dye	Thermo Fisher	Cat#65-0865-14
TALON metal affinity resin	Takara	Cat#635502
OptiMEM reduced serum media	Thermo Fisher	Cat#31985062
ViaFect Transfection Reagent	Promega	Cat#E4981
recombinant human IL-2, Proleukin	Novartis	N/A
Critical commercial assays		
KAPA HiFi PCR kit with GC buffer	Roche Diagnostics	Cat#07958846001
KAPA2G Fast ReadyMix kit	Sigma Aldrich	Cat#KK5102
QIAquick PCR Purification Kit	Qiagen	Cat#28106
SE Cell Line 4D-Nucleofector X Kit L	Lonza	Cat#V4XC-1024
SE Cell Line 4D-Nucleofector X Kit S	Lonza	Cat#V4XC-1032
PureLink RNA Mini kit	Invitrogen	Cat#12183025
QIAprep Spin Miniprep kit	Qiagen	Cat#27106
EasySep Human CD8+ T Cell Isolation kit	Stemcell Technologies	Cat#17953
P3 Primary Cell 4D-Nucleofector X Kit S	Lonza	Cat#V4XP-3032
Human IFN- γ ELISpot Pair	BD	Cat#551873
96-well ELISpot plates	Millipore	Cat#MSIPS4W10
Human IFN- γ Uncoated ELISA Kit	Thermo Fisher	Cat#88-7316-22
Deposited data		
Raw DMS FASTQ data	This paper	SRA: PRJNA869721, https://www.ncbi.nlm.nih.gov/bioproject/86972
Experimental models: Cell lines		
Human: Jurkat E6-1	ATCC	RRID:CVCL_0367
Human: A375Luc2	ATCC	RRID:CVCL_UR32
Human: T2	DSMZ	RRID:CVCL_2211
Human: EJM	DSMZ	RRID:CVCL_2030
Human: Colo 205	ECACC	RRID:CVCL_0218
Human: B-LCL 88	ECACC	RRID:CVCL_E416
Human: B-LCL 133	ECACC	RRID:CVCL_E347
Human: B-LCL 220	ECACC	RRID:CVCL_E382
Human: B-LCL 31708	ECACC	RRID:CVCL_E444
Human: B-LCL JS	ECACC	RRID:CVCL_E718
Human: B-LCL 129	ECACC	RRID:CVCL_E344
Human: Expi293	Thermo Fisher	Cat#A14527
Human: iCell Cardiomyocytes	Fujifilm CDI	Cat#R1224
Experimental models: Organisms/strains		
Mouse: Immunodeficient male NOD scid gamma (NOD.Cg-Prkdc ^{scid} /Il2rg ^{tm1Wjl} /SzJ)	The Jackson Laboratory	Strain#:005557
Oligonucleotides		
crRNA CCR5: tgacatcaattatacatat	PMID: 26424571	N/A
crRNA AAVS1: gggccactaggacaggat	PMID: 23287722	N/A

(Continued on next page)

Continued

REAGENT or RESOURCE	SOURCE	IDENTIFIER
crRNA CD4: gcactgagggctactacca	This paper	N/A
crRNA TRAC (Jurkat): cagggttctggatatctgt	PMID: 28225754	N/A
crRNA Fas: ttgaaaggcctgcataatcgat	This paper	N/A
crRNA CDR3β: tcgacctgtcggctaacta	This paper	N/A
crRNA TRAC (primary T cells): agagtctctca gctggatca	PMID: 31182835	N/A
crRNA TRBC1/2 (primary T cells): ggagaat gacgagtggacc	PMID: 31182835	N/A
Alt-R tracrRNA	IDT	Cat#1072534
Ultramers	IDT	Custom-made
Recombinant DNA		
Plasmid: pX458	Addgene	Cat#48138
Plasmid: AAVS1_Puro_Tet3G_3xFLAG_Twin_Strep	Addgene	Cat#92099
Plasmid: pGL4.30	Promega	Cat#E8481
Plasmid: pTwist Amp High Copy	Twist Bioscience	N/A
Plasmid: pTwist_CMV_WPRES	Twist Bioscience	N/A
Plasmid: pTwist Lenti SFFV	Twist Bioscience	N/A
Software and algorithms		
FlowJo X	FlowJo, LLC	https://www.flowjo.com/ solutions/flowjo
GraphPad Prism 9.2.0	GraphPad	https://www.graphpad.com/
R 4.1.3	R Core Team	https://cran.r-project.org/bin/ windows/base/old/4.1.3/
R ggplot2 3.3.6	https://doi.org/10.1007/ 978-0-387-98141-3	N/A
R ggseqlogo 0.1	https://doi.org/10.1093/ bioinformatics/btx469	N/A
R Biostrings 2.64.0	https://doi.org/10.18129/ B9.bioc.Biostrings	N/A
R VennDiagram 1.7.3	https://doi.org/10.1186/ 1471-2105-12-35	N/A
Original code	This paper	Github: https://github.com/LSSI-ETH/ Vazquez-Lombardi_2022 , Zenodo: https://doi.org/ 10.5281/zenodo.7006793
ScanProsite	PMID: 16845026	https://prosite.expasy.org/ scanprosite/
Other		
4D-Nucleofector, including LV unit	Lonza	N/A
BD LSRFortessa	BD	N/A
Beckman Coulter CytoFLEX	Beckman-Coulter	N/A
BD FACSAria III	BD	N/A
BD FACSAria Fusion	BD	N/A
AID ELR08 ELISpot reader	Autoimmun Diagnostika	N/A
Octet instrument	ForteBio	N/A

RESOURCE AVAILABILITY

Lead contact

Requests for resources and reagents should be directed to and will be fulfilled by the lead contact, Sai Reddy (sai.reddy@ethz.ch).

Materials availability

Reagents generated in this study will be made available on request, but we may require a completed Materials Transfer Agreement.

Data and code availability

- Raw FASTQ files from deep sequencing that support the findings of this study have been uploaded to SRA (NCBI) and are publicly available as of the date of publication, see [key resources table](#).
- Original code for the DMS analysis and peptide scanning processing has been deposited on Github and Zenodo, see [key resources table](#).
- Any additional information required to reanalyze the data reported in this paper is available from the lead contact upon request.

EXPERIMENTAL MODEL AND SUBJECT DETAILS

Animal studies

NSG mice (*NOD.Cg-Prkdc^{scid}/I2rg^{tm1Wjl}/SzJ*), males 8-12 weeks old, were purchased from the Jackson Laboratory (strain: 005557), bred in-house at the Department of Biomedicine (University of Basel) pathogen-free facility and provided with standard food and water without restriction (License: 1007-2H). All mouse experiments were approved by the local ethics committee (Approval 3036, Basel Stadt, Switzerland) and performed in accordance with the Swiss federal regulations.

Cells lines

The Jurkat leukemia E6-1 T cell line (TIB152) and the A375luc2 cell line (CRL-1619-LUC2) were obtained from the American Type Culture Collection (ATCC); the T2 hybrid cell line (#ACC598) and the EJM multiple myeloma cell line (#ACC560) were obtained from the German Collection of Cell Culture and microorganisms (DSMZ); and the Colo 205 colon adenocarcinoma cell line (#87061208) was obtained from the European Collection of Authenticated Cell Cultures (ECACC). Jurkat cells, engineered TnT cells and Colo 205 cells were cultured in ATCC-modified RPMI-1640 (Thermo Fisher, #A1049101), T2 cells were cultured in RPMI-1640 (Thermo Fisher, #11875093), EJM cells were cultured in IMDM (Thermo Fisher, #12440053). A375luc2 cells were cultured in high-glucose DMEM (Thermo Fisher, #10566016) supplemented with 10% FBS and 8 µg ml⁻¹ blasticidin (Sigma Aldrich, #15205). All media other than A375luc2 media were supplemented with 10% FBS, 50 U ml⁻¹ penicillin and 50 µg ml⁻¹ streptomycin. Detachment of EJM, Colo 205 and A375luc2 adherent cell lines for passaging was performed using the TrypLE reagent (Thermo Fisher, #12605010). All cell lines were cultured at 37 °C, 5% CO₂ in a humidified atmosphere. Jurkat E6-1 (RRID:CVCL_0367) and Colo 205 (RRID:CVCL_0218) cell lines are male. A375luc2 (RRID:CVCL_UR32) and EJM (RRID:CVCL_2030) cell lines are female. The T2 (RRID:CVCL_2211) is a hybrid cell line and thus of unspecified sex.

B-lymphoblastoid cell lines were purchased from the European Collection for (ECACC) and cultured in ATCC-modified RPMI (Thermo Fisher, #A1049101) supplemented with 10% FBS, 50 U ml⁻¹ penicillin and 50 µg ml⁻¹ streptomycin. The B-LCL cell lines 88 (RRID:CVCL_E416), 129 (RRID:CVCL_E344), 133 (RRID:CVCL_E347), 31708 (RRID:CVCL_E444) are female while the cell lines 220 (RRID:CVCL_E382) and JS (RRID:CVCL_E718) are male.

All cell lines were purchased from the vendors specified above, passaged twice, aliquoted and cryopreserved for long term storage. Each aliquot was used for up to 20 passages before discarding. We did not perform authentication of the cell lines.

Primary cell cultures

Human peripheral blood mononuclear cells were purchased from Stemcell Technologies (#70025) and CD8+ T cells isolated using the EasySep Human CD8+ T Cell Isolation kit (Stemcell Technologies, #17953). Primary human CD8+ T cells were cultured for up to 24 days in ATCC-modified RPMI (Thermo Fisher, #A1049101) supplemented with 10% FBS, 10 mM non-essential amino acids, 50 µM 2-mercaptoethanol, 50 U ml⁻¹ penicillin, 50 µg ml⁻¹ streptomycin and freshly added 20 ng ml⁻¹ recombinant human IL-2, (Peprotech, #200-02). According to Stemcell Technologies, donor 1 is Hispanic, male and age 26 while donor 2 is Pacific islander and male.

METHOD DETAILS

Polymerase chain reaction (PCR)

PCRs for cloning, generation of HDR templates, genotyping of mammalian cells, generation of TCR libraries and generation of amplicons for deep sequencing were performed using the KAPA HiFi PCR kit with GC buffer (Roche Diagnostics, #07958846001) and custom designed primers ([Table S6](#)). Annealing temperatures (x) were optimized for each reaction by gradient PCR and cycling conditions were as follows: 95°C for 3 min; 35 cycles of 98°C for 20 s, x°C for 15 s, 72°C for 30 s per kb; final extension 72°C for 1 min per kb. PCRs for genotyping of bacterial colonies after transformation were performed using the KAPA2G Fast ReadyMix kit (Sigma Aldrich, #KK5102) with custom designed primers and the following cycling conditions: 95°C for 3 min; 35 cycles of 95°C for 15 s, 60°C for 15 s, 72°C for 15 s per kb; final extension 72°C for 1 min per kb.

Development of TCR-accepting T cells (TnT)

In the first step, we equipped the Jurkat T cell line with constitutive Cas9 and human CD8 expression by CRISPR-Cas9 HDR targeting the CCR5 safe harbor locus (Sather et al., 2015). This was performed in order to simplify and increase genome editing efficiency (Mason et al., 2018), and to allow screening of CD8+ T cell-derived TCRs recognizing MHC class I-restricted peptides. In line with this, in the second step we knocked out the endogenous Jurkat CD4 co-receptor by CRISPR-Cas9 non-homologous end joining (NHEJ). In the third step, we introduced an NFAT-GFP construct into the AAVS1 safe harbor locus through CRISPR-Cas9 HDR, which provides a fluorescence reporter of TCR signaling and activation. Notably, our design incorporated a promoter-less mRuby cassette that acted as a PPP1R12C gene-trap (Hockemeyer et al., 2009) and served to identify successfully edited cells. In the fourth step, we targeted the endogenous Jurkat TCR α chain for knockout through CRISPR-Cas9 NHEJ, leading to the generation of a cell line with abolished surface expression of the TCR-CD3 complex. In addition to eliminating the possibility of transgenic TCR chains mispairing with the endogenous Jurkat TCR α chain, this approach allows us to use restoration of CD3 surface expression as a selectable marker for successful integration of transgenic TCRs (see Figure 2C). In the final step, we knocked out expression of the Fas cell surface death receptor (Fas) by CRISPR-Cas9 NHEJ with the aim of reducing activation-induced cell death (AICD). This resulting cell line constitutively expresses Cas9, human CD8, and mRuby, harbors an NFAT-GFP reporter of TCR signaling, and lacks expression of CD4, endogenous TCR and Fas, and thus represents the TnT platform used throughout this study. An overview of all genomic changes harboured by TnT cells is shown in Figure 1. The sequences of primers utilized for HDR template generation and clone genotyping are listed in Table S6.

We sought to reconstitute TnT cells with transgenic TCRs in a manner that would allow for monoallelic, homogenous and physiological TCR expression. To this end, we used CRISPR-Cas9 HDR to target integration of TCR transgenes to the recombined Jurkat TCR β locus. First, we confirmed that the Jurkat T cell line expresses a single TCR β chain by performing template-switching RT-PCR and Sanger sequencing (Figures S1A and S1B). We then designed and validated a gRNA molecule targeting the complementarity-determining region 3 (CDR3 β) of the Jurkat TCR β chain (Figure S1C). Since the CDR3 β sequence arises from the allele-independent recombination of V-, D- and J-genes, it provides a genomic target that is both highly specific and monoallelic. Having identified a suitable gRNA, we then proceeded to design TCR $\alpha\beta$ HDR templates for targeted TCR reconstitution in TnT cells. HDR templates contained sequences encoding TCR α variable (V δ) and constant (TRAC) domains, a self-processing T2A peptide and a TCR β variable (VDJ β) domain, flanked by ~900 bp homology arms mapping to the recombined Jurkat TCR β locus (see Figure 2B). During the extensive characterization of TnT cells reconstituted with TCR_{1G4} (NY-ESO-1), TCR_{DMF4} (MART-1) or TCR_{DMF5} (MART-1) using our approach, we confirmed TnT-TCR resistance to AICD (Figure S1G) and physiological down-regulation of surface TCR-CD3 expression with increasing amounts of presented antigen (Figure S1H).

Cloning and generation of HDR templates

DNA for gene-encoding regions and homology regions were generated by gene synthesis (Twist Bioscience) or PCR and introduced into desired plasmid backbones via restriction cloning (Table S7). The following plasmids were used as backbones: pX458 (Addgene, #48138), AAVS1_Puro_Tet3G_3xFLAG_Twin_Strep (Addgene, #92099), pGL4.30 (Promega, #E8481) and pTwist Amp High Copy (Twist Bioscience). Targeted knock-in of Cas9/GFP into the CCR5 locus was performed utilizing circular plasmid DNA as the HDR template. HDR templates for all other targeted knock-in experiments were provided as linear double-stranded DNA (dsDNA) generated by PCR. Prior to transfection, PCR products were column-purified using the QIAquick PCR Purification Kit (Qiagen, #28106). For targeted TCR reconstitution of TnT cells, homology arms flanking the recombined Jurkat TCR β VDJ locus were designed and cloned in pTwist (Twist Bioscience), resulting in pJurTCRB. TCR $\alpha\beta$ cassettes encoding transgenic TCRs were generated by gene synthesis (Twist Bioscience) and cloned into pJurTCRB using naturally occurring XbaI and BsaI restriction sites present within the homology arms. Next, HDR templates were generated by PCR using primer pair RVL-127/128 and PCR products purified prior to transfection. For targeted TCR reconstitution of primary human CD8+ T cells, TCR $\beta\alpha$ cassettes lacking TRAC exons 2-3 and flanked by homology arms mapping to TRAC exon 1 (Schober et al., 2019) were designed and cloned in pTwist (Twist Bioscience). HDR templates were generated by PCR using primer pair RVL-164/165 and PCR products purified prior to transfection.

CRISPR-Cas9 genome editing

Transfection of TnT cells and Jurkat-derived cell lines was performed by electroporation using the 4D-Nucleofector device (Lonza) and the SE cell line kit (Lonza, #V4XC-1024). The day before transfection, cells were seeded at 2.5×10^5 cells ml $^{-1}$ and cultured for 24 h. Prior to transfection, gRNA molecules were assembled by mixing 4 μ L of custom Alt-R crRNA (200 μ M, IDT) with 4 μ L of Alt-R tracrRNA (200 μ M, IDT, #1072534), incubating the mix at 95°C for 5 min and cooling it to room temperature. For transfection of Cas9-negative cell lines, 2 μ L of assembled gRNA molecules were mixed with 2 μ L of recombinant SpCas9 (61 μ M, IDT, #1081059) and incubated for > 10 min at room temperature to generate Cas9 RNP complexes. Immediately prior to transfection, cells were washed twice in PBS and 1×10^6 cells were re-suspended in 100 μ L of SE buffer. 1.5 μ g of HDR template and 7 μ L of assembled gRNA (or 4 μ L of Cas9 RNP complexes) were added to the cell suspension, mixed and transferred into a 1 mL electroporation cuvette. Cells were electroporated using program CK116, topped-up with 1 mL of complete media and rested for 10 min prior to transfer into a 12-well plate. Alt-R HDR enhancer (IDT, #1081073) was added at a 30 μ M final concentration and removed after 16 h of culture by centrifugation. HDR efficiency was assessed by flow cytometry on day 5 post-transfection. For transfections at the 20 μ L scale (Lonza, #V4XC-1032), cell numbers and reagent volumes were reduced 5-fold.

Flow cytometry and FACS

Flow cytometric analysis of cell lines and primary T cells was performed according to standard protocols. The following antibodies were purchased from BioLegend and used at $1 \mu\text{g ml}^{-1}$ in flow cytometry buffer (PBS, 2% FBS, 2 mM EDTA): PE-Cy7-conjugated or APC-conjugated anti-human CD3e (clone UCHT1, #300420 or #300458), APC-conjugated anti-human CD4 (clone RPA-T4, #300552), PE-conjugated anti-human CD8a (clone HIT8a, #300908), PE-Cy7-conjugated anti-human CD19 (clone HIB19, #302216), APC-conjugated anti-human CD69 (clone FN50, #310910), APC-conjugated anti-human Fas (clone DX2, #305611) and PE-conjugated anti-human TCR α/β (clone IP26, #306707). DAPI viability dye (Thermo Fisher, #62248) was added to antibody cocktails at a final concentration of $1 \mu\text{g ml}^{-1}$. Cells were washed once in flow cytometry buffer prior to staining, stained for 20 min on ice and washed twice in flow cytometry buffer before analysis using BD LSRFortessa or Beckman-Coulter CytoFLEX flow cytometers. Blocking of Fc receptors in T2 cells was performed prior to staining using the TruStain FcX reagent (BioLegend, #422301). Staining with peptide-MHC dextramers was performed for 10 min at room temperature (RT), followed by addition of 2X antibody cocktails ($2 \mu\text{g ml}^{-1}$ antibodies, $2 \mu\text{g ml}^{-1}$ DAPI) and incubation for 20 min on ice. The following peptide-MHC dextramers were commercially obtained from Immudex: NY-ESO-1₁₅₇₋₁₆₅ (SLLMWITQC, HLA-A*0201, #WB2696-APC); MART-1_{26-35(27L)} (ELAGIGILTV, HLA-A*0201, #WB2162-APC); MAGE-A3₁₆₈₋₁₇₆ (EVDPIGHLY, HLA-A*0101, #WA3249-PE) and titin_{24,337-24,345} (ESDPIVAQY, HLA-A*0101, custom-made, APC-conjugated). Peptide-MHC dextramers were used at a 3.2 nM final concentration (i.e., 1:10 dilution) for staining, unless indicated otherwise in figure legends. FACS was performed using BD FACSAria III or BD FACSAria Fusion instruments. Single-cell sorts were collected in 96-well flat-bottom plates containing conditioned media and clones were cultured for 2–3 weeks prior to characterization.

Genotyping of cell lines and transfectants

Genomic DNA was extracted from 2×10^5 cells by resuspension in 100 μL of QuickExtract solution (Lucigen, #0905T), incubation at 65°C for 6 min, vortexing for 15 s and incubation at 98°C for 2 min. 5 μL of genomic DNA extract were then used as templates for 25 μL PCR reactions. For genotyping by two-step RT-PCR, RNA from 1×10^5 cells was extracted using the TRIzol reagent (Invitrogen, #15596018) and column-purified using the PureLink RNA Mini kit (Invitrogen, #12183025). For reverse transcription, 100 pmol of oligo dT, 10 nmol of each dNTP, 5 μL RNA and sufficient nuclease-free water for a final 14 μL volume were mixed, incubated at 65°C for 5 min and chilled on ice for 5 min. This was followed by addition of 4 μL of 5X RT buffer, 40 units of RiboLock RNase inhibitor (Thermo Fisher, #EO0381) and 200 units of Maxima H-minus reverse transcriptase (Thermo Fisher, #EP0751) and mixing. In some experiments, 40 pmol of template-switching oligonucleotide (TSO, Table S6) was added for labelling of first-strand cDNA 3' ends (Picelli et al., 2014). Reverse transcription was performed at 50°C for 30 min, followed by inactivation at 85°C for 5 min. 5 μl of the resulting cDNA-containing reverse transcription mixes were then used as templates for 25 μL PCR reactions.

Peptides and peptide pulse

Peptides and peptide libraries were generated by custom peptide synthesis (Genscript), re-suspended at $10 \mu\text{g ml}^{-1}$ in DMSO and placed at -80°C for prolonged storage. For peptide pulsing, T2 cells or Colo 205 cells were harvested and washed twice in serum-free RPMI 1640 (SF-RPMI). Peptides were diluted to $10 \mu\text{g ml}^{-1}$ in SF-RPMI (or to concentrations indicated in figure legends) and the solution was used to re-suspend cells at 1×10^6 cells ml^{-1} . Cells were incubated for 90 min at 37°C, 5% CO₂, washed once with SF-RPMI, re-suspended in complete media and added to co-culture wells (see section below).

TnT stimulation and co-culture assays

For clone screening and assessment of AICD, TnT cells and Jurkat-derived cell lines were stimulated overnight with either $10 \mu\text{g ml}^{-1}$ plate-bound anti-human CD3e antibody (clone OKT3, BioLegend, #317326), 1X eBioscience Cell Stimulation Cocktail (81 nM PMA, 1.34 μM ionomycin; Thermo Fisher, #00497093), or $10 \mu\text{g mL}^{-1}$ soluble PHA (Invivogen, inh-phap). For co-culture experiments, TnT-TCR cells at $\sim 1 \times 10^6$ cells ml^{-1} density were harvested, pelleted by centrifugation and re-suspended in fresh complete media at 1×10^6 cells ml^{-1} . 1×10^5 TnT-TCR cells (100 μL) were seeded in wells of a V-bottom 96-well plate. Antigen-expressing cells (EJM) or peptide-pulsed cells (T2, Colo 205) were adjusted to 1×10^6 cells ml^{-1} in complete media and 5×10^4 cells (50 μL) added to each well. Anti-human CD28 antibody (clone CD28.2, BioLegend, #302933) was added at a final concentration of $1 \mu\text{g ml}^{-1}$ for co-stimulation of all samples (including negative controls) and plates were incubated overnight at 37°C, 5% CO₂. The next day, expression of NFAT-GFP and CD69 in TnT-TCR cells was assessed by flow cytometry. Flow cytometric discrimination between TnT-TCR cells and Colo 205 cells (or EJM cells) was based on side scatter area (SSC-A) and mRuby expression, while discrimination between TnT-TCR cells (CD19-negative) and T2 cells (CD19-positive) was based on CD19 expression.

Deep mutational scanning (DMS) library generation

DMS libraries of the CDR3 β regions of TCR_{A3} and TCR_{DMF4} were generated by plasmid nicking mutagenesis as described by Wrenbeck and colleagues (Wrenbeck et al., 2016). The protocol relies on the presence of a single BbvCI restriction site for sequential targeting with Nt.BbvCI and Nb.BbvCI nickases, digestion of wild-type plasmid and plasmid re-synthesis using mutagenic oligonucleotides. A plus-strand BbvCI restriction site was introduced into the pJutTCRB-TCR_{A3} plasmid by means of PCR and blunt-end ligation, while the endogenous minus-strand BbvCI site present in the TRBV10-3 gene of pJutTCRB-TCR_{DMF4} was targeted. The order of BbvCI nickase digestion was adjusted for each plasmid so that the plus DNA strand was digested first. Mutagenic oligonucleotides were designed using the QuikChange Primer Design online tool (Agilent) and assessed for the presence of secondary

structures using the Oligo Evaluator online tool (Sigma-Aldrich) ([Table S6](#)). Oligonucleotides showing strong potential for forming secondary structures were manually modified to reduce this propensity. After nicking mutagenesis, mutated plasmids were transformed into 100 µL of chemically competent *E. coli* DH5 α cells (NEB, #C2987H) and plated on ampicillin (100 µg mL⁻¹) LB agar in Nunc BioAssay dishes (Sigma-Aldrich, #D4803). Serial dilutions of transformed cells were plated separately to quantify bacterial transformants. Plasmid libraries were purified from bacterial transformants using the QIAprep Spin Miniprep kit (Qiagen, #27106). HDR templates were generated from plasmid libraries by PCR using primer pair RVL-127/128 and column-purified prior to transfection.

DMS library screening and selections

DMS library HDR templates and CDR3B gRNA were used to transfect 1x10⁶ TnT cells. In TCR_{A3} DMS selections, cells with restored CD3 surface expression and no binding to control titin peptide-MHC dextramer were isolated by FACS on day 8 post-transfection (SEL 1). Sorted cells were expanded for 13 days and either stained with MAGE-A3 peptide-MHC dextramer or co-cultured overnight with MAGE-A3-positive EJM cells. Dextramer-positive cells (SEL 2A) and activated CD69^{high} cells (SEL 2B) were then isolated by FACS. In TCR_{DMF4} DMS selections, cells with restored CD3 surface expression and no binding to control NY-ESO-1 peptide-MHC dextramer were isolated by FACS on day 8 post-transfection (SEL 1). Sorted cells were expanded for 13 days and either stained with MART-1 peptide-MHC dextramer or co-cultured overnight with MART-1 peptide-pulsed T2 cells. Dextramer-positive cells (SEL 2A) and activated NFAT-GFP-positive cells (SEL 2B) were then isolated by FACS.

Generation of combinatorial TCR_{A3} libraries

Degenerate codons reflecting the combined CDR3 β amino acid frequencies observed in TCR_{A3} DMS binding and signaling selections (SEL2A+2B) were determined as previously described ([Mason et al., 2018](#)). The library resulting from two iterations of our algorithm was modified to include VNB codons at CDR3 β positions 4 and 6. For library construction, ssDNA oligonucleotides containing a 28 nt complementary overlap were designed and purchased as custom ultramers (IDT, [Table S6](#)). The forward ultramer encoded exclusively wild-type TCR_{A3} codons, while the reverse ultramer contained the reverse complement of both wild-type and library degenerate codons. 200 pmol of each ultramer were mixed and subjected to single-cycle PCR using the following conditions: 95°C for 3 min, 98°C for 20 s, 70°C for 15 s, 72°C for 10 min. The resulting 270 bp dsDNA product was gel-purified (Zymogen, #D4002) and 8 ng were utilized as template for a 200 µL PCR reaction using external primers with the following cycling conditions: 95°C for 3 min; 25 cycles of 98°C for 20 s, 62°C for 15 s, 72°C for 15 s; final extension 72°C for 30 s. The PCR product was column-purified, digested with KpnI and BsaI restriction enzymes, and re-purified. In parallel, the pJurTCRB-TCR_{A3} plasmid was digested with KpnI and BsaI, de-phosphorylated (CIP, NEB, #M0290) and gel-purified. Digested PCR product (112.5 ng) and plasmid (750 ng) were ligated in a 75 µL reaction containing 1X T4 PNK buffer, 1 mM ATP and 3 units of T4 DNA ligase for 2 h at RT (all from NEB). Next, the ligation mix was transformed into 750 µL of chemically competent *E. coli* DH5 α cells (NEB, #C2987I) and plated on ampicillin LB agar in Nunc BioAssay dishes. Quantification of bacterial transformants, purification of plasmid library and generation of HDR templates was performed as described for DMS libraries.

Combinatorial TCR_{A3} library screening

Combinatorial library HDR templates (20 µg) and CDR3B gRNA (10 nmol) were used to transfect 1x10⁸ TnT cells using the 4D-Nucleofector LV unit (Lonza, #AAF-1002L). TnT cells with restored CD3 surface expression were bulk sorted (SEL 1) on day 6 post transfection. SEL 1 cells were expanded for 6 days prior to overnight co-culture with MAGE-A3-positive EJM cells followed by co-staining with MAGE-A3 and titin peptide-MHC dextramers. After co-culture, NFAT-GFP-positive cells displaying positive MAGE-A3 peptide-MHC binding and negative titin peptide-MHC binding were bulk-sorted (SEL 2) and expanded in culture for 12 days. SEL 2 cells were co-cultured overnight with either peptide MAGE-A3-pulsed (MAGE-A3) or titin-pulsed Colo 205 cells. Activated NFAT-GFP-positive cells from MAGE-A3 (SEL 3A) and titin (SEL 3B) co-cultures were bulk-sorted for RNA extraction, RT-PCR and deep sequencing.

Deep sequencing and analysis of TCR libraries

TCR amplicons for deep sequencing of plasmid libraries were generated by PCR using primer pair RVL-144/154, while TCR amplicons for deep sequencing of TnT-TCR selections were generated by two-step RT-PCR using primer pair RVL-144/145. In both cases, PCR was limited to 25 cycles. TCR amplicons were column-purified and deep-sequenced using the Amplicon-EZ service (Genewiz), which includes adaptor/index ligation and paired-end Illumina sequencing (250 cycles) followed by delivery of 50,000 assembled reads per sample with unique sequence identification and abundance analysis. For DMS plasmid libraries and selections, unique sequences with less than ten sequencing reads were excluded from enrichment analysis, as every library member had sequencing reads above this threshold. Sequence enrichment of unique DMS variants was determined by dividing their observed frequencies in SEL 1 (TCR-CD3 expression), SEL 2A (binding) and SEL 2B (signaling) over their plasmid DMS library frequencies, and heatmaps were generated using the GraphPad Prism software. For the TCR_{A3} combinatorial plasmid library and selections, unique clone frequency data was filtered to remove clones containing insertions, deletions or mutations outside CDR3 β . Filtered data was used to generate sequence logos weighted on amino acid frequencies at specific CDR3 β positions using R packages ggseqlogo ([Wagih, 2017](#)) and ggplot2. The frequencies of specific TCR_{A3} variants across selections were identified by merging unique clone datasets using a custom Python script. Sequence enrichment of unique TCR_{A3} combinatorial variants was determined by dividing their

observed frequencies in SEL 2 (MAGE-A3-induced activation and binding), SEL 3A (MAGE-A3-induced activation) and SEL 3B (titin-induced activation) over their SEL 1 (TCR-CD3 expression) frequencies.

Peptide scanning and off-target validation

A peptide scanning library of the target MAGE-A3₁₆₈₋₁₇₆ EVDPIGHLY peptide was designed and generated by custom peptide synthesis (Genscript). Each library member ($n = 171$) was individually pulsed at a 50 $\mu\text{g ml}^{-1}$ concentration on Colo 205 cells for co-culture with TnT-TCR cells ($n = 171$ co-cultures). Co-cultures with MAGE-A3-pulsed ($n = 3$), titin-pulsed ($n = 3$), CMV-pulsed ($n = 6$) peptides and unpulsed ($n = 6$) Colo 205 cells were included as controls. After overnight co-culture, TnT-TCR activation was assessed by NFAT-GFP and CD69 expression by means of flow cytometry. The mean background activation observed in CMV peptide controls (i.e., VTEHDTLLY peptide pulse) was subtracted from all samples and their responses normalized to the mean MAGE-A3 response. In the improved sensitivity protocol, Colo 205 were treated overnight with 200 ng mL^{-1} recombinant human IFN- γ (Peprotech, 300-02) prior to peptide pulsing. Normalized data was used to generate heatmaps (GraphPad Prism), weighted sequence logos (ggseqplot, ggplot2 in R) and peptide sequence motifs of allowed substitutions at discrete activation thresholds (Bioconductor package Biostrings in R). Peptide sequence motifs were then used to query the UniProtKB database (including splice variants) with the ScanProsite online tool. The output of these searches was processed using the Biostrings package in order to compute the number of unique peptide hits. Unique peptide hits shared between TCR_{a3a}, TCR_{A3-05} and TCR_{A3-10} were identified computationally (Bioconductor package Biostrings, and VennDiagram in R), with resulting 354 candidate off-targets synthesized (Genscript) for screening using peptide-pulsed Colo 205 (IFN- γ pre-treated) as target cells and TnT-TCR cells as effectors.

Primary T cell reconstitution with transgenic TCRs

For generation of CRISPR TCR-T cells, T cells were activated with anti-CD3/anti-CD28 tetrameric antibody complexes (Stemcell Technologies, #10971) on days 1 and 13 of culture and expanded every 3-4 days. Transfection of primary T cells with Cas9 RNP complexes and TCR $\beta\alpha$ HDR templates was performed 3-4 days following activation using the 4D-Nucleofector and a 20 μL format P3 Primary Cell kit (Lonza, V4XP-3032). Briefly, 1×10^6 primary CD8+ T cells were transfected with 1 μg of HDR template, 1 μl of TRAC Cas9 RNP complex and 1 μl of TRBC1/2 Cas9 RNP complex using the EO115 electroporation program (Cas9 RNP complexes = 50 μM gRNA, 30.5 μM recombinant SpCas9). For RT-PCR validation of TCR reconstitution, RNA was extracted from 1×10^6 T cells, quantified using a Nanodrop instrument, and 40 ng RNA used as input for reverse transcription. 2 μL of reverse transcription mixes were then utilized as templates for 25 μL PCR reactions.

For generation of lentivirally-transduced TCR-T cells, spinoculation with lentiviral particles packaging a TCR α -P2A-TCR β -T2A-GFP cassette (Vigene Biosciences) was performed on pan-human T cells at 24 hours post-activation with Human T Activator Dynabeads (Thermo Fisher, 11131D) following a previously described protocol (Prommersberger et al., 2020).

Co-culture of primary T cells and IFN- γ ELISpot

IFN- γ ELISpot assays were performed using the Human IFN- γ ELISpot Pair (BD, #551873), 96-well ELISpot plates (Millipore, #MSIPS4W10), Avidin-HRP (Biolegend, #405103) and precipitating TMB substrate (Mabtech, #3651-10). Wells were activated with 15% (v/v) ethanol for 30 s, washed twice with PBS and coated with 5 $\mu\text{g ml}^{-1}$ capture antibody (in PBS) at 4°C overnight (or up to a week). On the day of co-culture (i.e., day 5 post-transfection), wells were washed twice with PBS and blocked with primary T cell media lacking IL-2 (RP10-TC) for > 2 h at 37°C. In parallel, TCR-reconstituted primary CD8+ T cells were rested in the absence IL-2 for 6 h. After resting, T cells were washed and re-suspended in fresh RP10-TC media. A 100 μL volume of cell suspensions containing 5×10^4 to 4×10^5 T cells was then transferred into blocked ELISpot wells, as specified in figure legends. Next, 1.5×10^4 antigen-expressing (EJM) or peptide-pulsed (Colo 205) cells were added into wells in a 50 μL volume of RP10-TC media. Anti-CD28 monoclonal antibody was added into every well at a 1 $\mu\text{g ml}^{-1}$ final concentration and plates were incubated for 20 h at 37°C, 5% CO₂. Following co-culture, cells were removed, and wells washed three times with wash buffer (0.01% (v/v) Tween 20 in PBS). Detection antibody was then added at 2 $\mu\text{g ml}^{-1}$ in dilution buffer (0.5% (v/v) BSA in PBS) followed by 2 h incubation at RT. After incubation, wells were washed three times with wash buffer and 1:2000 avidin-HRP (in dilution buffer) added for 45 min at RT. Wells were washed three times with wash buffer and once in PBS, followed by development with precipitating TMB substrate for 3-10 min at RT. Development was stopped by washing with deionized water and plates were dried for > 24 h in the dark prior to analysis using an AID ELR08 ELISpot reader (Autoimmun Diagnostika).

Primary T cell cytotoxicity assay

TCR-reconstituted primary CD8+ T cells were washed and re-suspended in fresh RP10-TC media. A 100 μL volume of cell suspensions containing 1.25×10^5 T cells was then transferred into wells of a sterile U-bottom 96-well plate. Next, 1.5×10^4 EJM cells (MAGE-A3-positive, HLA-A*0101-positive) were added into wells in a 50 μL volume of RP10-TC media. Anti-CD28 monoclonal antibody (1 $\mu\text{g ml}^{-1}$) and recombinant human IL-2 (20 ng ml^{-1}) were added into every well and cells were incubated for 20 h at 37°C, 5% CO₂. After co-culture, supernatants were harvested by centrifugation and IFN- γ concentration determined by ELISA (Thermo Fisher, #88-7316-22) following manufacturer's instructions. The T cell-mediated cytotoxicity was determined by assessing EJM cell survival after co-culture. Briefly, 2×10^4 Calibrile™ beads (BD, #349502) were added to every sample, followed by washing once in PBS. Samples were resuspended in a 1 $\mu\text{l ml}^{-1}$ dilution of eFluor780 fixable viability dye (in PBS, Thermo Fisher, #65-0865-14) and incubated for 20 min on ice. Cells were washed twice in flow cytometry buffer, Fc γ receptors were blocked for 10 min on ice (TruStain FcX, Biolegend, #

422302), and samples were stained with anti-human CD8 and anti-human CD138 fluorescently labeled monoclonal antibodies for a further 20 min on ice. Samples were washed in flow cytometry buffer and analyzed by flow cytometry. The number of surviving EJM cells (eFluor780-negative, CD8-negative, CD138-positive) in each sample was calculated from the total number of acquired beads. Percentage EJM survival across samples was normalized to the mean number of live EJM cells observed in samples containing TCR KO T cells, which was then transformed into percentage cytotoxicity. For T cell cytotoxicity assays using lentivirally-transduced TCR-T cells as effectors, 5×10^4 EJM myeloma cells or 5×10^4 A375 melanoma cells were seeded in wells of a U-bottom 96-well plate and co-cultured with different amounts of effector T cells in a final 150 μL volume (see figure legends). Following overnight co-culture, EJM (target-specific marker: CD138) and A375 (target-specific marker: HLA-A2) cell survival was assessed by flow cytometry as described above, with normalization relative to control co-cultures with untransduced T cells.

B-LCL alloreactivity assay

CRISPR TCR-T cells were generated as described above and subjected to FACS enrichment in order to obtain pure populations of T cells expressing transgenic A3 TCRs (TRBV5-1-positive) as well as pure populations of negative control TCR knockout T cells (CD3-negative). Following FACS enrichment, 3×10^4 CRISPR TCR-T cells were co-cultured overnight with 3×10^4 B-LCL cells or appropriate positive controls in complete T cell media supplemented with 20 ng ml^{-1} IL-2 and 1 $\mu\text{g ml}^{-1}$ anti-CD28 monoclonal antibody. After co-culture, supernatants were harvested for assessment of IFN- γ secretion by means of ELISA following the manufacturer's instructions (Thermo Fisher, #88-7316-22).

TCR affinity measurements

TCRs were re-formatted for soluble expression as recently described (Froning et al., 2020). Briefly, TRAV and TRBV regions were genetically fused to stabilized constant domains containing the following mutations: T150I, A190T, S139F (in TRAC), and E134K, H139R, D155P, S170D (in TRBC1). An additional interchain disulphide bond was introduced by adding two further mutations (i.e., T166C in TRAC and S173C in TRBC1) (Boulter et al., 2003). Constant regions were truncated at positions C231 (TRAC) and C247 (TRBC1), thus retaining the native disulphide bond. A murine IGKV signal peptide (MVFTPQILGLMLFWISASRG) was used to drive secretion of both TCR chains from separate plasmids, and an N-terminal 8xHis tag was added to the TCR α chain construct to allow for purification. Designed TCR cassettes were generated by gene synthesis and cloned into the mammalian expression vector pTwist_CMV_WPREG (Twist Biosciences). Suspension-adapted HEK293 cells (Expi293, Thermo Fisher) were co-transfected with TCR α and TCR β plasmids and secreted soluble TCRs were purified from culture supernatants using the TALON metal affinity resin (Takara, #635502) as described previously (Vazquez-Lombardi et al., 2018). Biolayer interferometry (BLI) measurements were performed using the Octet instrument (ForteBio). Biotinylated MAGE-A3 peptide-MHC class I monomers (Biolegend, #280013) were loaded onto streptavidin biosensors at 10 $\mu\text{g ml}^{-1}$ for 600 s. Binding curves were obtained using soluble TCRs diluted serially in a 2-fold fashion with 120 s association and 300 s dissociation times. Scatchard plots were generated using the Prism GraphPad software.

TCR-T cell co-culture with beating cardiomyocytes

Cryopreserved cardiomyocytes differentiated from induced pluripotent stem cells (iPSC) were obtained commercially, thawed and cultured as per manufacturer's instructions (Fujifilm CDI, R1224) in 96-well flat-bottom plates pre-coated with 0.1% (v/v) gelatin at 2×10^4 cells per well. Beating activity was confirmed visually using an inverted light microscope as early as 4 days post-thawing. On day 7 post-thawing, beating cardiomyocytes were transfected by lipofection using the ViaFect reagent (Promega, E4981) and a custom designed pTwist_CMV_WPREG mammalian expression plasmid encoding an HLA-A*0101-P2A-BFP gene cassette (Twist Biosciences). Briefly, 8 μg of plasmid DNA were diluted in 800 μL of OptiMEM I reduced serum media (Thermo Fisher, 31985062), sterile-filtered and complexed with 16 μL ViaFect reagent (i.e., a 1:2 DNA:lipofection reagent ratio) for 20 min at RT. Each well was then transfected with a volume corresponding to 7.5 ng of plasmid following manufacturer's instructions (Fujifilm CDI, Application Protocol AP-CMCVIA160719). Transfection efficiency was measured in test wells at 48 hours post-transfection by flow cytometry detection of BFP expression. Co-cultures with LV TCR-T cells were performed at 72 hours post-transfection by addition of 1×10^5 LV TCR-T cells into each well (E:T ratio 5:1) in complete T cell media supplemented with 20 ng ml^{-1} recombinant human IL-2 and 1 $\mu\text{g ml}^{-1}$ anti-CD28 monoclonal antibody. Culture supernatants were harvested following overnight co-culture for assessment of IFN- γ secretion by means of ELISA following manufacturer's instructions (Thermo Fisher, #88-7316-22).

Xenogeneic A375 melanoma mouse tumor model

Immunodeficient male NOD scid gamma (NSG) mice at 6 weeks of age were inoculated subcutaneously (s.c.) with 5×10^6 A375luc2 cells (ATCC, CRL-1619-LUC2) in 200 μL of PBS in their left flanks. Mice were injected intravenously with vehicle (PBS), 1×10^7 untransduced T cells or 1×10^7 LV TCR T cells (injection volume = 200 μL) on days 23-27 as indicated in the figure legends. All mice received s.c. injections of 2.75 μg recombinant human IL-2 (ProleukinTM, Novartis) on the day of T cell injection, the subsequent two days, and on a biweekly basis for the first three weeks of the experiment, as previously described (Jespersen et al., 2017). Following inoculation, tumor volume was monitored every 2-3 days using calipers (tumor volume = length \times width 2 /2) and mice were euthanized if showing considerable weight loss (> 20% of initial body weight), displaying obvious signs of systemic illness or if tumors grew larger than 1500 mm^3 .

QUANTIFICATION AND STATISTICAL ANALYSIS

Data are displayed as mean \pm SEM or mean \pm SD as indicated in the figure legends, (*P<0.05, **P<0.01, ***P<0.001, ****P<0.0001, ns = not significant). Statistical analyses included one-way and two-way analysis of variance with Bonferroni post hoc test for multiple comparisons. EC50 values were derived from non-linear least squares fits. Linear regression analysis was added to enrichment scatter plots. Mouse survival was displayed using Kaplan-Meier plots and compared by the log-rank (Mantel-Cox) test. Data were analyzed using the Prism software (GraphPad).

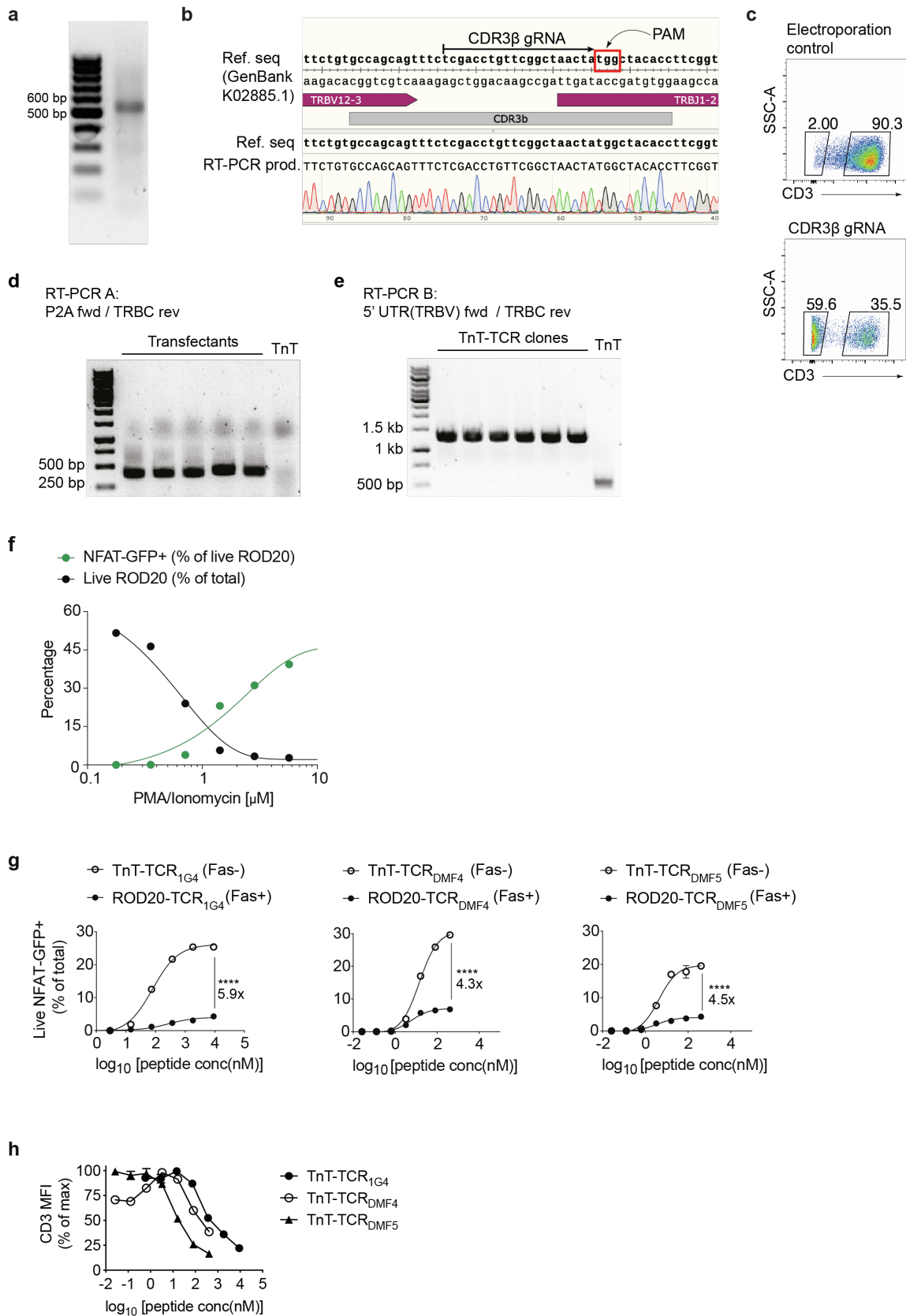
Supplemental information

**High-throughput T cell receptor engineering
by functional screening identifies candidates
with enhanced potency and specificity**

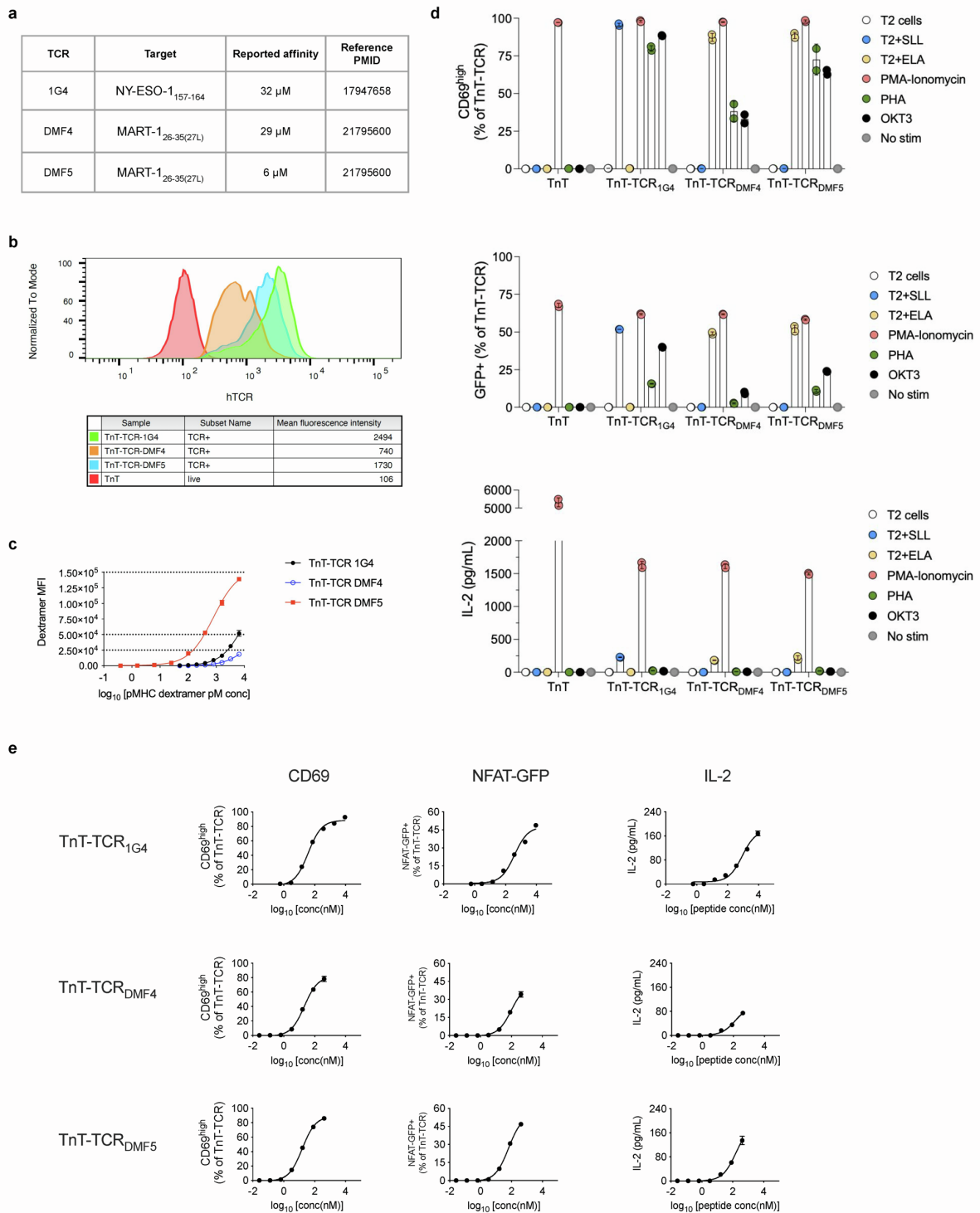
Rodrigo Vazquez-Lombardi, Johanna S. Jung, Fabrice S. Schlatter, Anna Mei, Natalia Rodrigues Mantuano, Florian Bieberich, Kai-Lin Hong, Jakub Kucharczyk, Edo Kapetanovic, Erik Aznauryan, Cédric R. Weber, Alfred Zippelius, Heinz Läubli, and Sai T. Reddy

Supplemental Information

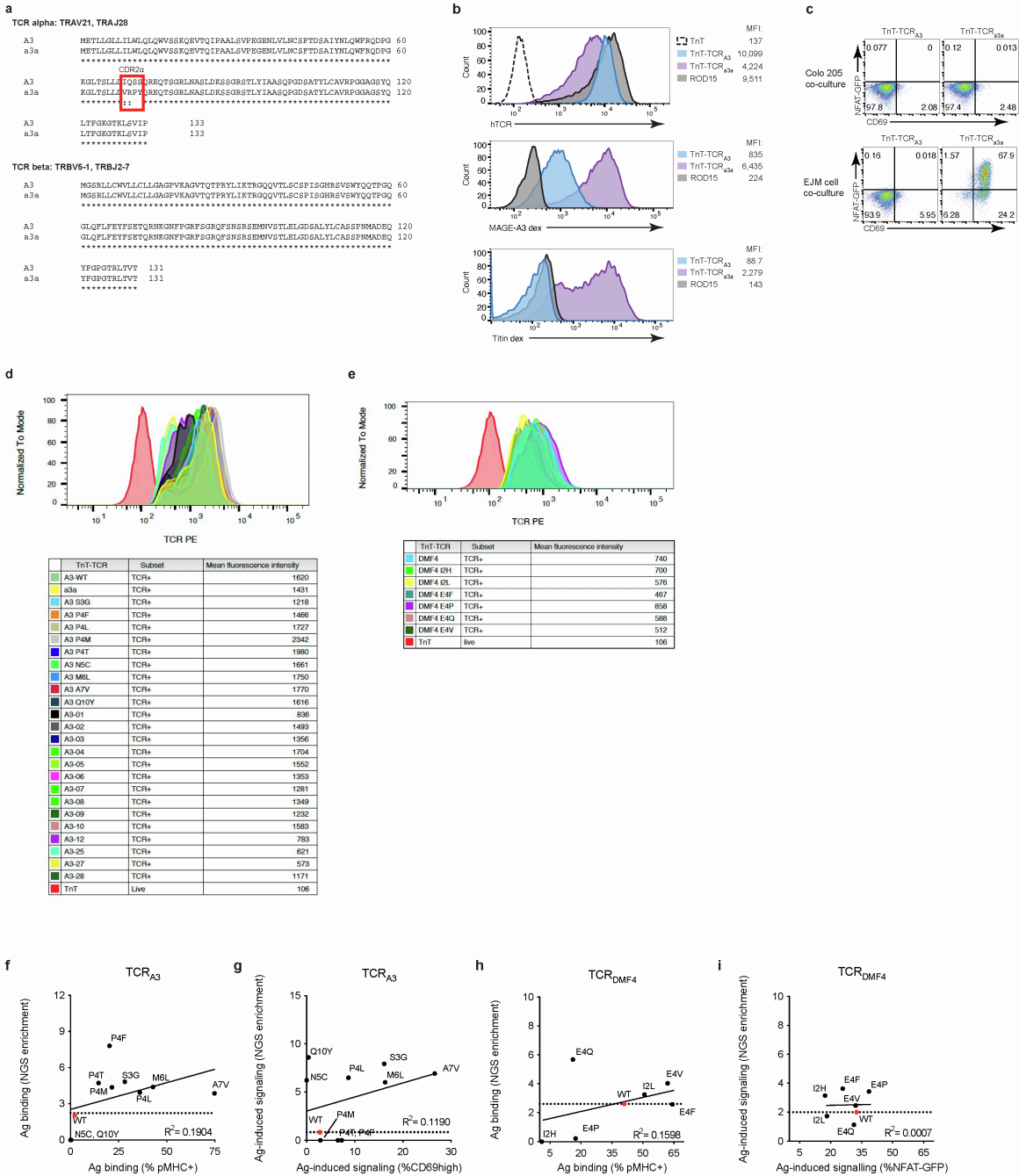
Supplemental Figures 1-7



Supplemental Fig. 1. The recombined Jurkat CDR β 3 sequence is an ideal target for monoallelic and physiological CRISPR-Cas9 TCR reconstitution of AICD-resistant TnT cells, Related to Figures 1 and 2. **a**, PCR amplification of TSO-labelled Jurkat cDNA with ISPCR forward and TRBC1/2 reverse (RVL-68) primers. **b**, Sanger sequencing of the ~ 550 bp band in **(a)** confirmed the expression of a single TCR β chain matching the Jurkat TCR β reference sequence (GenBank K02885.1). The designed CDR3 β gRNA is also displayed. **c**, Flow cytometry shows transfection of Cas9+ Jurkat cells with CDR3 β gRNA results in nearly 60% TCR β knockout efficiency, as measured by surface expression of CD3. **d**, Gel shows results of RT-PCR using a forward primer annealing to the P2A sequence within the TCR $\alpha\beta$ HDR template (RVL-144) and a reverse primer annealing to the endogenous Jurkat TRBC (RVL-145). Untransfected TnT cell samples display no PCR product, while samples derived from TCR transfectants display a 435 bp product consistent with targeted TCR integration and correct splicing with TRBC1. Products from RT-PCR were routinely utilized for deep sequencing of TCR selections (Genewiz Amplicon EZ). **e**, Gel shows results of RT-PCR using a forward primer annealing to the 5' UTR of the recombined Jurkat TCR β VDJ exon (RVL-67c) and a reverse primer annealing to the endogenous Jurkat TRBC (RVL-68). Untransfected TnT cells show a 500 bp band corresponding to the endogenous Jurkat TCR β , while TnT-TCR clones display a unique band at 1.3 kb demonstrating targeted integration of TCR $\alpha\beta$ cassettes and their correct splicing with TRBC1 (see Fig.1b). Sanger sequencing of RT-PCR products was routinely performed for clone validation purposes. **f**, Increased cell death in the ROD20 cell line (Cas9+ CD8+ CD4- mRuby+ NFAT-GFP CD3-) after non-specific stimulation with increasing concentrations of PMA-ionomycin. This increase was inversely correlated to the proportion of NFAT-GFP-positive cells within surviving cells, thus indicating that increased cell death resulted from AICD. **g**, TCR $_{1G4}$, TCR $_{DMF4}$ and TCR $_{DMF5}$ were introduced into ROD20 (Fas+) or TnT (Fas-) cells via CRISPR-Cas9 HDR and co-cultured overnight with T2 cells pulsed with serially-diluted target peptides ($n = 2$). Activated TnT-TCR cells displayed significantly higher proportions of live NFAT-GFP-positive cells relative to ROD20-TCR cells, thus indicating confirming resistance to AICD. **h**, CD3 mean fluorescence intensity (MFI) in TnT-TCR cells expressing TCR $_{1G4}$, TCR $_{DMF4}$ or TCR $_{DMF5}$ after co-culture T2 cells pulsed with serially-diluted target peptides ($n = 2$). Non-linear least squares fits and two-way ANOVA with Bonferroni post hoc test for multiple comparisons are displayed in **(f)**, **** $P < 0.0001$. PAM: protospacer adjacent motif. TSO: template-switching oligonucleotide. Experiments were performed once.

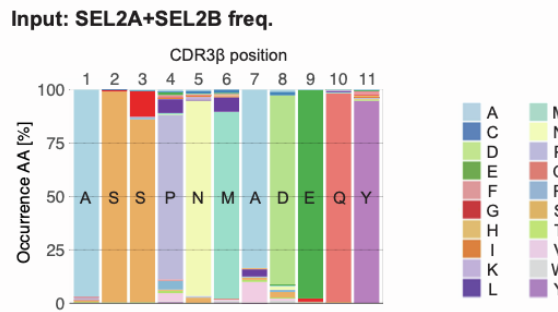


Supplemental Fig. 2. Profiling of TnT-TCR cell activity in response to antigen-dependent and antigen-independent stimulation, Related to Figure 2. **a**, Reported affinity levels of TCR_{1G4}, TCR_{DMF4} and TCR_{DMF5} for their cognate antigens. **b**, Histograms displaying TCR surface expression levels (mean fluorescence intensity) in TnT-TCR cells following CRISPR-targeted reconstitution with TCR_{1G4}, TCR_{DMF4} or TCR_{DMF5}, as assessed by flow cytometry. **c**, Serially diluted target peptide-MHC dextramers were used to assess the binding avidities of TnT-TCR_{1G4}, TnT-TCR_{DMF4} and TnT-TCR_{DMF5} (n = 3). Displayed are the mean fluorescence intensity in the dextramer channel (live TnT-TCR gate) and non-linear least squares fits. **D**, Activation profiling of TnT-TCR_{1G4}, TnT-TCR_{DMF4} and TnT-TCR_{DMF5} following stimulation with soluble PMA/ionomycin, soluble PHA, plate-bound anti-CD3 monoclonal antibody (OKT3), or T2 cells pulsed with NY-ESO-1 (SLL) or MART-1 (ELA) peptides. Shown are the levels of CD69 and NFAT-GFP following stimulation, as assessed by flow cytometry (percent of live TnT-TCR cells), as well as levels of secreted IL-2 as assessed by ELISA (n = 2). **e**, CD69 expression (flow cytometry), NFAT-GFP expression (flow cytometry), and IL-2 secretion (ELISA) levels in TnT-TCR cells after overnight co-culture with T2 cells pulsed with serially diluted cognate peptide (n = 2). Non-linear least squares fits and are shown for each plot. All data are displayed as mean ± SD. Experiments were performed once.



Supplemental Fig. 3. Assessment of TCR expression, antigen binding and antigen-induced signalling in TnT-TCR cells, Related to Figure 3. **a**, Protein sequence alignments of $\text{TCR}_{\text{A}3}$ and its phage display-engineered variant $\text{TCR}_{\text{a}3\alpha}$ (WO2012013913). The four substitutions introduced into the CDR2 α of $\text{TCR}_{\text{a}3\alpha}$ are highlighted in red. **b**, TnT clones expressing $\text{TCR}_{\text{A}3}$ and $\text{TCR}_{\text{a}3\alpha}$ were generated by CRISPR-Cas9 HDR followed by single-cell FACS. Levels of TCR expression (anti-TCR monoclonal antibody clone IP26), MAGE-A3 peptide-MHC dextramer binding and titin peptide-MHC dextramer binding in TnT- $\text{TCR}_{\text{A}3}$, TnT- $\text{TCR}_{\text{a}3\alpha}$ and negative control cell lines are displayed. **c**, Flow cytometry of NFAT-GFP and CD69 expression after overnight co-culture of TnT- $\text{TCR}_{\text{A}3}$ and TnT- $\text{TCR}_{\text{a}3\alpha}$ cells with Colo 205 (HLA-A*0101 MAGE-A3-) and EJM (HLA-A*0101+ MAGE-A3+) cancer cell lines. **d-e**, Histograms display the levels of TCR surface expression in TnT-TCR transfectants as assessed by flow cytometry. Mean fluorescence intensity levels of (d) $\text{TCR}_{\text{A}3}$ variants or (e) $\text{TCR}_{\text{DMF}4}$ variants alongside appropriate positive (i.e., $\text{TCR}_{\text{a}3\alpha}$, $\text{TCR}_{\text{DMF}5}$) and negative controls (TnT) are displayed. **f-i**, Simple linear regression analyses of deep sequencing enrichment data (**Figs. 3c-d**) and flow cytometry validation data (**Figs. 3e and 3g**) derived from selected $\text{TCR}_{\text{A}3}$ and $\text{TCR}_{\text{DMF}4}$ single mutants in terms of antigen binding and antigen-induced signalling. Dotted line represents the wild deep sequencing read enrichment observed for wild-type $\text{TCR}_{\text{A}3}$ or $\text{TCR}_{\text{DMF}4}$.

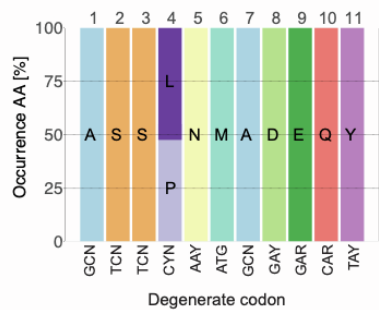
a



b

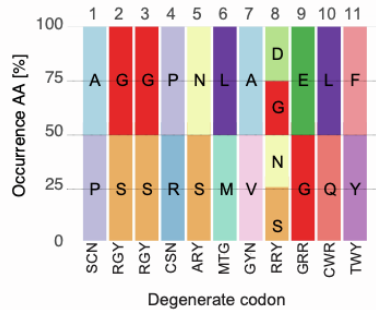
Round 1:

Theoretical diversity = 2



Round 2:

Theoretical diversity = 4,096

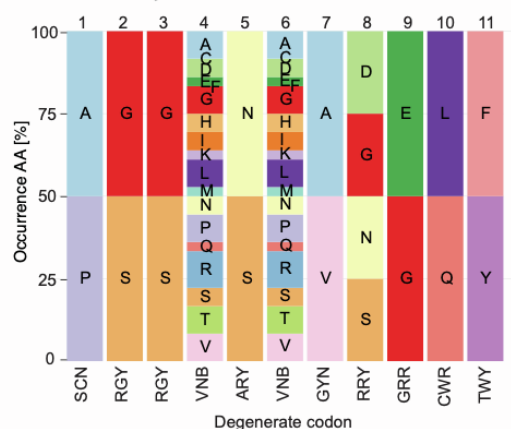


↓
2 x VNB
(positions 4 and 6)

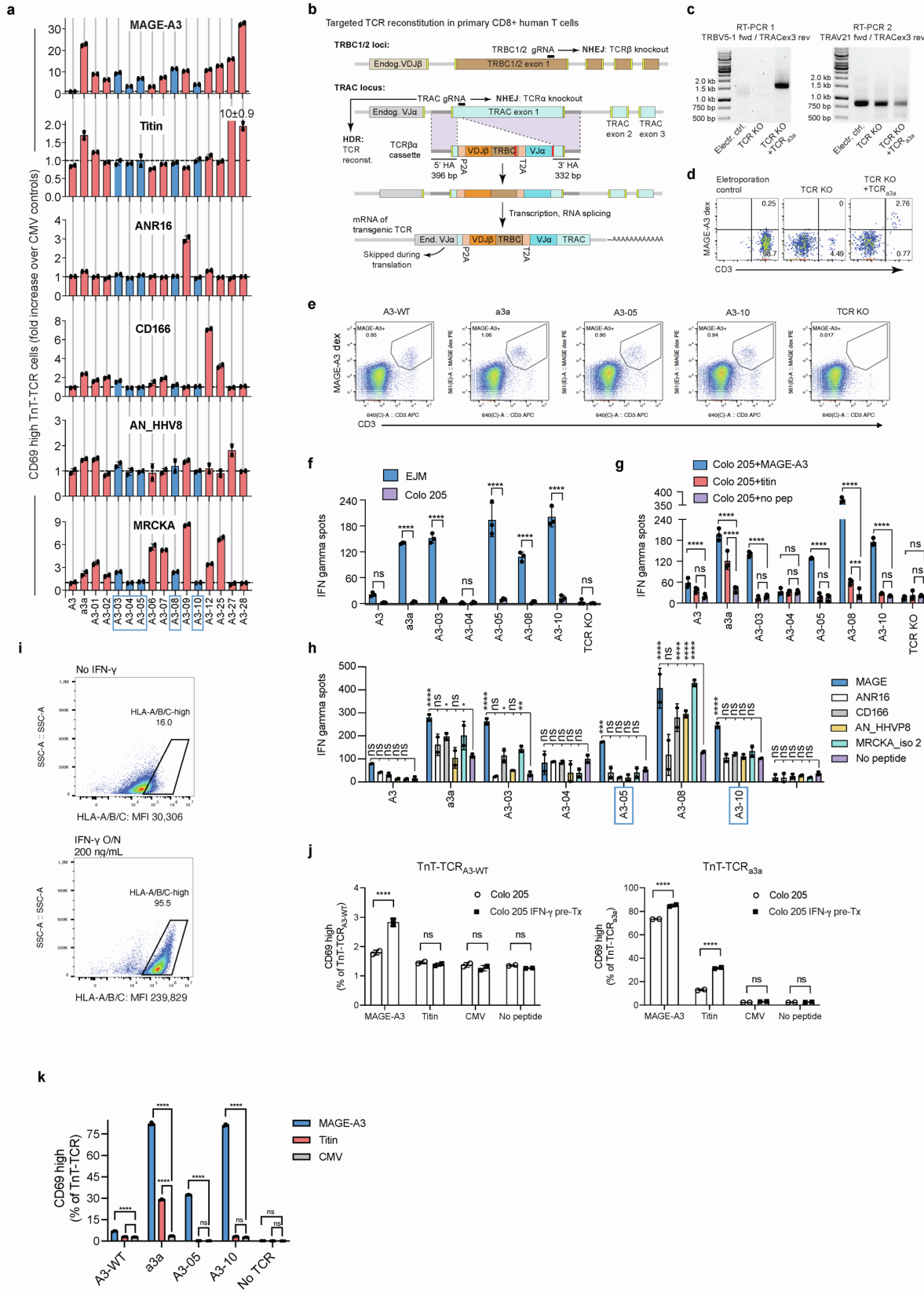
c

Final library:

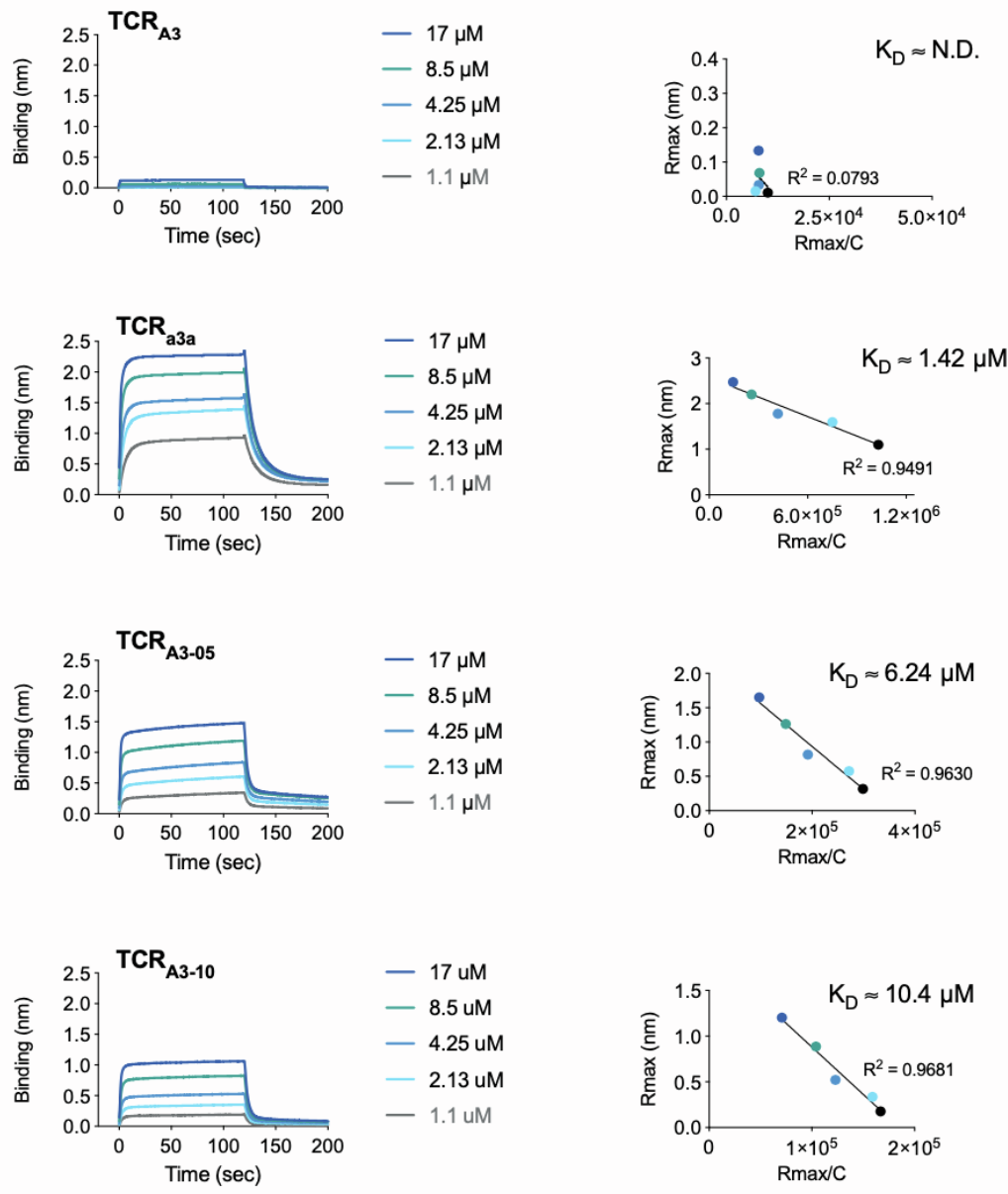
Theoretical diversity = 2.6×10^5



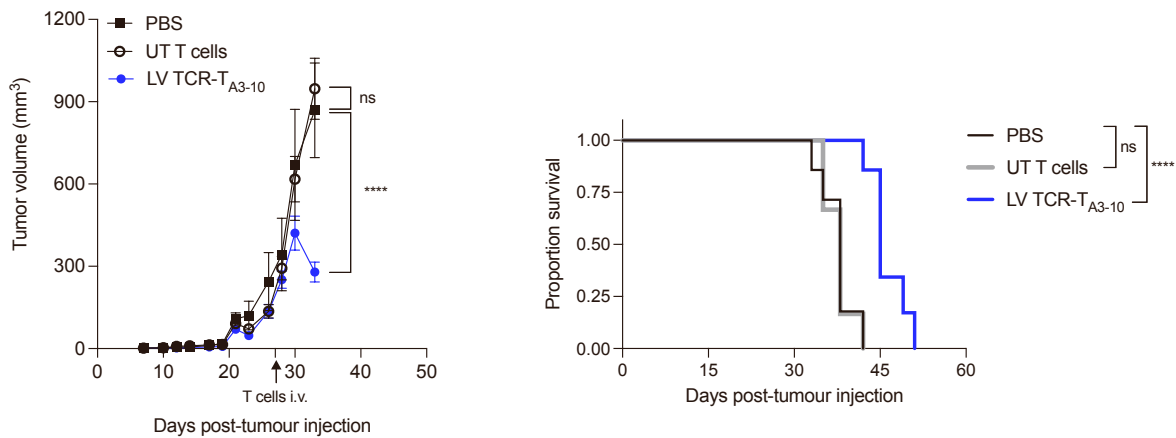
Supplemental Fig. 4. Combinatorial library design based on DMS of the TCR_{A3} CDR3 β , Related to Figure 4. **a**, Bar plots show the frequencies of single mutants present in TCR_{A3} DMS selections 2A (MAGE-A3 peptide-MHC+) and 2B (NFAT-GFP+) (added and normalized to 100%). **b**, Pooled DMS data was used as input for our previously described algorithm (Mason et al. 2018, PMID: 29931269) with the aim of re-capitulating observed amino acid frequencies with degenerate codons (two iterations with varying sensitivity to lower frequency amino acids are displayed). **c**, To take advantage of the full attainable diversity of mammalian cell display, the “Round 2” solution (theoretical diversity of 4,096 sequences) was rationally modified to include two “VNB” codons at positions 4 and 6 (high levels of enrichment in DMS), leading to a theoretical diversity of 2.6×10^5 variants. Degenerate base symbols: R = A, G; Y = C, T; S = G, C; W = A, T; K = G, T; M = A, C; B = C, G, T; D = A, G, T; H = A, C, T; V = A, C, G; N = any base.



Supplemental Fig. 5. TCR-Engine variants display high levels of specificity in TnT cells and primary human T cells, Related to Figure 4. **a**, TnT cells expressing TCR_{A3}, TCR_{a3a} and selected TnT_{A3} variants were co-cultured with Colo 205 cells pulsed with a subset of predicted off-target peptides. The percentages of CD69^{high} TnT-TCR cells were determined by flow cytometry and normalized to their respective CMV backgrounds (n = 2). Selected TnT-TCR_{A3} variants displaying favorable cross-reactivity profiles are highlighted in blue. **b-e**, CRISPR-targeted reconstitution of primary human CD8+ T cells with transgenic TCRs. **b**, Adapted CRISPR-Cas9-based method for dual knockout of endogenous TCRα and TCRβ chains and simultaneous reconstitution with transgenic TCRs targeted to the TRAC locus (see also STAR Methods). The lack of a complete TRAC region in the designed TCRβ_a HDR templates made splicing with endogenous TRAC exons a requirement for transgenic TCR surface expression. Regions highlighted in red were recoded in order to prevent targeting of HDR templates. Transgenic TCR expression is dependent on correct RNA splicing with endogenous TRAC exons 2 and 3. **c-d**, Validation of the approach is shown for TCR_{a3a}. **c**, RT-PCR with a forward primer annealing to the transgenic TRBV5-1 gene and a reverse primer annealing to the endogenous TRAC exon 3. Electroporation control and dual TCR knockout samples display no PCR product, while samples derived from TCR_{a3a} transfecants display a 1.6 kb product consistent with targeted TCR integration and correct splicing with endogenous TRAC. A second RT-PCR reaction amplifying both endogenous and transgenic TRAV21-TRAC TCRs is shown as a positive control. **d**, Flow cytometric assessment of CD3 expression and MAGE-A3 peptide-MHC dextramer binding in primary CD8+ T cells reconstituted with TCR_{a3a}. **e**, Flow cytometric assessment of CD3 expression and MAGE-A3 peptide-MHC dextramer binding in primary CD8+ T cells reconstituted with TCR_{a3a}. **f-g**, Example CRISPR-targeted TCR reconstitution experiment showing expression of TCR_{A3}, TCR_{a3a}, TCR_{A3-05}, TCR_{A3-10} in edited primary human CD8+ T cells, as determined by flow cytometry (n = 1). **f-g**, Functional assessment of selected TCR_{A3} variants expressed on the surface primary human CD8+ T cells, as measured by IFN-γ ELISpot. Primary human CD8+ T cells were transfected with Cas9 RNP complexes targeting the TRAC and TRBC regions, along with TCR-encoding HDR templates. A no-HDR-template control (TCR KO) was also included. **f**, Activation of edited CD8+ T cells following co-culture with MAGE-A3-positive EJM cells or MAGE-A3-negative Colo 205 cells (n = 3). 5x10⁴ T cell transfectants plus 1.5x10⁴ EJM or Colo 205 cells per well. **g**, Activation of edited CD8+ T cells following overnight co-culture with Colo 205 cells pulsed with MAGE-A3, titin, or no peptide (n = 3). 4x10⁵ T cell transfectants plus 1.5x10⁴ Colo 205 cells per well. **h**, Activation of edited CD8+ T cells following overnight co-culture with Colo 205 cells pulsed with a panel of potential off-target peptides (n = 2). 2.5x10⁵ T cell transfectants plus 1.5x10⁴ Colo 205 cells per well. Blue boxes highlight variants TCR_{A3-05} and TCR_{A3-10}, which display negligible cross-reactivity. **i**, Overnight stimulation of Colo 205 with 200 ng mL⁻¹ human IFN-γ results in a 8-fold increase in mean fluorescence intensity of surface HLA class I expression. **j**, Overnight stimulation of Colo 205 with 200 ng mL⁻¹ human IFN-γ significantly enhances the sensitivity of TnT-TCR cells to pulsed peptides (n = 2). **k**, Assessment of TnT-TCR activation in response to peptide-pulsed Colo 205 cells pre-treated with IFN-γ, as measured by flow cytometry detection of CD69 expression, reveals a lack of cross-reactivity to titin by TCR_{A3-05} and TCR_{A3-10} (n = 3). Asterisks indicate significant differences between indicated groups as determined by two-way ANOVA with Bonferroni post-hoc test for multiple comparisons. Data are displayed as mean ± SD. * P < 0.05, ** P < 0.01, *** P < 0.001, **** P < 0.0001, ns = not significant. Experiments were performed once.



Supplemental Fig. 6. TCR-Engine variants display enhanced binding affinity to MAGE-A3 pMHC, Related to Figure 6. Biolayer interferometry analyses of soluble TCR binding to immobilized MAGE-A3 HLA-A*0101 monomers. K_D values were approximated by Scatchard analyses of R_{max} vs. $R_{\text{max}}/\text{concentration}$ plots (K_D in molar \approx negative of linear regression slope).



Supplemental Fig. 7. LV TCR-T_{A3-10} cells mediate tumor regression and prolonged survival of NSG mice harboring established A375 melanoma tumors, Related to Figure 7. The antitumor activity of LV TCR-T_{A3-10} cells was assessed in a xenogeneic A375 melanoma mouse tumor model. NSG mice were injected s.c. in their left flanks with 5×10^6 A375luc2 cells on day 0 ($n = 6$), followed by treatment with a single i.v. dose of PBS, 1×10^7 UT T cells or 1×10^7 TCR-T_{A3-10} T cells on day 27. All mice (including those in the PBS group) were injected periodically with s.c. injections of recombinant human IL-2 (2.75 μ g per dose) in order to promote T cell engraftment (dosing schedule described in methods section). Following treatment, mice were monitored for tumor growth (left panel) and survival (right panel). Data are displayed as mean \pm SEM. Mouse survival (right panel) is displayed using Kaplan–Meier plots and compared by the log-rank (Mantel-Cox) test. Asterisks indicate significant differences as determined by two-way ANOVA with Bonferroni post hoc test for multiple comparisons. * $P < 0.05$, ** $P < 0.01$, *** $P < 0.001$, **** $P < 0.0001$, ns = not significant. Experiment was performed once.

Supplemental Tables 1-6

Supplemental Table 1. Previously discovered TCRs and target peptides utilized in this study, Related to Figures 2 and 3.

Name	Target protein(s)	Target peptide	MHC restriction	Peptide sequence	Comments
TCR _{1G4}	NY-ESO-1	NY-ESO-1 ₁₅₇₋₁₆₄	HLA-A*0201	SLLMWITQC	
TCR _{DMF4}	MART-1	MART-1 _{26-35(27L)}	HLA-A*0201	E <u>L</u> AGIGILTV	Anchor-modified peptide
TCR _{DMF5}	MART-1	MART-1 _{26-35(27L)}	HLA-A*0201	E <u>L</u> AGIGILTV	Anchor-modified peptide
TCR _{A3}	MAGE-A3	MAGE-A3 ₁₆₈₋₁₇₆	HLA-A*0101	EVDPIGHLY	
TCR _{a3a}	MAGE-A3 Titin	MAGE-A3 ₁₆₈₋₁₇₆	HLA-A*0101	EVDPIGHLY	
		Titin _{24,337-24,345}	HLA-A*0101	ESDPPIVAQY	

Supplemental Table 2. Unique clones identified in SEL 3A (MAGE-A3-induced signalling) and SEL 3B (titin-induced signalling) by means of deep sequencing, Related to Figure 4.

Total clones SEL 3A + 3B	Clones in SEL 3A only	Clones in SEL 3B only	Clones in both SEL 3A and SEL 3B	Clones enriched >2-fold in SEL 3A and not enriched in SEL 3B (enrich. over SEL 1)
1600	910	365	325	195

Supplemental Table 3. Top-ranked TCR_{A3} variants with predicted high specificity for MAGE-A3, Related to Figure 4. Experimentally validated variants are highlighted in bold.

TCR	SEL 2 (MAGE) enrichment over SEL 1	SEL 3A (MAGE) enrichment over SEL 1	SEL 3B (titin) enrichment over SEL 1	SEL 3A frequency rank	SEL 3A enrichment rank	Score
A3-001	41.9	130.5	0.0	45	8	53
A3-002	54.8	103.1	0.0	59	13	72
A3-003	53.1	78.2	0.0	76	19	95
A3-004	82.1	78.1	0.0	77	20	97
A3-005	25.9	65.7	0.0	21	24	45
A3-006	71.7	65.6	0.0	89	25	114
A3-007	43.5	63.3	0.0	93	26	119
A3-008	35.4	57.0	0.0	97	31	128
A3-009	32.2	55.9	0.0	99	33	132
A3-010	88.6	53.5	0.0	102	34	136
A3-011	19.1	48.9	0.0	31	40	71
A3-012	25.0	46.0	0.4	8	45	53
A3-013	39.5	43.4	0.0	124	50	174
A3-014	23.4	42.2	0.0	127	53	180
A3-015	20.9	41.0	0.0	132	55	187
A3-016	33.8	41.0	0.0	133	56	189
A3-017	26.1	40.4	0.0	70	58	128
A3-018	35.6	39.1	0.0	40	60	100
A3-019	29.0	38.5	0.0	136	61	197
A3-020	25.8	37.3	0.0	139	63	202
A3-021	26.1	34.7	0.0	83	68	151
A3-022	24.5	33.5	0.0	43	74	117
A3-023	9.2	31.6	0.0	92	76	168
A3-024	11.4	22.1	0.0	41	98	139
A3-025	12.1	21.8	0.5	88	99	187
A3-026	15.8	19.3	0.0	62	110	172
A3-027	4.9	17.9	0.2	50	117	167
A3-028	13.6	15.4	1.0	11	133	144
A3-029	10.3	15.4	0.1	29	134	163

Supplemental Table 4. List of candidate off-target peptides shared by TCR_{a3a}, TCR_{A3-05} and TCR_{A3-10}, as predicted from peptide scanning of the MAGE-A3₁₆₈₋₁₇₆ target using TnT-TCR cells as effectors, Related to Figure 6.

Pep No.	Protein	Start position	End position	Sequence	Pep No.	Protein	Start position	End position	Sequence	Pep No.	Protein	Start position	End position	Sequence	Pep No.	Protein	Start position	End position	Sequence	Pep No.	Protein	Start position	End position	Sequence	Pep No.	Protein	Start position	End position	Sequence
1	5HT2A	243	251	EIPIPLTMV	61	CHSTE	362	370	FAYPLPNVT	121	FNDC8	287	295	ENYPIQITV	181	MAGI1	540	548	QSIPFAGSV	241	PKL2	367	375	FGDPLWIVQ	301	TFFC	282	290	FSDPPLSYTF
2	A16L2	497	505	QVIPVGGRV	62	CLD15	146	154	FFDPLVPGT	122	FRIL6	977	985	QIVPV PANI	182	MARE1	234	242	ENDPVLQRI	242	PLD5	387	395	ETDPLTNRF	302	THIL	234	242	EVIPVTVT
3	A1CF	71	79	EIPLCEKI	63	CND2	240	248	EIDPMFOKT	123	FSO1L	201	209	EIDPVEELV	183	MED6	91	99	QVIPLAGDT	243	PP1R8	107	115	QQIPIDSTV	303	TIF1A	924	932	FDQPVPLT
4	AAK1	917	925	EIDPVPVLI	64	CNOT1	710	718	QIDPLAGMT	124	GATA1	76	84	QVYPLLNCM	184	MEF6	319	327	EGDPLVDGTC	244	PPM1H	298	306	EQIPMSSEF	304	TIGIT	138	146	FQIPLLGAM
5	ABCAC	531	539	QIPLIEAM	65	CNOT4	377	385	EIPIVSSST	125	GBG5	44	52	QHDPLLTGV	185	MGST2	58	66	EFYPIFIT	245	PR14L	705	713	QTIPQTKI	305	TITIN	2437	2443	ESPDIVAGY
6	ABCAC	858	866	QAPIMLQNT	66	CNOT5	162	170	EIPICLRLI	126	GFP72	217	225	EQIPILYRT	186	MNDA	208	216	QNDPVTVVV	246	PRC2B	1957	1965	QQIPISLHT	306	TKFC	128	136	EGIPVEMMV
7	ABC4	357	365	EVDPIEHT	67	CNTN2	524	532	QHPPLLDII	127	GLT16	270	278	EQIPLEKHM	187	MOC51	549	557	QLIPLHHV	247	PRD16	862	870	FDIPYLSRV	307	TML1	446	454	EDPPLAPAV
8	ABEC4	259	267	ESYPLINAF	68	COG6	1892	1900	EIIPVVITF	128	GPR18	196	204	FIPLFLIMI	188	M0D5	85	93	FVDFLVNTY	248	PRDM6	184	192	EIPLNQHT	308	TMW2	539	547	FNIPLMAYM
9	ACACA	2174	2182	EIPIYHQV	69	CG4	351	359	EIDLPILEV	129	GRHL3	257	265	QPVYTLRT	189	MORC1	570	578	QFIPDEIT	249	PRDX1	42	50	FFYPLDFTF	309	TPC11	993	1001	ENIPVTTV
10	ACADM	59	67	EIPVAAEY	70	COQ5	265	273	EIPIVPLGEV	130	GRIA1	531	539	FLDPLAYEI	190	MROH8	70	78	QQDPLSEAI	250	PR510	114	122	EVDPLVYNN	310	TR49B	22	30	FDIPVTD
11	AQL7A	231	239	EGYPLPSIT	71	CP2A6	390	398	EVYPMLGSV	131	GST2	110	118	FGIPLWVQV	191	MTFR2	56	64	ELIPLLNSV	251	PTPRB	1131	1139	QVDPVLQSF	311	TR64C	22	30	FDIPVTD
12	AEBP1	916	924	QIPIRANAT	72	CP3A5	215	223	EIPLPLLSI	132	GTC1	51	59	QTIPSEHY	192	MXRA5	1804	1812	ONIPMVSST	252	PUR4	92	100	EMIPREVWC	312	TR11	23	31	FTDPVMTD
13	AFAD	1217	1225	EAYPIPQT	73	CPED1	371	379	FMPYVLOV	133	HACD3	299	307	QSIPIFNET	193	MXRA5	2544	2552	FHDPISEKI	253	RAS4B	289	297	QLIPUIEET	313	TR117	23	31	FTDPVMT
14	AGRE4	300	308	FMYPVGYGI	74	CPLH1	363	371	EIPLHPLU	134	HAC4	996	1004	EDPLPKEV	194	MY15B	737	745	EAIPLAPGI	254	RBBP6	365	373	QDDPLMPV	314	TR41	27	35	FTDPVSI
15	AGR66	716	724	QVDPVLSI	75	CPLN1	2416	2424	QDPLNLII	135	HD	2801	2809	QLIPVSDY	195	MYBB	388	396	EIPLSPST	255	RBM25	753	761	FAYPLDWSI	315	TR51	22	30	FLDPVTD
16	AGR1L	42	50	EYGPIELRL	76	CRBG	1635	1643	EVPPMMPEV	136	HELQ	1009	1017	EIPLMEVT	196	MYO1H	174	182	QGIPVFVGH	256	RPB1	190	198	FGIPLADAV	316	TR158	267	275	ENIPMLEKT
17	AGR3L	37	45	ESYPIELRC	77	CRBG3	1706	1714	EIPIVTLAM	137	HELZ2	612	620	OTDPIVTLQY	197	MYO2Z	242	250	EIPIVTTT	257	RELCH	541	549	EULIPILCT	317	TRM4	19	27	FDQPV
18	ALPK3	1702	1710	EIPILYLIY	78	CRBN	79	87	EIPIVPLQV	138	HERC1	4283	4281	QCIPLVLAGV	198	NCHL1	145	153	EODPVLPC	258	RELN	1226	1234	QIPVINP	318	TR10	2687	2695	FVPLSEV
19	AMPE	711	719	EIPLMEEY	79	CSE01	279	287	QNDPLPGRI	139	HERC1	4647	4655	EMPLDSFV	199	NELF0	571	579	EHDPIVTEI	259	REV3L	2317	2325	EDPFLCAFL	319	TSH1	466	474	QSLPLPPT
20	AN13A	377	385	QVPIPLDLM	80	CSKP	767	775	EIAYPIHPT	140	HEXD	82	90	EIPIVQTF	200	NEMF	388	396	QGDPLVASAI	260	RFIP3	118	126	ELDPFLSWT	320	TSH1	95	103	FSYPLVASC
21	AN10B	980	988	QIPLQGKF	81	CSPG2	1360	1368	EIDPVHDL	141	HMHCN1	994	1002	EIPIVPLCP	201	NEMF	995	1003	FAPICAPY	261	RGP24	1369	1377	EULPTARM	321	TT21A	441	449	OQIPGLSEY
22	ANR16	147	155	EGDPLILQY	82	CTR4	540	548	FQIPMVPV	142	HNRC1	250	258	EIDPLDDDV	202	NEP1	178	186	FSIPIVSDV	262	RHAG	49	57	EYPLPQDFV	322	TT30A	438	446	ENYPMVEKV
23	ARMD3	143	151	QFIPPLTRT	83	CWC22	121	129	EIPLPLTRT	143	HRH3	86	94	EIPIVPPV	203	NFE2	178	182	EMYPPVEY	263	RP1R1	720	728	QADPMAPRT	323	TT30B	438	446	ENYPMVEK
24	ARRD1	328	336	FIDPVFLST	84	DDX1	56	64	EISPIVQIV	144	HFS2	259	267	EINPIVPEI	204	NPF2	169	177	EYFPVPPY	264	RM11	62	70	EQIPLPTK1	324	TTC14	535	543	ECYPLVANT
25	ARRD2	199	207	EIVIPVFAEI	85	DDX23	445	453	EIPLVLLVI	145	HSP7E	365	373	EIVIGAAI	205	NLGNX	497	505	FGIPMIGPT	265	RM40	81	89	EUDPEOFI	325	TTL2	176	184	QFIPLTVF
26	ARRD4	210	218	EIPIYAEI	86	DDX24	247	255	EIAYPIHMAV	146	IDD	43	51	QCIPLWPQG	206	NMES1	121	20	EIPLVLFM	266	RNP37	263	271	FLDPLTLEI	326	TRW2	246	254	EGDPLLESV
27	ARSGD	18	26	FIDPVDFC	87	DDX46	224	232	EIDPLVDAYM	147	IFNA2	74	82	EITPIVHEM	207	NOX3	397	405	FHYPLVFCVC	267	RP1	1070	1078	QDPIEET	327	TX13C	154	162	QVYPMODF
28	ASHL1	2748	2756	EIPILEAVV	88	DEN6B	427	435	EIPILEHYM	148	GSF2	35	43	EGYPSVIGC	208	NPBW1	212	220	EAIPLVSTIC	268	RPB2	86	94	ETDPLIAMI	328	UBE2W	76	84	ENIPVPHV
29	AT11B	351	359	EIPIYSLV	89	DHK9	1123	1131	QIDPVNERM	149	GSF3	159	167	EQDPLLETC	209	NTRK2	609	617	EODPLIMVF	269	RRBP1	1284	1292	QDIPVOLKT	329	UBP38	242	250	QHIPLOM
30	AT11C	356	364	EIPIVSMYV	90	DIPI2A	1561	1569	EIPLPVAY	150	L7RA	237	245	EMDPLILLT	210	NUPBL	197	205	QNIPRTGAV	270	RSH4A	527	535	EIPVPLVELV	330	UBP8	658	666	FLDPLTGTF
31	AT13A	544	552	QGDPLDKM	91	DIPI2B	426	434	EIVIPVPIEV	151	IQN	341	349	QTYPVWSVT	211	SPD1	202	220	EIPIVMIIF	271	SCAP1	284	292	EIPLVTTT	331	URAS1	24	32	FLIPVALR
32	ATP7A	660	668	EIPIVGMGL	92	DLG1	822	830	EIPLVPSI	152	LBFB	393	401	EIPIVVARM	212	OS1A7	27	35	EISPLCMY	272	S12A3	487	495	QLYPLGF	332	UTP20	236	234	EIPPLCLMT
33	ATP7B	660	668	EIPIVVALM	93	DLG2	788	796	EIPLVIAIFI	153	ITAB8	1008	1016	EISPLVWII	213	ODAM	107	115	QVDPLOLOT	273	S15A1	10	18	FGYPLSIFF	333	VAFNB	57	95	EMYPVPPIT
34	B3A3	930	938	EIPLVSLISL	94	DLGP1	61	69	EISDPLASST	154	ITBT7	148	156	EYGPYDLYY	214	OMA1	510	518	EIPLVITIV	274	S6A20	117	125	QDQPLPWVSI	334	VATA	417	425	FSDPVLSI
35	B3GN7	321	329	EIPLDODFV	95	DNA13	38	46	EIPLVLLTT	155	JAK2	34	42	QDIPLOVY	215	OPLA	732	740	QDPLQSLSI	275	SCAF4	349	357	QDQPMHQQV	335	VDLR	126	134	QCIPVSWRC
36	B3GN8	64	72	EIPLPFFAY	96	DND1	73	81	EIPLPQFQV	156	JIP14	919	927	EITDPLGVQI	216	OPRK	235	243	FIVPLVIII	276	SCAM1	256	264	QNIPVGIMM	336	WB5B1	49	57	FVYPLDECT
37	BCL7C	179	187	EAYPVPEV	97	DSCAM	714	722	EIYPVPTV	157	K1210	525	533	QGYPMSAA	217	OPSD	212	220	EIPLVMIIF	277	SCAP1	284	292	EIPLVTTT	337	WASH1	188	196	FLDPLAGAV
38	BDH	225	233	EIYPLGVKV	98	DUS18	82	90	EFDPIADH	158	K154L	1245	1253	EIPLVQET	218	OR101	23	31	EIPLRFLV	278	SCN1A	788	796	EHYMPDHF	338	WDFY4	313	321	EYGPLLKV
39	BEND1	348	356	EISIPVPCQI	99	DUS21	84	92	EFDPIADU	159	KALRN	2853	2861	EIPLVPSLGT	219	OR211	252	260	EIPLVMCMY	279	SCN2A	779	787	EHYMPTEQF	339	WDR27	491	499	EAYPVCEAV
40	BRWD3	1007	1015	EIDPLSGKM	100	DYH11	3798	3806	EIDPLLEDF	160	KCNK1	139	147	EIPLMFLV	220	RSK4	202	210	FSIPIQIFT	280	SCN4A	598	606	EHYPTEHF	340	WFS1	343	351	FFPLVLLT
41	BUD13	541	549	EQIPMANP	101	DYH7	836	844	EIPLQIVI	161	KDM2A	303	311	EINPLMQLK	221	OR6K6	55	63	EIPLLIIY	281	SCNNA	110	118	FSYPLVSLNI	341	XPO2	40	48	ONPLPLLT
42	C10L1																												

Supplemental Table 5. HLA-typed B-LCL lines used for alloreactivity screening (European Collection of Authenticated Cell Cultures, ECACC), Related to Figure 6.

B-LCL	HLA-A		HLA-B		HLA-C	
B-LCL 88	3	24	13	62	6	-
B-LCL 133	1	2	8	60	3	7
B-LCL 220	25	11	14	18	5	8
31708	2301	6802	1503	35	0202	0401
JS	3003	0301	0702	1801	0501	0702
B-LCL 129	1	3	7	8	7	-

Supplemental Table 6. Sequences of DNA oligonucleotides utilized in this study, Related to STAR Methods.

Purpose	Oligo name	Sequence 5'-3'	Annealing temp (°C)
CD8 α -P2A-CD8 β PCR	RVL-50	cgtacaggatccgtatggccttaccagtgaccgc	72
	RVL-51	tgc当地caacgcgtactgtcactaagatacattgtatggttgg	
CD4 PCR	RVL-101	gatgttggacggcgataatggaa	65
	RVL-102	tgtggagctaggcaacaagaa	
Labeling of cDNA 3' ends	TSO	AAGCAGTGGTATCAACGCAGAGTGAATrGrG+G	n/a
Jurkat TCR α template-switching RT-PCR	ISPCR	aaggcagtgttatcaacgcagagt	64
	RVL-70	tctcagctgttacacggcag	
Jurkat TCR β template-switching RT-PCR	ISPCR	aaggcagtgttatcaacgcagagt	62
	RVL-68	agatctctgttctgtatggcctc	
Jurkat TCR α RT-PCR	RVL-69	cagtccgtgacccagcttgg	62
	RVL-70	tctcagctgttacacggcag	
NFAT-GFP HDR template generation (AAVS1)	RVL-119	tgctttctgtaccaggattctctc	72
	RVL-120	agagcagagccaggaaccc	
AAVS1 PCR 1	RVL-137	cacctactcagacaatgcgtatgc	60
	RVL-138	gaactctgcctctaacgcgtc	
AAVS1 PCR 2	RVL-139	ctgggataccccaagagtgagt	65
	RVL-140	ccgcctggaaagggttagagggaaa	
TnT-TCR PCR	RVL-71	gtgccctctcttttgttgc	61.5
	RVL-72	gattcaggcagagggtggagtt	
TnT-TCR RT-PCR A (amplicon for deep seq.)	RVL-144	gaggagaacccctggacctatg	60
	RVL-145	ggaacacccgttgcaggctc	
TnT-TCR RT-PCR B	RVL-67c	ttcttgctcatgctcacagagg	62
	RVL-68	agatctctgttctgtatggcctc	
Plasmid library PCR (amplicon for deep seq.)	RVL-144	gaggagaacccctggacctatg	66
	RVL-154	ctagagacccccagccttacc	
Primary T cell RT-PCR 1	TRBV5-1_fwd	atccctggtaccaacagaccccaggacag	68
	TRACex3_rev1	gtcatgagcagattaaacccggccac	
Primary T cell RT-PCR 2	TRAV21_fwd	atggaaaccccttgggcctg	62.3
	TRACex3_rev2	aaacccggccactttcag	
TCR $\alpha\beta$ HDR template generation (TnT cells)	RVL-127	gcatgcctctgtccaaacag	70
	RVL-128	tttatctgtcatggccgtgacccg	
TCR $\beta\alpha$ HDR template generation (1° T cells)	RVL-166	ctgcctttactctgtccagagttatattgc	62
	RVL-167	gacatcatgaccagagctctgg	
Nicking mutagenesis TCR α DMS	A3_NNK1	ggccctttatcttgcnnkagcagcccaaatatggcg	n/a
	A3_NNK2	ggccctttatcttgcnnkagcccaaatatggcgatgaaca	
	A3_NNK3	ggccctttatcttgcnnkagcccaaatatggcgatgaaca	
	A3_NNK4	ggccctttatcttgcnnkagcccaaatatggcgatgaacagtc	
	A3_NNK5	ggccctttatcttgcnnkagcccaaatatggcgatgaacagtc	
	A3_NNK6	tcttgcggcaggccggaaatnnkgcggatgaacagtc	
	A3_NNK7	cgccaggccggaaatnnkgcggatgaacagtc	
	A3_NNK8	gcagccggaaatnnkgcggatgaacagtc	
	A3_NNK9	ccgaatatggcgatrnkcgacttggccggcaccagg	
	A3_NNK10	gaatatggcgatgaannktactcggccggcaccagg	
	A3_NNK11	atatggcgatgaacagnnkttcgccggccggcaccagg	
Nicking mutagenesis TCR α DMS	DMF4_NNK1	cagacatctgtgtactctgtgnkcatcagtggatgggttggg	n/a
	DMF4_NNK2	atctgtgtactctgtgcnnkagtggatgggttggg	
	DMF4_NNK3	gtgtactctgtgcnnkagtggatgggttggg	
	DMF4_NNK4	tacttctgtgcnnkagtggatgggttggg	
	DMF4_NNK5	ctgtgcnnkagtggatgggttggg	
	DMF4_NNK6	gtgcnnkagtggatgggttggg	
	DMF4_NNK7	ccatcgtggatgggttggg	
	DMF4_NNK8	tgtgcnnkagtggatgggttggg	
	DMF4_NNK9	cagtggatgggttggg	

DMF4_NNK10	gaggtaggggtgggcagnnkcgacatttgtatggg		
DMF4_NNK11	gttaggggtggcagccnnkcattttgtatgggact		
DMF4_NNK12	gggtgggcagccccagnnktttgtatggactcg		
Nicking mutagenesis (2nd strand synthesis)	RVL-128	tttatctgtcatggccgtgaccg	n/a
Combinatorial TCR _{A3} library OE-PCR	A3_fwd_ultramer	atcctgttaccaacagaccccaggacaggccctcagtccctttgaa tacttcagtgagacacagagaacaaaggaaactccctggtcattc tcaggccgcaggctctaactctcgctctgagatgaatgtgagcacctt ggagct	70
	A3_rev_ultramer	taggctctccatagagaccccccagccttacctgtgaccgtgagcctggtg cccgcccaarwaywgyccryynrcvnbrytvnbcrycrysngsc aaagataaaaggccgagtcggccagctccaagggtgtcacattcatct cag	
Combinatorial TCR _{A3} library flanking PCR	A3_flank_fwd	atcctgttaccaacagaccccaggacag	62
	A3_flank_rev	taggctctccatagagaccccccagccttacc	

rG = riboguanosine; +G = locked nucleic acid guanine; r = a, g; y = c, t; s = g, c; w = a, t; k = g, t; m = a, c; b = c, g, t; d = a, g, t; h = a, c, t; v = a, c, g; n = any base.